OPEN ACCESS

ISSN 2587-3458
e-ISSN 2587-3466

Category A

OH&RM ONE HEALTH & RISK MANAGEMENT

THE SCIENTIFIC JOURNAL
OF THE MOLDAVIAN BIOSAFETY AND BIOSECURITY ASSOCIATION

January 2026 | Volume 7 | Issue 1

https://doi.org/10.38045/ohrm.2026.7(1)

The Moldovan Association for Biosafety and Biosecurity (MDBBA) is a scientific and practical, instructive and educational, non-governmental, apolitical and non-profit professional organization, founded in 2017.

The main objective of the association is the development of good practices and culture in the field of biosafety and biosecurity and the promotion of knowledge within professional and research-innovation groups.

BIOSAFETY includes security principles, technologies and rules to be followed to prevent unintended exposure to pathogens and toxins or their accidental release/ leakage.

"Protection of personnel, population from unintended exposure to pathogens/ biohazardous material".

BIOSECURITY includes a wide spectrum of measures (biosecurity policies, regulatory regime, scientific and technical measures) applied in an organized framework, necessary to minimize risks (prevention of actions, terrorist attacks by the intentional release of pathogens or toxins as well as loss, their theft or misuse).

"Protection and prevention of theft, intentional misuse of pathologies/biohazardous material".

RISK MANAGEMENT is a decision-making process in which the results of risk assessment (the process of estimating workplace hazards) are integrated with economic, technical, social and political principles to generate strategies for risk reduction.

One Health is an integrated, unifying approach that aims to sustainably balance and optimize the health of people, animals and ecosystems.

It recognizes that the health of humans, domestic and wild animals, plants, and the wider environment (including ecosystems) are closely linked and interdependent.

While health, food, water, energy and environment are all wider topics with sector-specific concerns, the collaboration across sectors and disciplines contributes to protect health, address health challenges such as the emergence of infectious diseases, antimicrobial resistance, and food safety and promote the health and integrity of our ecosystems.

By linking humans, animals and the environment, One Health can help to address the full spectrum of disease control – from prevention to detection, preparedness, response and management – and contribute to global health security.

CONTENTS | TABLE DES MATIÈRES

FOREWORD – AVANT-PROPOS

Dániel Cadar
Genomics, One Health, and the Future of Infectious Disease Preparedness 3

RESEARCH ARTICLES – ARTICLES DE RECHERCHE

Ludmila Rudi, Tatiana Chiriac, Inga Zinicovscaia, Liliana Cepoi, Dmitrii Grozdov
IN VIVO evaluation of gold nanoparticles functionalized with *Arthrospira platensis* protein extract 4

Hashim Abed Abass, Muthanna Abdlkhader Salh Al-Mahdawi, Mohammed Sabea Challoob, Hayder H. Abed
Evaluation of *Thymus vulgaris* aqueous extract as a natural antimicrobial agent against urinary tract infection pathogens 15

Liliia Vygovska, Artem Ushkalov, Liubov Zelena, Valerii Ushkalov, Cristina Sirbu, Yurii Vishovan
Biological properties of *Serratia liquefaciens* 1/2024, isolated from chicken 22

Gala Matevska, Golubinka Boshevska, Elizabeta Jancheska, Teodora Karevska, Maja Vukovikj
Single Nucleotide Polymorphism test for rapid detection of SARS-CoV-2 lineages in the Republic of North Macedonia 39

Doina Secu, Daniela Blanita, Natalia Usurelu, Victoria Sacara
Clinical, biochemical, and genetic distinctions in patients with mitochondrial involvement versus other genetic disorders 49

Liliana Cepoi, Ludmila Rudi, Tatiana Chiriac, Vera Miscu, Ecaterina Plingau
Astaxanthin and Cellular Metabolites Production in *Haematococcus lacustris* Exposed to Silver Nanoparticles 60

EXPERT OPINION – AVIS D'EXPERT

Dániel Cadar
Metagenomics at the Interface of Diagnostics and Surveillance: a near-term perspective 74

REQUIREMENTS FOR AUTHORS 77
CERINȚE PENTRU AUTORI 78
EXIGENCES POUR LES AUTEURS 79

Quarterly edition
Languages of publication: English, French
Founder: Asociația de Biosiguranță și Biosecuritate din Republica Moldova

Category A
Scopus®

ISSN 2587-3458 (Print)
e-ISSN 2587-3466 (Online)
Registered at the Ministry of Justice with no. 476676, 05th of July, 2017

Genomics, One Health, and the Future of Infectious Disease Preparedness

Dániel CADAR, DVM, MSc.PH, PhD.
Head of Virus Metagenomics and Evolution Group
Bernhard Nocht Institute for Tropical Medicine
WHO Collaborating Centre for Arbovirus and
Hemorrhagic Fever Reference and Research
National Reference Centre for Tropical Infectious Diseases Hamburg, Germany

In recent years, the landscape of infectious disease surveillance and diagnostics has undergone a profound transformation, driven by rapid advances in molecular biology, sequencing technologies, and bioinformatics. Emerging and re-emerging pathogens, increasing global mobility, climate-driven ecological changes, and intensified human-animal-environment interactions continue to challenge public health systems worldwide. In this context, the ability to detect, characterize, and monitor pathogens with high resolution and speed has become a cornerstone of effective preparedness and response.

Metagenomic and targeted genomic approaches now offer unprecedented opportunities to move beyond pathogen detection alone toward a deeper understanding of transmission dynamics, pathogen evolution, and population-level risk. These technologies enable unbiased discoveries of known and novel agents, support real-time outbreak investigations, and provide critical insights into genomic diversity that inform diagnostics, therapeutics, and public health decision-making. Importantly, they also bridge traditionally separated domains-human health, veterinary medicine, wildlife surveillance, and environmental monitoring embodying the principles of the One Health approach.

At the same time, translating these powerful tools into routine public health practice remains a complex task. Challenges related to sensitivity, standardization, cost-effectiveness, data interpretation, and integration into existing surveillance frameworks must be addressed thoughtfully and collaboratively. Capacity building, interdisciplinary cooperation, and the sharing of methodological experience across regions and institutions are therefore essential to ensure that genomic technologies deliver their full societal benefit.

This volume brings together expert perspectives that reflect both the promise and the practical realities of modern pathogen genomics. By highlighting methodological advances, applied case studies, and future directions, it contributes to a more informed and resilient public health infrastructure. I hope that the contributions presented here will stimulate dialogue, foster collaboration, and support the continued integration of genomic approaches into evidence-based public health action.

Sincerely,

Dániel Cadar

RESEARCH ARTICLES – ARTICLES DE RECHERCHE

BIOLOGICAL SCIENCES

OPEN ACCESS

IN VIVO EVALUATION OF GOLD NANOPARTICLES FUNCTIONALIZED WITH *ARTHROSPIRA PLATENSIS* PROTEIN EXTRACT

Ludmila RUDI[1], Tatiana CHIRIAC[1], Inga ZINICOVSCAIA[2,3], Liliana CEPOI[1], Dmitrii GROZDOV[2]

[1] Institute of Microbiology and Biotechnology, Technical University of Moldova, Chisinau, Republic of Moldova
[2] Joint Institute for Nuclear Research, Dubna, Russia
[3] Horia Hulubei National Institute for R&D in Physics and Nuclear Engineering, Magurele, Romania

Corresponding author: Ludmila RUDI, e-mail: ludmila.rudi@imb.utm.md

https://doi.org/10.38045/ohrm.2026.1.01 CZU: [546.59:582.232]:57.083

ABSTRACT

Introduction Gold nanoparticles (AuNPs) have gained increasing attention in nanomedicine due to their biocompatibility and unique physicochemical properties, which make them suitable for targeted therapies against cancer and other chronic diseases. Functionalizing AuNPs with bioactive compounds further enhances their biocompatibility and therapeutic potential. This study aimed to evaluate the effects of 10 nm citrate-stabilized AuNPs functionalized with a protein extract from *Arthrospira platensis* (AuNPs-APE) on biodistribution, as well as hematological and biochemical parameters, in Wistar rats.

Material and methods FTIR spectroscopy confirmed AuNPs' functionalization. Wistar rats received oral doses of AuNPs or AuNPs-APE for 28 days, followed by a 28-day clearance period. Gold biodistribution was analyzed in organs collected at the end of the experiment. Hematological and biochemical profiles were assessed using standard methods.

Results FTIR analysis confirmed stable AuNPs-protein interactions. Both AuNPs and AuNPs-APE exhibited notable renal accumulation, suggesting extraglomerular retention. The protein extract showed mild immunomodulatory effects, reducing oxidative stress and inflammation associated with nanoparticle exposure.

Conclusions The AuNPs–APE complex shows promise as a renal-targeted nanotherapeutic system, demonstrating improved biocompatibility and reduced systemic stress compared with unmodified AuNPs. Further studies are required to elucidate the underlying mechanisms and to optimize the formulation and safety profile.

Keywords Gold nanoparticles, *Arthrospira platensis*, protein extract, Wistar rats, biodistribution, hematological assessment, biochemical profile.

EVALUAREA *IN VIVO* A NANOPARTICULELOR DE AUR FUNCȚIONALIZATE CU EXTRACT PROTEIC DIN *ARTHROSPIRA PLATENSIS*

Introducere Nanoparticulele de aur (AuNP) sunt utilizate tot mai frecvent în nanomedicină datorită biocompatibilității și proprietăților fizico-chimice unice, care le susțin aplicabilitatea în terapiile țintite pentru cancer și boli cronice. Funcționalizarea cu ajutorul compușilor bioactivi le optimizează potențialul terapeutic și biocompatibilitatea. Acest studiu a evaluat efectele funcționalizării AuNP stabilizate cu citrat de 10 nm, cu un extract proteic din *Arthrospira platensis* (AuNP-APE) asupra biodistribuției, profilurilor hematologic și biochimic la șobolani Wistar.

Material și metode Funcționalizarea AuNP a fost caracterizată prin spectroscopie FTIR. Șobolanii au primit oral AuNP sau AuNP-APE timp de 28 de zile, urmate de o perioadă de repaus de 28 de zile. Biodistribuția aurului a fost analizată în organele colectate la finalul experimentului. Profilurile biochimic și hematologic au fost evaluate prin metode standard.

Rezultate Spectroscopia FTIR a confirmat interacțiuni stabile între AuNP și proteinele din extract. Atât AuNP, cât și AuNP-APE s-au acumulat în rinichi, sugerând mecanisme extraglomerulare de retenție. Extractul proteic a avut efecte imunomodulatoare favorabile, reducând stresul oxidativ și inflamația sistemică, cauzată de nanoparticule.

Concluzii Complexul AuNP–APE prezintă potențial ca sistem nanoterapeutic, demonstrând biocompatibilitate superioară și un impact sistemic redus, față de AuNP nefuncționalizate. Sunt necesare cercetări suplimentare pentru clarificarea mecanismelor implicate și optimizarea profilului de siguranță și al formulării.

Cuvinte-cheie Nanoparticule de aur, *Arthrospira platensis*, extract proteic, șobolani Wistar, biodistribuție, evaluare hematologică, profil biochimic.

INTRODUCTION

Gold nanoparticles have emerged as essential tools in nanomedicine due to their significant potential in cancer diagnosis and treatment. In recent years, their applications have expanded considerably to include therapies for degenerative and infectious diseases and innovative oncological treatment strategies (1-3). Their unique physicochemical properties and nanoscale dimensions allow AuNPs to accumulate preferentially in tumor tissues and interact selectively with target cells while maintaining low systemic toxicity (4).

To enhance therapeutic effectiveness and improve the risk-benefit balance, recent research has focused on functionalizing AuNPs with bioactive molecules or complex delivery systems (4-6). Standard methods included functionalization with polyethylene glycol (PEG) or citrate, which boost colloidal stability and influence biodistribution (7-9). Additionally, attaching peptides, amino acids, or other specific ligands has shown potential for increasing the selectivity of AuNPs for tumor cells (4, 10).

Bionanosynthesis has emerged as a novel approach to nanoparticle functionalization, using natural reducing agents derived from plant or microbial sources to generate nanoparticles with enhanced biological properties (5, 6, 11). One such innovative strategy involves the incorporation of gold nanoparticles into the biomass of the cyanobacterium *Spirulina (Arthrospira) platensis*, followed by functionalization with bioactive protein fractions extracted from this biomass. These strategies improve the biocompatibility of nanoparticles and provide new opportunities for the development of advanced targeted therapies (12, 13).

The biomass of *Arthrospira (Spirulina) platensis* is recognized as a natural source of bioactive compounds with well-documented immunomodulatory and antioxidant properties, making it an ideal biological matrix for nanoparticle biofunctionalization (12–14).

This study aimed to evaluate the effects of 10 nm citrate-stabilized AuNPs functionalized with a protein extract from *Arthrospira platensis* biomass on biodistribution and *in vivo* hematological and biochemical profiles in a Wistar rat model.

MATERIAL AND METHODS

Preparation of *Arthrospira platensis* Protein Extract

The protein extract was prepared from the biomass of the cyanobacterial strain *Arthrospira (Spirulina) platensis* CNMN-CB-02, maintained in the National Collection of Non-Pathogenic Microorganisms at the Institute of Microbiology and Biotechnology, Technical University of Moldova. The strain was cultivated under photoautotrophic conditions in a mineral growth medium with the following composition (g/L): $NaNO_3$, 2.25; $NaHCO_3$, 8.0; NaCl, 1.0; K_2SO_4, 0.3; Na_2HPO_4, 0.2; $MgSO_4 \cdot 7H_2O$, 0.2; $CaCl_2$, 0.024; $FeSO_4$, 0.01; EDTA, 0.08; H_3BO_3, 0.00286; $MnCl_2 \cdot 4H_2O$, 0.00181; $ZnSO_4 \cdot 7H_2O$, 0.00022; $CuSO_4 \cdot 5H_2O$, 0.00008; MoO_3, 0.000015. The protein content of the dry biomass ranged from 68% to 72%, as determined by the Lowry method (15). For protein extraction, the bio-

mass was treated with a 0.45% (w/v) sodium hydroxide solution (SIGMA-ALDRICH CHEMIE GmbH, Germany) at a ratio of 1 g of biomass to 0.5 L of extraction solution. The extraction was carried out at 25 ± 1 °C with constant stirring for 60 min. The mixture was subsequently centrifuged, and the supernatant was collected. A second extraction was performed using an additional 200 mL of the same alkaline solution for 30 min under identical conditions. The two supernatants were combined and dialyzed until a neutral pH (7.0–7.2) was reached. The final *Arthrospira platensis* protein extract (APE) was standardized to a 1% (w/v) dry matter concentration, containing a total protein content of 52%.

Functionalization of AuNPs and Preparation of the AuNPs-APE Functional Complex (12)

Citrate-stabilized gold nanoparticles (AuNPs) with an average diameter of 10 ± 0.2 nm (0.02 mg/mL; SIGMA-ALDRICH CHEMIE GmbH, Germany) were used to prepare the functional complex. A 20 mL volume of the AuNP suspension was slowly added to 200 mL of a 1% (w/v) *Arthrospira platensis* protein extract (APE) solution. The mixture was stirred at 2000 rpm for 120 minutes at 25 ± 1 °C to facilitate interaction between the protein extract and the nanoparticles. The resulting bio-nanoconjugate (AuNPs–APE) had a final concentration of 1.0 mg/mL APE and 1 µg/mL AuNPs.

Characterization of AuNPs-APE

Fourier Transform Infrared (FTIR) Spectroscopy was performed on both APE and AuNPs-APE to assess functional group interactions. After being dehydrated at 40°C, the samples were analyzed at room temperature. Spectra were recorded in the range of 4000–400 cm^{-1} using a PerkinElmer spectrometer equipped with a DTGS detector.

Animals and Experimental Design

The *in vivo* study was conducted at the Laboratory of Stress Physiology, Adaptation, General Sanocreatology and Vivarium of the Institute of Physiology and Sanocreatology, Republic of Moldova. All procedures were approved by the Institute's Ethics Committee (Approval No. IREC/12/03.11.2020). A total of 48 adult Wistar albino rats (28 males and 20 females) were used. The animals were randomly divided into four experimental groups (n=12 per group, with 7 males and 5 females in each) and housed under standard laboratory conditions (22 ± 2 °C, 55 ± 5% relative humidity, 12-hour light/dark cycle) with *ad libitum* access to food and water. The experimental groups received the following dietary regimens for 28 consecutive days: C (–): negative control – standard diet only; C (+): positive control – standard diet supplemented with APE; Group 1 (AuNPs): standard diet with non-functionalized gold nanoparticles; and group 2 (AuNPs-APE): standard diet with the functionalized AuNPs-APE complex. Each animal received a daily dose of 1 µg of gold, administered in breadcrumbs made from whole rye flour. After the 28-day treatment period, seven animals from each group (4 males and 3 females) were euthanized for the collection of blood and organs (brain, liver, spleen, kidneys, testes, and ovaries). The remaining animals were maintained on a standard diet for a further 28 days to assess nanoparticle clearance.

Analysis of Gold Content in Animal Tissues by ICP-MS

Tissue samples were dried at 70 °C until a constant weight was achieved. For gold analysis, a 0.1 g aliquot of each sample was digested with 3 mL of HNO_3 and 1 mL of H_2O_2 (both from Sigma-Aldrich, Germany) in an ETAS-6 autoclave at 180 °C, 20 bar, and 400 W for 90 minutes. After cooling, the digests were diluted to a final volume of 20 mL with deionized water. Gold concentrations were determined using inductively coupled plasma mass spectrometry (ICP-MS; XSeries II, Thermo Scientific, USA), with a measurement uncertainty of 5–10%.

Hematological and Biochemical Analysis

Hematological parameters were analyzed using an automated hematology analyzer (Sysmex XT-2000i, GMI Inc., USA). Biochemical parameters were measured with a semi-automatic photometer (StarDust MC15, DiaSys Diagnostic Systems, Germany).

Statistical Analysis

All experiments were conducted in triplicate, and data are expressed as the mean ± standard deviation. Statistical comparisons between groups were made using Student's t-test, with a $p < 0.05$ considered statistically significant.

RESULTS

Characteristics of AuNPs Biofunctionalized with *Arthrospira platensis* Protein Extract (AuNPs-APE)

The FTIR spectra in Figure 1 illustrate the structural characteristics of the *Arthrospira platensis* protein extract (APE) and the changes following its interaction with gold nanoparticles (AuNPs-APE).

The APE spectrum (blue curve) shows characteristic absorption bands for protein structures. The peaks at 3138 and 3050 cm^{-1} are assigned to O–H and N–H stretching vibrations, respectively, while the band at 2853 cm^{-1} is attributed to C–H stretching in alkyl side chains. The amide I and II bands appear at ~1657 and 1618 cm^{-1}, respectively. A peak at 1403 cm^{-1} corresponds to symmetric COO^- stretching, and the band at 1284 cm^{-1} is assigned to C–N stretching vibrations from amines or amide III. Additional vibrations between 1218–1125 cm^{-1} and 1200–1000 cm^{-1} are attributed to C–O and C–N bonds in ether, alcohol, and amide groups (fig. 1).

The AuNPs–APE spectrum (black curve) retains several native features but exhibits noticeable shifts and variations in band intensity, indicating interactions between the biomolecule and the nanoparticle. A weak, broadened band observed around 3260–3270 cm^{-1} (O–H/N–H stretching) shows decreased intensity, suggesting its involvement in nanoparticle binding. The C–H stretching bands (2920–2850 cm^{-1}) remain detectable but appear less intense. The amide I (~1640–1650 cm^{-1}) and amide II (~1530–1540 cm^{-1}) bands exhibit reduced intensity, implying interactions likely mediated by peptide carbonyl and amine groups (fig. 1).

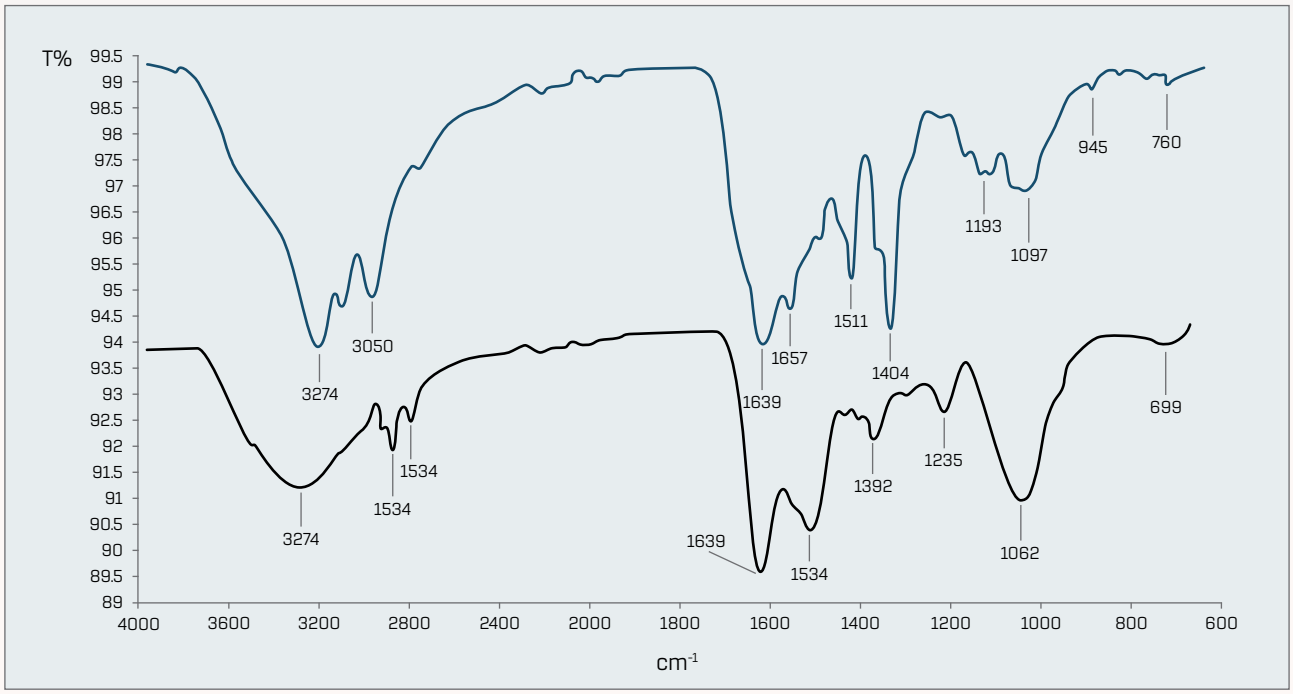

Figure 1. FTIR spectra of the *Arthrospira platensis* protein extract (APE) and the functionalized AuNPs–APE complex. Blue curve – the APE spectrum, and black curve – the AuNPs–APE spectrum.

Changes in the 1400–1200 cm^{-1} region, including band shape and position, suggest a structural reorganization of functional groups upon nanoparticle binding. In the 1100–1000 cm^{-1} region, the C–O stretching bands become less defined, likely due to reduced mobility of the involved groups. Further evidence of interaction with the metallic surface comes from the 1000–800 cm^{-1} region, where bands between 900–800 cm^{-1} are more attenuated. Finally, a weak band at 650–600 cm^{-1} may indicate coordination of the gold nanoparticles with donor atoms like nitrogen or sulfur from amino acids or peptide residues (fig. 1).

Gold Accumulation in Rat Organs

Table 1 shows the gold concentration in the kidneys of rats following 28 days of oral administration of AuNPs and the AuNPs-APE complex. Gold was detected only in the kidneys and was measured immediately after the administration and clearance period (CET). It was not detected in any other organs examined, including the brain, liver, ovaries, and testes.

Table 1. Gold accumulation in rat organs following AuNPs and AuNPs-APE administration, and a subsequent 28-day clearance period.

Experimental Groups	Kidney (ng/g)	Kidney, CET (ng/g)	Spleen (ng/g)	Spleen, CET (ng/g)
AuNPs	6.4±0.42	2.8±0.38	ND	ND
AuNPs-APE	10.4±0.66*	4.3±0.41	1.0±0.40	ND

Note: Concentrations were measured immediately after 28 days of treatment or following a 28-day clearance period (CET). *p < 0.01 indicates statistically significant differences between adjacent groups. ND – non-detected.

Quantitative analysis of kidney tissue revealed significantly different gold concentrations between non-functionalized gold nanoparticles (AuNPs) and those functionalized with *Arthrospira platensis* protein extract (AuNPs-APE). Following administration, the gold concentration in the kidneys was 6.4 ng/g in the AuNPs group, compared to 10.4 ng/g in the AuNPs-APE group – a 62.59% increase (tab. 1).

After the clearance period, gold levels in renal tissue decreased to 2.8 ng/g in the AuNPs group and 4.3 ng/g in the AuNPs-APE group. This corresponds to the elimination of 56.25% and 58.65% of the initially accumulated gold from the AuNPs and AuNPs-APE groups, respectively (tab. 1).

In the spleen, gold accumulation was detected only in the AuNPs-APE group (1.0 ng/g) and was undetectable after the clearance period (tab. 1).

Hematological and Biochemical Profiles in Experimental Animals

Table 2 presents the hematological and biochemical parameters measured in the experimental groups at two time points: following nanoparticle administration and at the end of the clearance period (CET).

Table 2. Hematological and biochemical indices in rats after 28 days of AuNPs and AuNPs-APE administration, followed by a clearance period of 28 days.

Indices	C (-)	AuNPs	AuNPs, CET	C (+)	AuNPs-APE	AuNPs-APE, CET
HB g/L	156.43±5.9	155.2±3.3	152.0±8.5	145.57±7.1	151.40±3.0	158.5±0.7
RBC, 10^{12}/L	8.77±0.30	8.56±0.39	8.14±0.08	8.15±0.38	8.21±0.46	8.53±0.15
WBC, 10^{9}/L	17.08±2.55	11.96±3.49*	9.70±1.65*	12.73±3.52	15.18±2.52*	12.85±0.05
PMN, %	28.59±6.69	22.38±2.77*	22.3±1.13*	22.37±7.51	26.42±2.38*	23.06±1.20
LY, %	57.40±6.21	67.36±5.78*	62.30±3.11	62.00±9.19	59.22±3.74	61.17±1.65
MON, %	7.56±2.33	4.98±4.59*	8.0±1.13	7.36±2.55	8.06±2.34	9.43±1.24*
EOS, %	5.43±1.61	4.78±0.96*	6.6±1.56*	6.33±1.67	5.70±1.98	5.85±0.49
BAS, %	0.53±0.33	0.56± 0.25	0.7±0.71	0.5 ±0.22	0.60 0.42	0.5±0.28
RET, %	3.35±1.08	3.45±1.15	5.08±0.16*	3.66±0.81	4.20±0.38	3.66±0.46
Prot, g/L	58.97±5.68	64.71±7.13	62.46±4.04	64.17±6.47	61.53±8.81	57.57±6.25
Glu, mmol/L	5.49± 0.77	4.64±1.10	5.65±0.47	5.87±0.86	5.42±0.75	4.91±1.05
Crea, μM/L	86.43±14.9	69.64±28.7	68.04±3.92*	100.93±7.77	71.70±10.6*	58.53±2.13*
Urea, mg/dL	29.03±5.69	25.65±5.51	33.72±0.36	25.53±5.97	24.27±1.73	23.71±1.59
ALT, U/L	162.4±39.6	131.0±27.9	188.2±13.5	184.9±50.2	218.6±23.5*	208.6±10.6
AST, U/L	3.57±2.31	5.61±2.57	5.43±0.80	2.84±1.90	2.83±1.08	7.03±0.68

Note: C (-) – Negative control; C (+) – Positive control (*Arthrospira platensis* protein extract); CET – clearance period; AuNPs – Experimental group administered with gold nanoparticles; AuNPs-APE – Experimental group administered with AuNPs functionalized with *Arthrospira platensis* protein extract; HB – hemoglobin; RBC – erythrocytes; WBC – leukocytes; PMN – polymorphomultinuclear neutrophil granulocytes; LY – lymphocytes; EOS – eosinophils; BAS – basophils; MON – monocytes; RET – reticulocyte; Prot – Total protein; Glu – Glucose; Crea – Creatinine; ALT – Alanine aminotransferase; AST – Aspartate aminotransferase; *p<0.05.

At the end of the 28-day daily administration period of non-functionalized gold nanoparticles, the treated rats exhibited a significant 30% decrease ($p < 0.05$) in total white blood cell count. Among the leukocyte subpopulations, neutrophil counts decreased by 21.72% ($p < 0.05$) and monocyte counts by 34.13% ($p < 0.05$) (tab. 2).

After the clearance period, monocytes showed signs of recovery. However, the total leukocyte count continued to decline, reaching a level 43.21% lower ($p<0.05$) than that of the negative control group, while neutrophil levels remained low and unchanged. Notably, significant increases were recorded in eosinophils (21.55%, $p<0.05$) and reticulocytes (51.64%, $p<0.05$). Most biochemical parameters did not remain within normal range and showed no significant changes (tab. 2).

In contrast, rats treated with protein extract-functionalized gold nanoparticles showed a significant increase in total leukocyte count (19.25%, $p<0.05$) and neutrophil levels (18.10%) after the 28-day administration period. A significant elevation in serum ALT levels (18.20%, $p<0.05$) was also observed (tab. 2).

Following the clearance period, most hematological parameters returned to baseline. Monocyte levels, however, continued to rise, reaching values 17% higher than those recorded during the administration period and 28.12% above those in the positive control group ($p < 0.05$). ALT levels remained elevated, and a significant increase in AST was recorded (41.90%, $p < 0.05$; tab. 2).

A decrease in serum creatinine levels was observed across all experimental groups. In the AuNPs and AuNPs (CET) groups, creatinine levels decreased by 19.43% and 21.28% ($p < 0.05$), respectively. The reductions were more pronounced in the AuNPs-APE and AuNPs-APE (CET) groups, with decreases of 28.93% and 42% ($p < 0.05$), respectively (tab. 2).

DISCUSSIONS

This study provides valuable insights into the functionalization of gold nanoparticles with protein extract components from derived the cyanobacterium *Arthrospira platensis*. FTIR spectral analysis revealed significant structural and functional changes upon the formation of the AuNPs–protein complex. Specifically, a reduction in the intensity of O–H and N–H bands, together with shifts in the carbonyl and amine regions, indicates coordinative or electrostatic interactions between the AuNPs and the protein matrix.

The emergence of characteristic signals for direct coordination bonds between the nanoparticles and donor atoms—such as nitrogen or sulfur from amino acids and peptides—further confirms the stable anchoring of biomolecules onto the gold surface. When compared to the original protein extract, the spectral changes in the fingerprint region of the AuNPs-APE complex confirm the formation of a new bio-nano system where the extract components interact directly with the AuNP surface.

The biodistribution data in rat organs are particularly noteworthy. Both non-functionalized and functionalized AuNPs were detected in the kidney, with a notable distinction: AuNPs-APE also accumulated in the spleen, albeit in very low amounts. For 10 nm citrate-stabilized AuNPs, intestinal transit and biliary excretion are the primary elimination routes, resulting in significant systemic bioavailability, particularly in the liver and spleen. In fact, 10 nm AuNPs are typically known to preferentially accumulate in the liver. As AuNPs are among the most inert nanoparticles and do not release gold ions, their absence in brain tissue is consistent with previous findings. The most prominent difference between AuNPs-APE and unmodified AuNPs is the significantly higher accumulation of the functionalized nanoparticles in renal tissue (13, 16, 17).

The stabilization medium of nanoparticles influences their aggregation behavior, absorption, and circulation properties (16). For instance, PEG-stabilized AuNPs have been detected in the brain, liver, kidneys, and testes. Likewise, functionalization with compounds derived from *Spirulina platensis* biomass has resulted in accumulation in the ovaries (13). AuNPs of 20 nm diameter, functionalized with peptides and administered intravenously to rats, showed predominant hepatic accumulation with minimal renal retention (10). However, other studies have experimentally demonstrated AuNP accumulation in the kidneys.

While 10 nm nanoparticles exceed the glomerular filtration threshold (~6–8 nm), they can still cross the fenestrated endothelium. This alternative route, independent of classical glomerular filtration, has been documented for PEGylated AuNPs ranging from 26 to 100 nm in size (9).

The exclusive detection in kidney tissue of AuNPs functionalized with *Arthrospira platensis* protein extract supports the hypothesis that the mesangium is the primary retention site for 10 nm particles. The proteins may facilitate receptor-mediated recognition, which could prolong circulation time and enhance renal retention (18).

The accumulation of citrate-stabilized 10 and 30 nm gold nanoparticles (AuNPs) in the kidneys was confirmed after intraperitoneal administration. The low urinary gold content indicates that these particles were not eliminated by glomerular filtration. Instead, they likely accumulated via extraglomerular pathways or were retained in the tubules through cellular interactions. These findings support the hypothesis that AuNPs smaller than 30 nm can be retained in renal tissue and are not efficiently excreted. Their accumulation appears to depend more on structural properties and specific tissue interactions than on classical glomerular filtration (7). This result highlights a promising research direction, particularly given the growing interest in kidney-targeted nanoparticles for drug delivery. This approach aims to deliver therapeutics directly to diseased tissue, minimize off-target effects, and improve treatment tolerability in patients requiring long-term pharmacotherapy for chronic kidney disease (4).

Correlations between the hematological and biochemical data present a coherent picture of the differential systemic impact of functionalized

versus non-functionalized nanoparticles. In the AuNP-treated groups, the decrease in total leukocytes, neutrophils, and monocytes suggests either immune suppression from oxidative stress or a subacute inflammatory response consuming these cells. This systemic reaction could also explain the moderate rise in AST without a corresponding ALT increase, pointing to extrahepatic mitochondrial damage, most likely in the kidneys, as further suggested by alterations in renal function markers.

Key Improvements and Rationale:

In contrast, the groups treated with AuNPs-APE exhibited a more stable immunological profile, with preserved or even elevated levels of monocytes and total leukocytes. This pattern suggests that the bioactive components in the protein extract may have an immunomodulatory or protective function. However, the functionalization process appeared to enhance hepatic toxicity, as indicated by high ALT levels and a further increase in AST in the post-clearance group.

This divergence between hematological stability and biochemical liver impairment suggests a potential compensatory mechanism against hepatotoxicity induced by the complexation of AuNPs with the protein matrix. It is also plausible that the hepatic toxicity might be an indirect effect of bioactive metabolites generated from the AuNPs–APE complex during enteric transit or systemic circulation.

Notably, the positive control group, which received only the *Arthrospira platensis* protein extract, exhibited hepatic and renal biochemical parameters comparable to, or even better than, those of the negative control group. No signs of enzymatic, hematological, or renal impairment were observed, indicating that the protein extract itself is non-toxic. Moreover, functionalizing the AuNPs the *Arthrospira platensis* protein extract appears to reduce their overall toxicity.

A common observation across all experimental groups was decreased serum creatinine levels. This reduction was particularly pronounced in female mice treated with PEGylated AuNPs, which showed a significant decline in creatinine without a corresponding changes in urea levels. This phenomenon may be linked to a subtle impairment of glomerular filtration or to transient metabolic alterations (8).

These findings highlight the need to further explore the biological mechanisms by which protein-extract-functionalized gold nanoparticles influence immune and biochemical parameters. Such research is essential for determining the optimal balance between the therapeutic benefits and toxicological risks of this nanotherapeutic approach.

CONCLUSIONS

1. FTIR analysis confirms the successful biofunctionalization of the AuNPs with *Arthrospira platensis* protein extract by forming direct interactions between the functional groups of the protein extract and the nanoparticle surface, indicating stabilization of the complex through coordinative or electrostatic bonds.
2. Unlike non-functionalized nanoparticles, AuNPs-APE accumulated in the kidneys at a three-fold higher level, thus, supporting the hypothesis that 10 nm particles penetrate renal tissue through extraglomerular mechanisms. This characteristic, combined with a noticeable reduction in systemic toxicity, highlights the potential of these bio-nano complexes in therapeutic for targeted renal therapy.
3. Combined hematological and biochemical data indicate that the APE has a beneficial immunomodulatory effect, attenuating the oxidative stress and systemic inflammation triggered by the nanoparticles. When administered alone, the *Arthrospira platensis* protein extract was non-toxic and showed a potentially protective effect. Functionalization with APE thus improves the stability and biocompatibility of the AuNPs, alters their tissue distribution, and reduces their overall toxicity.
4. The AuNP–APE complex emerges as a highly promising candidate for developing new targeted renal nanotherapeutics. Further research is needed on elucidating the underlying molecular mechanisms and establishing an optimal therapeutic window to ensure both efficacy and safety.

CONFLICT OF INTEREST The authors of the article deny the existence of any conflict of interest in the publication of this material.

FUNDING ACKNOWLEDGEMENT This research was supported by the Government of the Republic of Moldova – National Agency for Research and Development, project 20.80009.5007.05 “Biofunctionalized metal nanoparticles – obtaining using cyanobacteria and microalgae”.

ETHICAL APPROVAL This study is part of a larger research study entitled ”Biological effects of Au and Ag nanoparticles on physiological, hematological, biochemical indices and behavioral biology of laboratory animals”, which was approved by the Ethics Committee of the Institute of Physiology and Sanocreatology, decision no. 26 dated 06/02/2023.

REFERENCES

1. Eker F, Akdaşçi E, Duman H, Bechelany M, Karav S. Gold Nanoparticles in Nanomedicine: Unique Properties and Therapeutic Potential. *Nanomaterials*. 2024;14(22):1854. https://doi.org/10.3390/nano14221854.
2. Haume K, Rosa S, Grellet S, Śmiałek MA, Butterworth KT, Solov'yov AV, Prise KM, Golding J, Mason NJ. Gold nanoparticles for cancer radiotherapy: a review. *Cancer Nanotechnol.* 2016;7(1):8. https://doi.org/10.1186/s12645-016-0021-x.
3. Bansal SA, Kumar V, Karimi J, Singh AP, Kumar, S. Role of Gold Nanoparticles in Advanced Biomedical Applications. *Nanoscale Adv.* 2020;2:3764–3787. https://doi.org/10.1039/D0NA00472c.
4. Gerosa C, Crisponi G, Nurchi VM, Saba L, Cappai R, Cau F, Faa G, Van Eyken P, Scartozzi M, Floris G, Fanni D. Gold Nanoparticles: A New Golden Era in Oncology? *Pharmaceuticals.* 2020;13(8):192. https://doi.org/10.3390/ph13080192.
5. Niżnik Ł, Noga M, Kobylarz D, Frydrych A, Krośniak A, Kapka-Skrzypczak L, Jurowski K. Gold Nanoparticles (AuNPs)—Toxicity, Safety and Green Synthesis: A Critical Review. *Int J Mol Sci*. 2024;25(7):4057. https://doi.org/10.3390/ijms25074057.
6. Yadav P, Bandyopadhyay A, Sarkar K. Enhancement of gold-curcumin nanoparticle mediated radiation response for improved therapy in cervical cancer: a computational approach and predictive pathway analysis. *Discover Nano.* 2024;19(1):153. https://doi.org/10.1186/s11671-024-04104-7.
7. Lopez-Chaves C, Soto-Alvaredo J, Montes-Bayon M, Bettmer J, Llopis J, Sanchez-Gonzalez C. Gold nanoparticles: Distribution, bioaccumulation and toxicity. In vitro and in vivo studies. *Nanomedicine.* 2018;14(1):1-12. https://doi.org/10.1016/j.nano.2017.08.011.
8. Chen J, Wang H, Long W, Shen X, Wu D, Song SS, Sun YM, Liu PX, Fan S, Fan F, Zhang XD. Sex differences in the toxicity of polyethylene glycol-coated gold nanoparticles in mice. *Int J Nanomedicine.* 2013;8:2409-2419. https://doi.org/10.2147/IJN.S46376.
9. Choi HS, Liu W, Misra P, Tanaka E, Zimmer JP, Itty Ipe B, Bawendi MG, Frangioni JV. Renal clearance of quantum dots. *Nat Biotechnol.* 2007;25(10):1165-70. https://doi.org/10.1038/nbt1340.
10. Morais T, Soares ME, Duarte JA, Soares L, Maia S, Gomes P, Pereira E, Fraga S, Carmo H, Bastos Mde L. Effect of surface coating on the biodistribution profile of gold nanoparticles in the rat. *Eur J Pharm Biopharm.* 2012;80(1):185-193. https://doi.org/10.1016/j.ejpb.2011.09.005.
11. Hanisha R, Balaganapathy M, Eswar B, Kathirvelan P, Rajabathar JR, Dinakarkumar Y. Biogenic synthesis of silver nanoparticles using *Spirulina maxima* extract and their bactericidal activity. J *Umm Al-Qura Univ Appl Sci.* 2024. https://doi.org/10.1007/s43994-024-00203-4.
12. Rudi L, Zinicovscaia I, Cepoi L, Chiriac T, Grozdov D, Kravtsova A. The Impact of Silver Nanoparticles Functionalized with *Spirulina* Protein Extract on Rats. *Pharmaceuticals*. 2024; 17(9):1247. https://doi.org/10.3390/ph17091247.
13. Cepoi L, Rudi L, Chiriac T, Zinicovscaia I, Grozdov D, Rudic V. Effect of Gold Nanoparticles Functionalized by *Arthrospira Platensis* on Rats. In: Sontea, V., Tiginyanu, I., Railean, S. eds. *6th International Conference on Nanotechnologies and Biomedical Engineering. ICNBME 2023.* Vol 91. Springer; 2023. https://doi.org/10.1007/978-3-031-42775-6_40.
14. Lowry OH, Rosebrough NJ, Farr AL, Randall RJ. Protein measurement with the Folin phenol reagent. J Biol Chem. 1951;193:265-275.
15. Huang H, Lang Y, Zhou M. A comprehensive review on medical applications of microalgae. *Algal Res.* 2024;80:103504. https://doi.org/10.1016/j.algal.2024.103504.
16. Kozics K, Sramkova M, Kopecka K, Begerova P, Manova A, Krivosikova Z, Sevcikova Z, Liskova A, Rollerova E, Dubaj T, et al. Pharmacokinetics, Biodistribution, and Biosafety of PEGylated Gold Nanoparticles In Vivo. *Nanomaterials.* 2021;11(7):1702. https://doi.org/10.3390/nano11071702.
17. Abdelhalim MAK, Moussa SAA. The gold nanoparticle size and exposure duration effect on the liver and kidney function of rats: In vivo. *Saudi J Biol Sci.* 2013;20(2):177-181. https://doi.org/10.1016/j.sjbs.2013.01.007.
18. Huang Y, Wang J, Jiang K, Chung EJ. Improving kidney targeting: The influence of nanoparticle physicochemical properties on kidney interactions. J Control Release. 2021;334:127-137. https://doi.org/10.1016/j.jconrel.2021.04.016.

Date of receipt of the manuscript: 23.04.2025

Date of acceptance for publication: 18.12.2025

Ludmila RUDI, WoS Researcher ID: AAY-3219-2020, SCOPUS ID 55681134100;

Tatiana CHIRIAC, WoS Researcher ID: AIB-8864-2022, SCOPUS ID 38861074900;

Inga ZINICOVSCAIA, WoS Researcher ID: H-1656-2016, SCOPUS ID 36492597400

Liliana CEPOI, WoS Researcher ID: J-9640-2019, SCOPUS ID 55246094000;

Dmitrii Grozdov, SCOPUS ID 25723199300.

MEDICAL SCIENCES

OPEN ACCESS

EVALUATION OF *THYMUS VULGARIS* AQUEOUS EXTRACT AS A NATURAL ANTIMICROBIAL AGENT AGAINST URINARY TRACT INFECTION PATHOGENS

Hashim ABED ABASS[1], Muthanna Abdlkhader Salh AL-MAHDAWI[2], Mohammed Sabea CHALLOOB[1], Hayder H. ABED[3]*

[1] Department of Pathology, College of Medicine, University of Diyala, Diyala, Iraq
[2] Department of Biotechnology, College of Sciences, University of Diyala, Iraq
[3] Department of Chemistry and Biochemistry, Faculty of Medicine, Al Muthanna University, Samawah, Iraq

Corresponding author: Hayder H. Abed, e-mail: Hayderhussein862@mu.edu.iq

https://doi.org/10.38045/ohrm.2026.1.02 CZU: [615.322:582.949.27]:616.6-022.7

ABSTRACT

Introduction Urinary tract infections (UTIs) are often caused by bacteria such as *Staphylococcus aureus* (*S. aureus*) and *Escherichia coli* (*E. coli*) which can lead to major health problems. The purpose of this study was to to examine the antibacterial effects of extract of *Thymus vulgaris* aqueous against these uropathogens.

Material and methods The aqueous extract of *Thymus vulgaris* was prepared via hot water decoction (yield: 3.6 g from 30 g dried plant material 12%). Bacterial strains were isolated from 25 clinical urine samples and identified using selective culture media using the Gram staining and biochemical characterization. Antibacterial activity was assessed by using the agar well diffusion method with extract concentrations (50, 100 and 200 mg/mL) of *Thymus vulgaris* extract.

Results The results of this study showed dose dependent of inhibition zone with *S. aureus* showing greater susceptibility (ZOI: 10–27 mm) compared to *E. coli* (ZOI: 9–23 mm). Ciprofloxacin shown larger inhibition zone (28–30 mm).

Conclusions These findings demonstrate promising antibacterial potential of *T. vulgaris* aqueous extract as a natural alternative to combat antibiotic-resistant UTIs. These results support previous investigation about *T. vulgaris* as an alternative or complementary treatment for bacterial infections.

Keywords Ciprofloxacin, *E. coli*, *S. aureus*, *Thymus vulgaris*, urinary tract infections

EVALUAREA EXTRACTULUI APOS DE *THYMUS VULGARIS* CA AGENT ANTIMICROBIAN NATURAL ÎMPOTRIVA AGENȚILOR PATOGENI ALE INFECȚIILOR TRACTULUI URINAR

Introducere Infecțiile tractului urinar (ITU) sunt adesea cauzate de bacterii, precum *Staphylococcus aureus* (*S. aureus*) și *Escherichia coli* (*E. coli*), care pot cauza probleme majore de sănătate. Scopul acestui studiu a fost de a examina efectele antibacteriene ale unui extract apos de *Thymus vulgaris* împotriva acestor agenți patogeni.

Material și metode Extractul apos de *Thymus vulgaris* a fost preparat prin decoct în apă fierbinte, obținându-se 3,6 g din 30 g de material vegetal uscat (12%). Tulpinile bacteriene au fost izolate din 25 de probe de urină și identificate prin medii de cultură selective, folosind colorația Gram și caracterizarea biochimică. Activitatea antibacteriană a fost evaluată utilizând metoda de difuzie în agar cu godeuri la concentrații variabile (50, 100 și 200 mg/ml) de extract de *Thymus vulgaris*.

Rezultate Rezultatele acestui studiu au arătat o dependență de doză în funcție de zona de inhibiție, *S. aureus* prezentând o sensibilitate mai mare (ZI: 10–27 mm) comparativ cu *E. coli* (ZI: 9–23 mm). Ciprofloxacina a prezentat o zonă de inhibiție mai mare (28–30 mm).

Concluzii Extractul apos de *Thymus vulgaris* a demonstrat efecte antibacteriene distincte, evidențiind potențialul său ca alternativă naturală sau terapie complementară pentru combaterea infecțiilor urinare, susținând în același timp eforturile de a reduce rezistența la antibiotice. Aceste rezultate susțin investigațiile anterioare despre *Thymus vulgaris* ca tratament alternativ sau complementar contra infecțiilor bacteriene.

Cuvinte-cheie Ciprofloxacină, *E. coli*, *S. aureus*, *Thymus vulgaris*, infecții ale tractului urinar.

INTRODUCTION

Thymus vulgaris (commonly known as thyme) is a widely used medicinal herb with a long history in both traditional and modern therapeutics (1). Its pharmacological properties are largely attributed to bioactive constituents such as thymol and carvacrol, which exhibit strong antibacterial, antifungal, antiviral, and antioxidant activities (2, 3). Due to these properties, *T. vulgaris* has been traditionally applied in the treatment of respiratory infections, skin disorders, and urinary tract infections (UTIs), demonstrating effectiveness against pathogens including *Pseudomonas aeruginosa*, *Escherichia coli*, *Staphylococcus aureus*, and *Klebsiella pneumoniae* (4).

Previous studies have shown that *T. vulgaris* is active against both Gram-positive and Gram-negative bacteria, including antibiotic-resistant strains such as methicillin-resistant *S. aureus* (MRSA) (5). Its broad-spectrum antimicrobial potential has led to increasing interest in its application in medicine, food preservation, and personal care products, particularly as a natural alternative to synthetic antimicrobials (6).

In addition to its antimicrobial effects, *T. vulgaris* is valued for its expectorant, antispasmodic, anti-inflammatory, and antioxidant properties, which contribute to its use in managing respiratory ailments, inflammatory conditions, and oxidative stress-related disorders (7–9). As antimicrobial resistance (AMR) continues to pose a global public health challenge, there is a growing need to identify safe and effective plant-based alternatives that align with the One Health framework and help reduce reliance on conventional antibiotics.

Given this context, aqueous extracts of *T. vulgaris* may offer a promising natural therapeutic option for managing UTIs**.** We hypothesize that the aqueous extract of *T. vulgaris* exerts antibacterial effects against UTI-causing pathogens in a concentration-dependent manner. Therefore, this study aims to evaluate the antibacterial activity of aqueous *T. vulgaris* extract against *S. aureus* and *E. coli* isolated from human urinary tract infections. The agar well-diffusion method was employed to assess antimicrobial efficacy and compare the extract's activity with that of ciprofloxacin, a commonly used antibiotic.

MATERIALS AND METHODS

This study was conducted at Baquba Teaching Hospital in Baquba, Iraq, from May 2024 to January 2025. *Thymus vulgaris* was procured from a local market in Samawah. The plant material was washed three times with distilled water to remove surface contaminants and air-dried at room temperature. After drying, the plant material was ground into a fine powder using an electric blender and stored in a sealed container until extraction.

The aqueous extract of *T. vulgaris* was prepared using the decoction method. Briefly, 30 g of dried plant powder were mixed with 200 mL of distilled water in a beaker and heated until boiling. The mixture was then filtered through Whatman No. 1 filter paper to remove solid residues. The clear filtrate was collected in a sterile glass container and refrigerated at 4 °C for no longer than seven days prior to antimicrobial testing (10).

Urine samples were obtained from 25 patients clinically diagnosed with urinary tract infections (UTIs). Samples were collected in sterile containers and streaked onto MacConkey agar and eosin methylene blue (EMB) agar for *E. coli* isolation, and mannitol salt agar for *S. aureus* isolation. Blood agar was also used to support general bacterial recovery. Plates were incubated aerobically at 37 °C for 24 hours. Suspected colonies were selected based on

morphological characteristics and subjected to biochemical identification (11). Confirmed isolates were maintained on nutrient agar slants at 4 °C for subsequent analysis.

Antibacterial activity was evaluated using the agar well diffusion method. Mueller–Hinton agar plates were prepared and allowed to solidify. A standardized bacterial inoculum (100 µL) was evenly spread on each plate using a sterile cotton swab (12, 13). Wells of 6 mm diameter were created using a sterile cork borer. A volume of 100 µL of *T. vulgaris* extract at concentrations of 50 mg/mL (low), 100 mg/mL (medium), and 200 mg/mL (high) was dispensed into the wells. Sterile distilled water served as the negative control, while ciprofloxacin was used as the positive control. Plates were incubated at 37 °C for 24 hours, after which inhibition zones (mm) were measured. Larger inhibition zones indicated stronger antibacterial activity (14). The performance of the extract was compared with ciprofloxacin to assess relative efficacy.

All experiments were performed in triplicate, and results were expressed as mean ± standard deviation (SD). One-way ANOVA followed by Tukey's post hoc test was used to determine statistical significance using GraphPad Prism software (Version 8). Differences were considered statistically significant at $p \leq 0.05$ (15, 16).

RESULTS

The hot-water extraction of *Thymus vulgaris* yielded 3.6 g of extract from 30 g of dried plant material, corresponding to a 12% (w/w) yield. This value falls within the commonly reported range of 10–30% for aqueous herbal extractions, which varies depending on factors such as temperature, extraction duration, and plant composition.

A total of 25 urine samples from patients with urinary tract infections (UTIs) were cultured on selective and differential media to isolate *Escherichia coli* and *Staphylococcus aureus*. After 24 hours of incubation at 37 °C, bacterial growth was observed on MacConkey agar, eosin methylene blue (EMB) agar, mannitol salt agar (MSA), and blood agar. On EMB agar, *E. coli* produced characteristic green metallic sheen colonies due to vigorous lactose fermentation (fig. 1A). On MSA, *S. aureus* formed yellow colonies indicative of mannitol fermentation (fig. 1B). Blood agar cultures showed β-hemolytic colonies for *S. aureus*, whereas *E. coli* colonies were non-hemolytic or occasionally α-hemolytic (fig. 1C). Microscopic and biochemical analyses were performed to confirm species identity. Gram staining revealed *E. coli* as Gram-negative, rod-shaped bacteria occurring singly or in pairs, while *S. aureus* appeared as Gram-positive cocci arranged in clusters (17).

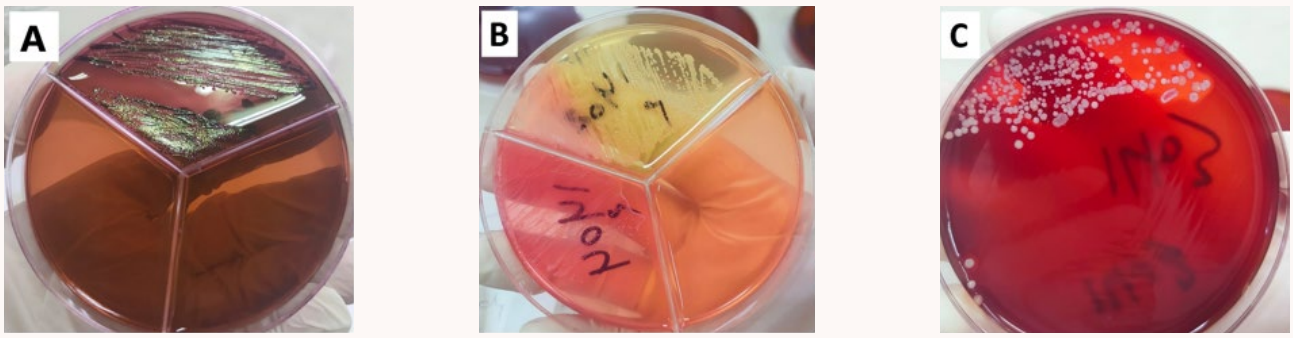

Figure 1. Identification of *Escherichia coli* and Staphylococcus aureus:
(A) *E. coli* identified on EMB agar, (B) *S. aureus* mannitol salt agar,
(C) *E. coli* and *S. aureus* colonies on blood agar.

The antibacterial activity of *Thymus vulgaris* extract was assessed against *Escherichia coli* and *Staphylococcus aureus* using the well diffusion method as illustrated in Figure 2.

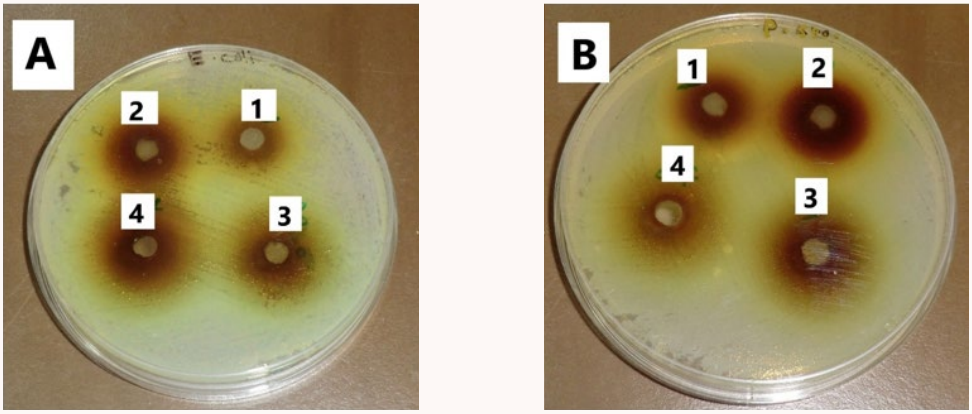

Figure 2. Comparison of inhibition zones of *Thymus vulgaris* extract:
(A) E. coli, (B) S. aureus. (1) Low concentration (50 mg/mL), (2) Medium concentration (100 mg/mL), (3) High concentration (200 mg/mL), (4) Ciprofloxacin (5 µg/disc).

The results, expressed as mean ± standard deviation (SD) of the inhibition zone diameter (ZOI) in millimeters, are summarized in Table 1. The results showed the zone of inhibition (ZOI) widths varied but the extract had inhibitory effects on both bacterial species. The antibacterial activity was assessed by measuring the diameter in mm of inhibition zones formed around the wells containing the extract. The results are summarized in Table 1 and Figure 3.

Table 1. Zone of inhibition (ZOI) for *Thymus vulgaris* extract (mm) against *E. coli* and *S. aureus*, p value ≤ 0.05.

Thymus vulgaris Extract (mg/mL)	N	*E. coli* mean ± SD of ZOI in mm	P value	*S. aureus* mean ± SD of ZOI in mm	*p value*
50 mg/mL (Low Concentration)	9	8.844 ± 1.51 ^{c***}	< 0.0001	10.37 ± 1.86 ^{c***}	< 0.0001
100 mg/mL (Medium Concentration)	9	13.94 ± 4.65 ^{c***}	< 0.0001	15.08 ± 4.61 ^{c***}	< 0.0001
200 mg/mL (High Concentration)	9	22.81 ± 3.80 ^{b**}	= 0.0015	26.98 ± 4.67 ^{a*}	= 0.0500
Ciprofloxacin (5 µg/disc)	9	28.32 ± 2.09	-	30.44 ± 5.53	-

*ZOI: Zone of inhibition

(a) Low Significant *, (b) Significant **, (c) High Significant *

For *E. coli*, the inhibition zones increased in a concentration-dependent manner. The lowest extract concentration (50 mg/mL) produced a zone of inhibition (ZOI) of 8.84 ± 1.51 mm ($p < 0.0001$), while the medium concentration (100 mg/mL) yielded a significantly larger ZOI of 13.94 ± 4.65 mm ($p < 0.0001$). The highest concentration (200 mg/mL) resulted in a ZOI of 22.81 ± 3.80 mm ($p = 0.0015$). However, all extract concentrations produced smaller inhibition zones than the positive control, ciprofloxacin (28.32 ± 2.09 mm).

A similar trend was observed for *S. aureus*. The low concentration (50 mg/mL) produced a ZOI of 10.37 ± 1.86 mm ($p < 0.0001$), while the medium concentra-

tion (100 mg/mL) generated a ZOI of 15.08 ± 4.61 mm ($p < 0.0001$). The highest concentration (200 mg/mL) exhibited the strongest antibacterial effect, with a ZOI of 26.98 ± 4.67 mm ($p < 0.05$), closely approaching the activity of ciprofloxacin (30.44 ± 5.53 mm).

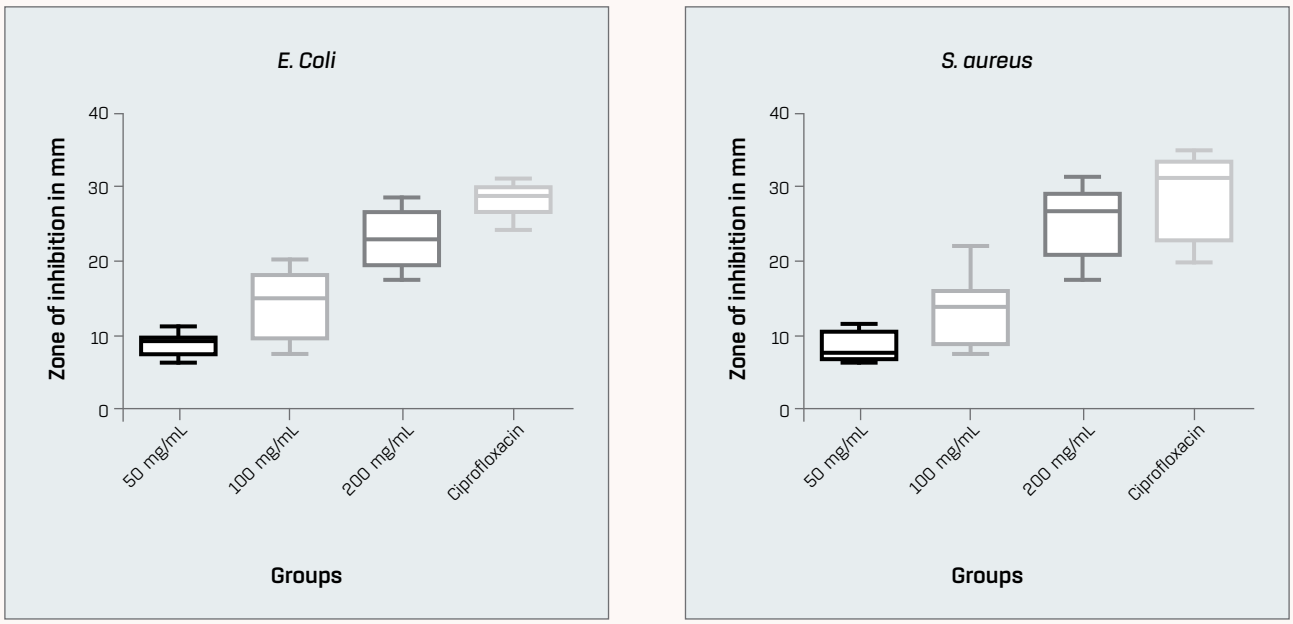

Figure 3. Statistical analysis of inhibition zones of *Thymus vulgaris* extract against *E. coli* and *S. aureus*, p value ≤ 0.05.

DISCUSSION

Thyme contains numerous bioactive compounds with demonstrated biological activity against a wide range of infectious agents. The findings of this study indicate that hot-water extraction was effective in isolating hydrophilic phytochemicals such as polyphenols, flavonoids, and tannins, all of which are known for their antimicrobial properties (18). However, because water has limited ability to dissolve hydrophobic compounds, aqueous extraction generally yields a lower quantity of extract compared to organic solvents such as ethanol or methanol (19). Despite this, the extract obtained in the present study provided a sufficient concentration of bioactive constituents to exert measurable antibacterial activity against *Escherichia coli* and *Staphylococcus aureus*.

The virulence of *E. coli* in UTIs is primarily attributed to its fimbriae-mediated adhesion, biofilm formation, and multiple antibiotic resistance mechanisms, all of which contribute to its high prevalence in clinical urine samples (20). In contrast, *S. aureus*–associated UTIs are often linked to immunocompromised conditions, catheter use, or hospital-acquired infections (HAIs).

As shown in Figure 2, inhibition-zone diameters increased proportionally with extract concentration, confirming a clear dose-dependent antibacterial effect. Moreover, *S. aureus* exhibited larger inhibition zones than *E. coli*, suggesting that Gram-positive bacteria are more susceptible to *Thymus vulgaris* extract than Gram-negative bacteria (21). This difference is likely related to structural distinctions in bacterial cell envelopes; the outer membrane of Gram-negative bacteria, such as *E. coli*, acts as a barrier that restricts the penetration of many antimicrobial compounds (22).

The antimicrobial activity of *T. vulgaris* can be attributed to its rich phytochemical profile, particularly thymol and carvacrol, which possess strong antibacterial properties. These compounds disrupt bacterial cell membranes, alter membrane permeability, and interfere with essential metabolic processes, ultimately leading to leakage of intracellular components and cell death (23).

Although the inhibition zones produced by the extract were smaller than those produced by ciprofloxacin, the results still demonstrate that *T. vulgaris* has meaningful antibacterial activity and may serve as a promising natural antimicrobial agent. Its bioactive constituents – including thymol, carvacrol, flavonoids, and phenolic acids – are known to damage bacterial membranes, inhibit enzymatic activity, and disrupt overall metabolic function (24).

A limitation of this study is the relatively small sample size (25 bacterial isolates), which may reduce the statistical power and generalizability of the findings. Larger studies with expanded sample sets are recommended to further validate and strengthen these observations.

CONCLUSIONS

1. *Thymus vulgaris* extract exhibits significant antibacterial activity against *E. coli* and *S. aureus* in a concentration-dependent manner.
2. The strong antimicrobial effects of the extract are primarily attributed to its diverse phytochemical composition, including thymol, carvacrol, and flavonoids, which disrupt bacterial cell membranes and interfere with essential cellular functions.
3. Although the extract produced inhibition zones smaller than those of ciprofloxacin, it demonstrated particularly potent activity against *S. aureus*, highlighting its potential as a natural antimicrobial agent and its promise for the management of urinary tract infections.

CONFLICT OF INTEREST

Author declare there is no conflict of interest

ACKNOWLEDGMENTS

The authors express their thank to “General Al Muthanna Teaching Hospital” and “Baquba Teaching Hospital” in Iraq for providing the necessary facilities and support to complete this study.

FUNDING

There are no organization support for this work.

ETHICAL APPROVAL

All experimental procedures involving animals were reviewed and approved by “the Ethics Committee of the College of Science, University of Diyala” (Approval No.: 2024 AEBT 144, Date: 8/2/2024). All procedures were done in accordance with the principles of research integrity, biosafety, and environmental protection.

REFERENCES

1. Cianfaglione K, Bartolucci F, Ciaschetti G, Conti F, Pirone G. Characterization of *Thymus vulgaris* subsp. *vulgaris* community by using a multidisciplinary approach: A case study from Central Italy. *Sustainability*. 2022;14(7):3981. https://doi.org/**10.3390/su14073981**.
2. Kowalczyk A, Przychodna M, Sopata S, Bodalska A, Fecka I. Thymol and thyme essential oil—new insights into selected therapeutic applications. *Molecules*. 2020;25(18):4125. https://doi.org/**10.3390/molecules25184125**.
3. Kachur K, Suntres Z. The antibacterial properties of phenolic isomers, carvacrol and thymol. *Crit Rev Food Sci Nutr*. 2020;60(18):3042-3053. https://doi.org/**10.1080/10408398.2019.1675585**.
4. Khameneh B, Eskin NAM, Iranshahy M, Fazly Bazzaz BS. Phytochemicals: A promising weapon in the arsenal against antibiotic-resistant bacteria. Antibiotics. 2021;10(9):1044. https://doi.org/**10.3390/antibiotics10091044.**
5. Vallejo MG, Bontti S, Perez Girabel RB, Patiño MS, Quintero CA. Natural extracts as a promising solution for gram-positive antibiotic resistance: A comprehensive review. 2023 ; 31(35): 26-44. https://doi.org/**10.48141/SJS.v31.n35.2023.04_QUINTERO_pgs_26_44.pdf**.
6. Yetgin A. Investigating medicinal plants for antimicrobial benefits in a changing climate. *Int J Second Metab*. 2024;11(2):364-377. https://doi.org/**10.21448/ijsm.1279531**.
7. Morya S, Pillai GS, Dinesh A, Alotaibi AS, Alatawi HA, Menaa F. Herbal Wine and Health Benefits. *Herb Nutraceuticals Prod Process*. Published online 2024:135-153. https://doi.org/**10.1002/9781394241576.ch7**
8. Gabbai-Armelin PR, Sales LS, Ferrisse TM, et al. A systematic review and meta-analysis of the effect of thymol as an anti-inflammatory and wound healing agent: A review of thymol effect on inflammation and wound healing. *Phyther Res*. 2022;36(9):3415-3443. https://doi.org/**10.1002/ptr.7541**.
9. Jovanović AA, Balanč B, Petrović P, Pravilović R, Djordjević V. Pharmacological potential of Thymus serpyllum L.(wild thyme) extracts and essential oil: A review. *J Eng Process Manag*. 2021;13(2):32-41. https://doi.org/**10.7251/JEPM2102032J**.
10. Abdullah HT, Al-Bayati AM, Saleh ANA, AlSalihi KA, Abed HH. Effect of Ocimum basilicum herbs extract on pro-inflammatory cytokines in ethanol-induced liver damage in rats. Wiad Lek. 2025;78(8):1522–9. https://doi.org/**10.36740/WLek/208443.**
11. Mbim EN, Mboto CI, Edet UO. Prevalence and antimicrobial susceptibility profile of bacteria isolated from the environment of two tertiary hospitals in Calabar Metropolis, Nigeria. *J Adv Med Pharm Sci*. 2016;10(4):1-15. https://doi.org/**10.9734/JAMPS/2016/29316**.
12. Majumder MMI, Mahadi AR, Ahmed T, Ahmed M, Uddin MN, Alam MZ. Antibiotic resistance pattern of microorganisms causing urinary tract infection: a 10-year comparative analysis in a tertiary care hospital of Bangladesh. Antimicrob Resist Infect Control. 2022;11(1):156. https://doi.org/**10.1186/s13756-022-01197-6.**
13. Riddell SW, Sanyal S. Essentials of diagnostic microbiology. *Introd to Clin Infect Dis A Probl Approach*. Published online 2019:439-460. https://doi.org/**10.1007/978-3-319-91080-2_42**
14. López-Malo A, Mani-López E, Davidson PM, Palou E. Methods for activity assay and evaluation of results. In: *Antimicrobials in Food*. CRC Press; 2020:13-40. https://doi.org/**10.1201/9780429058196-2**.
15. Ali AM, Hussein NA, Jawad D, Abed HH, Mekkey SM. Hepatotoxic effects of Stevia rebaudiana leaf extract and commercial stevia on rats: a comparative study. *Rev Clin Pharmacol Pharmacokinet*. 2024;38(2):69-72. https://doi.org/**10.61873/XFAQ5379**.
16. Abed HH, Ali AM, Mahdi ZS. Effect of Vitamin D3 Supplement on the Semen Quality in Human Patients with Vitamin D Deficiency. *HAYATI J Biosci*. 2022;29(5):562-569. https://doi.org/**10.4308/hjb.29.5.562-569**.
17. Iram D, Sansi MS, Puniya AK, Gandhi K, Meena S, Vij S. Phenotypic and molecular characterization of clinically isolated antibiotics-resistant *S. aureus* (MRSA), *E. coli* (ESBL) and *Acinetobacter* 1379 bacterial strains. *Brazilian J Microbiol*. 2024;55(3):2293-2312. https://doi.org/**10.1007/s42770-024-01347-5**.
18. Kelly NP, Kelly AL, O'Mahony JA. Strategies for enrichment and purification of polyphenols from fruit-based materials. *Trends Food Sci Technol*. 2019;83:248-258. https://doi.org/**10.1016/j.tifs.2018.11.010**.
19. Lajoie L, Fabiano-Tixier AS, Chemat F. Water as green solvent: methods of solubilisation and extraction of natural products – past, present and future solutions. *Pharmaceuticals*. 2022;15(12):1507. https://doi.org/**10.3390/ph15121507**.
20. Gajdács M, Kárpáti K, Nagy ÁL, Gugolya M, Stájer A, Burián K. Association between biofilm-production and antibiotic resistance in *Escherichia coli* isolates: A laboratory-based case study and a literature review. *Acta Microbiol Immunol Hung*. 2021;68(4):217-226. https://doi.org/**10.1556/030.2021.01487**.
21. Jung IG, Jeong JY, Yum SH, Hwang YJ. Inhibitory effects of selected medicinal plants on bacterial growth of methicillin-resistant *Staphylococcus aureus*. *Molecules*. 2022;27(22):7780. https://doi.org/**10.3390/molecules27227780**.
22. Tavares TD, Antunes JC, Padrão J, et al. Activity of specialized biomolecules against gram-positive and gram-negative bacteria. *Antibiotics*. 2020;9(6):314. https://doi.org/**10.3390/antibiotics9060314**.
23. Patil SM, Ramu R, Shirahatti PS, Shivamallu C, Amachawadi RG. A systematic review on ethnopharmacology, phytochemistry and pharmacological aspects of *Thymus vulgaris* Linn. *Heliyon*. 2021;7(5). https://doi.org/**10.1016/j.heliyon.2021.e07054**.
24. Wirtu SF, Ramaswamy K, Maitra R, Chopra S, Mishra AK, Jule LT. Isolation, characterization and antimicrobial activity study of *Thymus vulgaris*. *Sci Rep*. 2024;14(1):21573. https://doi.org/**10.1038/s41598-024-71012-2.**

Date of receipt of the manuscript: 04.05.2025

Date of acceptance for publication: 18.12.2025

Hayder H. Abed, WoS Researcher ID: AFK-2197-2022, SCOPUS ID 57211337747.

BIOLOGICAL SCIENCES

OPEN ACCESS

BIOLOGICAL PROPERTIES OF *SERRATIA LIQUEFACIENS* 1/2024, ISOLATED FROM CHICKEN

Liliia VYGOVSKA[1], Artem USHKALOV[1], Liubov ZELENA[2], Valerii USHKALOV[1], Cristina SIRBU[4], Yurii VISHOVAN[3]

[1] Department of Veterinary Epidemiology and Animal Health, Faculty of Veterinary Medicine, National University of Life and Environmental Sciences of Ukraine, Kyiv, Ukraine
[2] Department of Virus Reproduction, Zabolotny Institute of Microbiology and Virology, National Academy of Sciences of Ukraine, Kyiv, Ukraine
[3] Department of Microbiological research Ukrainian Laboratory of Quality and Safety of Agricultural Products of National University of Life and Environmental Sciences of Ukraine, Kyiv, Ukraine
[4] National Food Safety Agency of the Republic of Moldova

Corresponding author: Valerii Ushkalov, e-mail: ushkalov63@gmail.com

https://doi.org/10.38045/ohrm.2026.1.03 CZU: 579.842.21:636.52/.52+615.281.9.015.8

ABSTRACT

Introduction According to a study by the European Centre for Disease Prevention and Control (ECDC) for 2022-2023, *Serratia* spp. caused 54,406 cases of disease in 28 countries worldwide. *Serratia liquefaciens* is considered the second most frequently isolated organism from human clinical samples after *Serratia marcescens*. The aim of this study was to investigate the biological properties of *S. liquefaciens* isolated from chickens.

Material and methods The study investigated a *Serratia liquefaciens* strain isolated in 2024 from chickens kept in a vivarium with clinical manifestations of gastrointestinal tract disorders. The aim of the study was to examine the strain *S. liquefaciens*. When studying the biological properties of the isolate, morphological characteristics, growth typicality, biochemical properties, pathogenicity for laboratory animals, and antibiotic sensitivity were taken into account.

Results The isolated microorganism formed colonies typical of the *Serratin* genus, and the cells were motile at 37°C. The enzymatic profile matched the known characteristics of *S. liquefaciens*. The strain produced a denser biofilm at 23°C, exhibited pathogenicity in white mice, and showed resistance to several classes of antimicrobial agents. Based on the sequencing of a 16S rRNA gene fragment, the strain was deposited in the NCBI GenBank database under accession number PQ308601.1.

Conclusions The results obtained suggest that the *S. liquefaciens* 1/2024 may be used as a reference strain for the differential diagnosis of enterobacteria, assessment of antimicrobial activity, and application as a laboratory control strain in experimental studies.

Keywords Antibiotic resistance, biofilm, pathogenicity, sequencing, *Serratia* spp.

PROPRIETĂȚILE BIOLOGICE ALE *SERRATIA LIQUEFACIENS* 1/2024, IZOLATĂ DE LA PUI

Introducere Conform unui studiu ECDC pentru perioada 2022-2023, *Serratia* spp. a cauzat 54.406 cazuri de boală în 28 de țări din întreaga lume. *Serratia liquefaciens* este considerată al doilea cel mai frecvent izolat organism din probele clinice umane, după *Serratia marcescens*. Scopul studiului a fost de a investiga proprietățile biologice ale *S. liquefaciens* izolate de la pui.

Material și metode Obiectul cercetării au fost tulpinile de *S. liquefaciens*, izolate în 2024 de la puii crescuți într-un vivariu cu manifestări clinice de afecțiuni ale tractului gastrointestinal. La studierea proprietăților biologice ale izolatului, s-au luat în considerare proprietățile morfologice, culturale, biochimice, patogenitatea pentru animalele de laborator și sensibilitatea la antibiotice.

Rezultate Microorganismul izolat a format colonii tipice genului *Serratia*, iar bacteriile au fost mobile la 37°C. Activitatea enzimatică a izolatului a corespuns caracteristicilor *S. liquefaciens*. Bacteriile au fost capabile să formeze un biofilm mai dens la 23°C, au fost patogene pentru șoarecii albi și au prezentat semne de rezistență multiplă la agenții antimicrobieni. Pe baza rezultatelor secvențierii unui fragment al genei ARNr 16S, datele despre tulpină au fost introduse în GenBank NCBI sub numărul PQ308601.1.

Concluzii Rezultatele obținute oferă motive pentru utilizarea tulpinii *S. liquefaciens* 1/2024 în calitate de standard pentru diagnosticul diferențial al enterobacteriilor, determinarea activității preparatelor antibacteriene, ca tulpină de control, de testare etc.

Cuvinte-cheie Rezistența la antibiotice, biofilm, patogenitate, secvențiere, *Serratia* spp.

INTRODUCTION

S. marcescens is a prominent member of the genus *Serratia* and is of considerable significance in medical practice due to its role in numerous hospital-acquired infections. According to the ECDC study, "Point Prevalence Survey of Healthcare-Associated Infections and Antimicrobial Use in European Acute Care Hospitals" for 2022–2023, *Serratia* spp. accounted for 54,406 cases across 28 countries globally (1).

Infectious illnesses attributable to *Serratia* spp. demand meticulous scrutiny from veterinary and medical practitioners due to the ubiquity of *Serratia* in the environment (soil, water, and the gastrointestinal tracts of diverse animals) and their role as agents of nosocomial infections in humans.

S. marcescens predominantly induces respiratory tract infections in intubated patients, urinary tract infections in individuals with permanent catheters, and surgical wound infections, superinfections, and sepsis in cases involving intravenous catheterization or complicated local infections. It can also induce meningitis, brain abscesses, and several other illnesses, primarily in hospitalized patients, neonates, and individuals with diabetes (2, 3, 4, 5, 6, 7, 8).

Noncompliance with sanitary and hygienic norms and rules when handling plant-based food products increases the risk of *Serratia* spp. accumulation and infection of humans and animals. Soil serves as a reservoir for the pathogen; therefore, vegetables pose a potential risk of infection to animals, plants, and humans (9, 10). Animal products, such as cured ham, smoked bacon, and sausage, if not properly manufactured and handled, can also be contaminated with *Serratia* spp. and serve as a source of infection for consumers (11, 12, 13).

Among *S. marcescens* strains, a significant proportion produces a red pigment, which led to their use as bioindicators in studies of microbial dissemination and transmission. This practice was long facilitated by the misconception that bacteria of this genus were non-pathogenic. The first documented experiment was conducted in 1906 by M. H. Gordon at the request of the British government (14). The most significant tests involving this biological agent were carried out by the U.S. military between 1940 and 1960 to simulate the dissemination of biological weapons in the event of potential bioterrorist attacks. The "bioindicator" was released at military training facilities and in civilian locations, including San Francisco (1950); the Pentagon in Washington, D.C.; Mechanicsburg, Pennsylvania (1950); Panama City, Florida (1951); Point Mugu-Port Hueneme, California (1953); the New York City underground system (1966); and several other sites across the United States. A journalistic investigation into associated illnesses and fatalities led to hearings in the United States Senate in 1977 (14).

The importance of regulating the proliferation of bacteria belonging to the genus *Serratia* is evidenced by the following findings. In one medical center in southern Taiwan, during the period 1999–2003, 69 nonrepetitive bloodstream isolates were analyzed. Among these, 11 isolates produced extended-spectrum beta-lactamase, while 58 isolates carried an AmpC-encoding gene, including a novel S4 gene with 98% identity to the SRT-1 gene (n = 50), the SRT-2 gene (n = 3), the SST-1 gene (n = 1), and others (n = 4). Isolates carrying S4 exhibited a phenotype of resistance to cefotaxime (CTX) but not ceftazidime (15). In a university hospital in Madrid, Spain, between 2005 and 2020, 141 *Serratia* spp. isolates causing bloodstream infections were identified in 139 patients (16). Studies conducted in Poland in 2003–2004 showed that *S. marcescens* was the fifth most frequently detected clinical isolate (4%) among members of the family Enterobacteriaceae (17). Additionally, a study conducted in Japan in 2008 found that *S. marcescens* accounted for 6.4% of urinary tract infections, making it the fifth most common etiological agent (18).

The prevalence of *Serratia* in farm and wild animals is confirmed by numerous scientific publications. For example, scientists from the Department of Epidemiology at the Indian Veterinary Research Institute demonstrated the prevalence of antimicrobial-resistant Serratia spp. in farm and wild animals, poultry, and reptiles. Isolates were obtained from the cardiac blood of poultry, horses, goats, spotted deer and turtles (19). Additionally, outbreaks of mastitis were reported in cows from 2 different herds on a farm in Finland, where 18 isolates of *S. marcescens* were identified (20).

Researchers in Japan obtained 30 isolates from clinical specimens collected from dogs and cats that exhibited resistance to extended-spectrum cephalosporins. This finding raises concerns for both medical and veterinary practice, as third- and fourth-generation cephalosporins are frequently employed as "last-line" therapies for bacterial infections (21).

Clinical Microbiology Laboratory at the University of Melbourne Veterinary Clinic and Hospital performed 4,536 bacterial identifications in animal patients, with Serratia spp. isolated in 0.7% of cases (11 dogs, 9 cats, 6 horses, 1 rabbit, and 1 bird). Analysis of antibiotic susceptibility testing for 18 *Serratia* spp. isolates showed that 50% were resistant to sulfafurazole/trimethoprim, enrofloxacin, and third-generation cephalosporins. One strain also exhibited resistance to chlorhexidine, which is used for disinfecting tools and work surfaces in the veterinary facility (22). Similar findings have been reported by other authors (7, 23, 24).

Numerous authors have experimentally demonstrated the ability of *Serratia*, particularly *S. marcescens* and *S. liquefaciens*, to produce heat-stable enterotoxins (astA) that act via guanylate cyclase, increasing the level of cGMP in intestinal cells and causing secretory diarrhea. Some strains of *S. marcescens* secrete hemolysins that destroy erythrocytes. These toxins may damage the intestinal epithelium and induce inflammation (16).

Taxonomically, the genus *Serratia* remains ambiguous, and it currently comprises 14 recognized species and 2 subspecies (tab. 1).

Human infections caused by *Serratia*, particularly *S. marcescens*, were not well understood until the latter half of the 20th century. This was likely due to challenges in the taxonomic characterization of the genus and the fact that several species were not identified until the 1970s and 1980s. *S. marcescens* is now recognized as an important human pathogen. Another member of the genus, *S. liquefaciens*, is considered the second most common isolate from human clinical specimens. It is an environmental bacterium associated with disease and was first described in 1931 by Grimes and Hennerty as *Aerobacter liquefaciens*. In 1963, the organism was assigned to the genus *Enterobacter* and was subsequently reclassified as *S. liquefaciens* in 1973 based on phenotypic characteristics (14, 24).

The pathogenicity of *S. liquefaciens* has been established in humans, where it is a recognized pathogen of nosocomial infections. It also causes diseases in productive animals, insects and fish. The ubiquity of *Serratia* spp., together with the risks of disease outbreaks caused by representatives of this species, which do not belong to generally recognized pathogens, justifies the need for further investigation of its circulation and the arsenal of pathogenicity factors. Standard strains are essential for laboratory diagnostics, for evaluating the suitability of nutrient media, and for conducting comparative studies with the characteristics of epizootic isolates.

The aim of this study was to investigate the biological properties of the isolate *S. liquefaciens* obtained from chicken faeces.

Table 1. Current taxonomic map of the genus *Serratia* (14).

Species and subspecies	Year of detection	Habitat	Pathogenicity
S. entomophila	1988 (169)	Insects (*Costelytra zealandica*)	Insects
S. ficaria	1979 (167)	Plants, insects (cycle common fig-fig of wasp)	Humans
S. fonticola	1979 (145)	Water	Humans
S. glossinae	2010 (146)	Insects (*Glossinapalpalis gambiensis*)	Not reported
S. grimesii	1983 (163)	Water, soil	Not reported (isolated from humans)
S. liquefaciens	1931 (158)	Water, soil, animals, insects, plants	Humans, insects
S. marcescens subsp. *marcescens*	1823 (37, 264)	Water, soil, animals, insects, plants	Humans, animals, insects
S. marcescens subsp. *sakuensis*	1998 (109)	Water	Not reported
S. nematodiphila	2009 (425)	Nematodes (*Heterorhabditidoideschong mingensis*)	Not reported
S. odorifera	1978 (165)	Plants	Humans
S. plymuthica	1896 (162)	Water, animals, insects, plants	Humans
S. proteamaculans	1919 (291)	Water, soil, animals, insects, plants	Insects, plants
S. quinivorans	1982 (163)	Water, soil, animals, insects, plants	Humans
S. rubidaea	1940 (363)	Water, plants	Humans
S. ureilytica	2005 (36)	Water	Not reported

MATERIALS AND METHODS

Location of research

Investigations of morphological and biochemical characteristics, evaluation of antibiotic sensitivity, determination of pathogenicity, and establishment of biofilms formation were conducted at Kharkiv Regional State Laboratory of the State Service of Ukraine for Food Safety and Consumer Protection and at the Department of Veterinary Epidemiology and Animal Health, Faculty of Veterinary Medicine, National University of Life and Environmental Sciences of Ukraine, Kyiv, Ukraine. Molecular genetic studies of the isolate were performed at Danylo Zabolotny Institute of Microbiology and Virology of the National Academy of Sciences of Ukraine.

Selection of samples

Research samples were collected from chickens exhibiting diarrhea that were kept under laboratory vivarium conditions and were delivered to the laboratory in accordance with the state standards of Ukraine (DSTU 8703-1:2017, DSTU 8703-2:2017). A total of 23 samples were collected.

Object of research

S. liquefaciens isolate obtained in 2024 from chickens (*S. liquefaciens* 1/2024).

1. *Study of biological properties of Serratia liquefaciens*

1.1. *Isolation of pure culture and determination of morphological properties*

The study was conducted in accordance with current international and national regulatory documents for the detection of enterobacteria (ISO 21528-1:2017, ISO 21528-2:2017).

The conventional bacteriological approach, namely growing on liquid and solid nutrient medium, was employed to ascertain the morphological features.

Bacteriological examination of pathological material was conducted by inoculating cloacal washings onto nutrient broth using a sterile swab. Cultivation was carried out at the optimal temperature for *Serratia* growth, 37°C, for 24 hours.

To obtain a pure culture, the nutrient broth cultures were subcultured using a bacteriological loop with frequent wide strokes onto separate Petri dishes with Endo ta xylose-lysine-deoxycholate agar (XLD-agar), covering the entire agar surface, and thereafter incubated in a thermostat for 24 hours at 37°C. Subsequently, individual representative colonies were extracted from the agar surface using a bacteriological loop, subcultured into meat peptone nutrition broth and meat peptone nutrient slant agar, and incubated at 37°C for 24 hours.

Morphological properties were determined by microscopy of Gram-stained smears, while growth typicality was determined by inoculating *S. liquefaciens* cultures on liquid and solid nutrient media.

To assess bacterial motility, the isolated cultures were grown at 37°C in semi-liquid MPA (0.25 – 0.3%). Inoculation was performed by introducing the sample into a column of semi-liquid agar. Motility was also assessed by microscopy of daily agar cultures using the “crushed drop” technique.

1.2. *Assessment of biochemical properties*

The biochemical characteristics of the isolate were investigated by inoculation on Hiss media supplemented with various sugars (maltose, glucose, mannitol, sucrose, lactose, rhamnose, and raffinose). Additionally, the ability to produce enzymes, ornithine decarboxylase, phenylalanine deaminase, lysine decarboxylase, and arginine dehydrolase, was assessed, along with urea and indole production. The Voges-Proskauer reaction was also performed.

1.3. *Assessment of pathogenicity*

The pathogenicity of the isolate was assessed in 30 white male mice, 4 months old, weighing 21-23 g, by intraperitoneal injection of a 24-hour broth culture of *S. liquefaciens* at doses ranging from 10^1 to 10^9 CFU (3 mice per dose). The control group of mice received sterile MPB injection. The observation period lasted 72 hours. The LD_{100} was defined as the minimum dose of the tested culture that caused 100% mortality in the experimental animals.

Animal experiments were conducted in accordance with the current “General Ethical Principles of Animal Experiments”, adopted by the First National Congress of Bioethics and aligned with international bioethical standards (materials of the IV European Convention for the Protection of Vertebrate Animals Used for Experimental and Other Purposes, Strasbourg, 1985) (25). The research programme was reviewed and approved by the Bioethics Commission of the National University of Life and Environmental Sciences of Ukraine (approval No. 022/2024, dated 26.11.2024).

1.4. *Assessment of antibiotic sensitivity*

The sensitivity of the investigated isolate to antibacterial drugs was assessed by the disk fusion method. A specialized nutritional medium, Mueller Hinton Agar, was employed to evaluate sensitivity (26).

Four identical, distinctly separate colonies were picked from a 24-hour agar culture on meat-peptone agar in Petri plates and subsequently transferred to a test tube containing sterile saline using a bacteriological loop to generate a microbial suspension (inoculum). The optical density of the bacterial suspension was adjusted with a densitometer, measuring 0.5 according to McFarland standards.

Standardized antibiotic discs (26 medicines from several pharmacological categories) were used to assess sensitivity. The discs were placed on the agar surface using sterile tweezers, onto which the inoculum (1.0 ml) had been previously deposited. Following disc application, the Petri dishes were positioned in a thermostat and incubated at 37°C for 24 hours. The results (measurement of the growth inhibition zone) were recorded using a specialized ruler. Data were interpreted according to EUCAST guidelines, 2023. The experiments were performed in seven replicates.

1.5. *Evaluation of film formation*

An indirect assessment of bacterial biofilms biomass was performed using the adsorption/resorption of crystal violet, following the established methodology (27). The biofilms were stained using a 0.1% aqueous solution of crystal violet at 30°C for 60 minutes. The study was conducted under two culture temperatures: 23°C and 37°C. Sterile MPB served as the control. To ensure data reliability, the experiments were performed in seven replicates.

2. *Molecular-genetic research*

The molecular genetic methods for studying bacteria, particularly the sequencing of 16S rRNA gene fragments and phylogenetic analysis, were implemented according to the procedures outlined by Tkachuk et al. (28). In summary, genomic DNA was extracted from a pure bacterial culture for 16S rRNA gene sequencing and subsequently amplified using 27F and 1492r primers. PCR products were purified and sequenced in both directions using the ABI 310 (Applied Biosystems). The resulting sequences were compared with those in the GenBank database using BLASTn, and the highest percentage of sequence similarity (>98.7%) was used for species identification. Sequences showing greater than 98.7% similarity were further analyzed for variable and parsimony-informative sections utilizing MEGA6 (29) for identification.

3. *Statistical studies*

The data obtained from the biofilm formation studies under different temperature conditions were analyzed using SPSS Statistics software.

RESULTS

1.1. *Isolation of a pure culture and assessment of morphological characteristics*

After 24 hours of initial inoculation on Endo agar, small, homogenous pink colonies exhibiting an S-shape and measuring 1-2 mm in diameter were observed. On XLD-agar, the isolated culture produced uniform, colorless colonies exhibiting an S-shape, measuring 1-2 mm in diameter. Gram-stained smears were prepared from isolated colonies. Microscopic examination revealed small, homogenous, gram-negative rods with rounded ends, resembling ovoids, measuring 3-5 x 0.8-1.5 microns. In MPB, the pure culture produced consistent turbidity in the medium after 24 hours. In smears from broth cultures, the cells appeared singly; the dimensions of the bacteria cultured on nutritional media measured 3-5 x 0.8-1.5 microns. Small transparent colonies, occasionally exhibiting a faint yellowish hue, were detected on the MPA, characterized by a rounded, convex, S-shaped morphology.

Upon assessment of motility, *S. liquefaciens 1/2024* was identified as motile.

1.2. *Assessment of biochemical characteristics*

Under cultivation conditions in a thermostat at 37°C for 24 hours, *S. liquefaciens* 1/2024 metabolised maltose, glucose, mannitol, and sucrose, while failing to metabolise lactose, rhamnose, or raffinose. It produced ornithine decarboxylase and lysine decarboxylase but did not produce urea, phenylalanine deaminase, arginine dihydrolase, or indole. The Voges-Proskauer test yielded a negative result (tab. 2).

Table 2. Enzymatic properties of the isolate *S. liquefaciens* 1/2024 and *S. marcescens*.

Indicator name	*S. liquefaciens*	*S. marcescens*
Maltose	+	+
Glucose	+	+
Mannitol	+	+
Sucrose	+	+
Lactose	–	–
Rhamnose	–	+/–
Raffinose	–	–
Ornithine decarboxylase	+	+

Indicator name	*S. liquefaciens*	*S. marcescens*
Urea production	–	–
Phenylalanine deaminase	–	–
Lysine decarboxylase	+	+
Arginine dihydrolase	–	–
Indole	–	–
Voges-Proskauer (VP)	–	–

Note: «+» – reaction present, «-» – reaction absent.

1.3. *Assessment of pathogenicity*

No mortality was observed in mice within 72 hours following the administration of *S. liquefaciens 1/2024* culture at doses ranging from 10^1 to 10^7 CFU. However, 100% mortality occurred in groups receiving doses of 10^8 to 10^9 CFU within 12 to 18 hours. These results indicate that the specified isolate is pathogenic to white mice at a dose of 10^8 CFU.

1.4. *Antibiotic sensitivity testing*

The European Committee on Antimicrobial Susceptibility Testing (EUCAST) defines the area of technical uncertainty (ATU) as a situation in which antimicrobial susceptibility testing results do not allow for a definitive classification of an isolate as either susceptible or resistant. This may arise due to discrepancies in testing methodologies or the unique characteristics of the individual microbe. EUCAST does not establish distinct clinical breakpoints for *S. liquefaciens.*

The tested culture exhibited resistance to semisynthetic and inhibitor-protected penicillins (Ticarcillin, Ampicillin/Sulbactam, Amoxicillin/Clavulanicacid, Ticarcillin/Clavulanicacid), with the exception of Piperacillin, for which an inhibition zone of 18 mm was observed (tab. 3).

Table 3. Sensitivity of *S. liquefaciens* 1/2024 to β-lactam antibiotics.

Antibacterial drug	Diameter of inhibition of culture growth around the disk with antibacterial drug, mm	[4]ATU, mm
Ampicillin/sulbactam, [2]20, [3]SAM	6	[5]14
Amoxicillin/clavulanic acid, [2]10, [3]AMC	6	[5]19-20
Ticarcillin, [2]75, [3]TI	6	[5]20-23
Ticarcillin/clavulanicacid, [2]75\10, [3]TCC	7	[5]20-23
Piperacillin, [2]100, [3]PI	18	[5]20
Cefalotin, [1](I), [2]30, [3]CEP	6	[5]15-17
Cephalexin, [1](I), [2]30, [3]CL	12	[5]14
Cefaclor, [1](II), [2]30, [3]CF	10	[5]15-17
Cefuroxime, [1](II), [2]30, [3]CXM	6	[5]19
Cefamandole, [1](II), [2]30, [3]MA	14	[5]15-17
Cefixim, [1](III), [2]5, [3]CFM	13	[5]17
Cefoperazone, [1](III), [2]75, [3]CPZ	18	[5]16-20
Meropenem, [2]10, [3]MEM	44	[5]16-22 ([6]<28)

Notes: «[1]» – AMP generation; «[2]» – AMP concentration (μg); «[3]» – AMP code as indicated on the disc; «[4]» – Area of technical uncertainty for microorganism sensitivity/resistance to AMP; «[5]» – Interpretation of results per EUCAST (Version 13.1, valid from 2023-06-29); «[6]» – in carbapenemase screening, the meropenem screening limits> 0.125 mg/L (zone diameter <28 mm); «*» – indicates uniform growth of resistant colonies in the specified range (mm).

The culture exhibited sensitivity to cephalosporins (Cephalexin, Cefaclor, Cefamandole, Cefixim), with the exception of Cefalotin and Cefuroxime (tab. 3).

The culture exhibited sensitivity to carbapenems (Meropenem), with a growth inhibition zone of 44 mm. (tab. 3).

The culture exhibited sensitivity to aminoglycosides (Gentamicin, Netilmicin). Inhibition zones about 24 mm in diameter were observed surrounding the discs containing Netilmicin (tab. 4).

The tested culture was sensitive to tetracyclines (the culture's sensitivity to Tetracycline, and Doxycycline was manifested with growth inhibition zones of 23 mm and 26 mm, respectively) and to quinolones (a culture inhibition zone with a diameter of 36 mm was recorded around the disc with Nalidixic acid).

A growth inhibition zone measuring 30 mm was observed around the Lomefloxacin disc, while double zones of growth inhibition of 40/32 mm, 30/27 mm, and 30/27 mm were noted around the Ciprofloxacin, Ofloxacin, and Chloramphenicol discs, respectively, indicating an enhanced sensitivity of the cultures. The culture exhibited sensitivity to Polymixin B and Furazolidone, shown by zones of growth inhibition of 15 mm and 14 mm in diameter, respectively. The isolate exhibited moderate sensitivity to Fusidic acid, with a growth inhibition zone of 7 mm, indicating in vitro resistance to this medication at the specified dose.

Table 4. Sensitivity of *S. liquefaciens* 1/2024 to antimicrobial agents.

Antibacterial drug	Diameter of inhibition of culture growth around the disk with antibacterial drug, mm	[4]ATU, mm
Gentamicin, [1](I), [2]10, [3]CN	19	[5]17
Netilmicin, [1](III), [2]30, [3]NET	24	[6]13-14
Tetracycline, [2]30, [3]TE	23	[6]≥19
Doxycycline, [2]30, [3]DO	26	[6]≥19
Nalidixic acid, [1](I), [2]30, [3]NA	36	[6]14-18
Ciprofloxacin, [1](II), [2]5, [3]CIP	*40/32	[5]22-24
Ofloxacin, [1](II), [2]5, [3]OFX	*30/27	[5]22-24
Lomefloxacin, [1](II), [2]10, [3]LOM	30	[6]19-21
Chloramphenicol, [2]30, [3]C	*32/28	[6]13-17
Polymixin, [1]B, [2]300, [3]PB	16	[7]-
Furazolidone, [2]50, [3]FX	14	[7]-
Fusidic acid, [2]10, [3]FC	7	[7]-

Notes: «[1]» – AMP generation; «[2]» – AMP concentration (μg); «[3]» – AMP code as indicated on the disc; «[4]» – Area of technical uncertainty for microorganism sensitivity/resistance to AMP; «[5]» – Interpretation of results per EUCAST (Version 13.1, valid from 2023-06-29); «[6]» – Interpretation per Ministry of Health of Ukraine guidelines (2007); «[7]» – Thresholds not defined; «*» – indicates uniform growth of resistant colonies in the specified range (mm).

1.5. Biofilm formation study

When analyzing the biofilm-forming capacity of *S. liquefaciens* 1/2024, it was found (tab. 5) that denser biofilm production occurred during cultivation at 23°C compared to 37°C. Under these conditions, *S. liquefaciens* 1/2024 formed a biofilm that was 92.1% denser at 23°C ($P < 0.05$), which may indicate the bacterium's adaptation to more favorable environmental conditions.

Table 5. Results of studying the capacity of *S. liquefaciens* 1/2024 to form biofilms at 23°C and 37°C (M±m, n=7).

Culture conditions	The optic density of formed biofilm, λ 570
+23°C	0.265±0.05*
+37°C	0.138±0.038
Control (sterile MPB)	0.035±0.01

Note: P<0.05 compared to culture at +37°C

To check if the data followed a normal distribution, the Kolmogorov-Smirnov test (with Lilliefors correction) and the Shapiro-Wilk test were applied to two experimental temperature conditions: 23°C and 37°C. In both cases, the p-values were less than 0.05. For t23, the p-values were p = 0.043 (Kolmogorov-Smirnov) and p = 0.039 (Shapiro-Wilk). For t37, the p-values were p = 0.045 (Kolmogorov-Smirnov) and p = 0.030 (Shapiro-Wilk).

Q-Q plots were constructed to visually assess the normality of the distribution. The 23°C graph (fig. 1) shows significant deviations of the points from the diagonal line, especially at the extreme values. This indicates asymmetry or outliers. Similarly, the graph for 37 °C (fig. 2) also deviates from linearity, with the data points not aligning closely with the expected quantiles of a normal distribution. This is consistent with the test results.

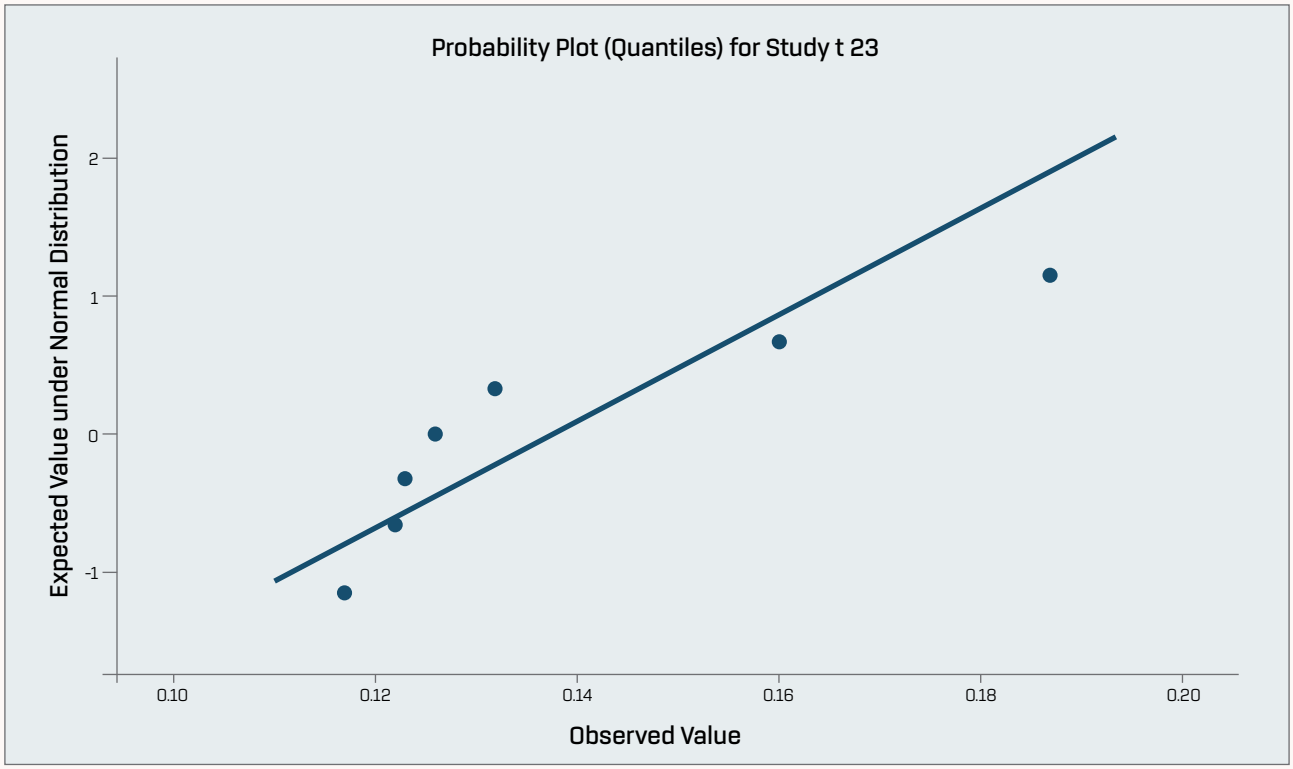

Figure 1. Visual assessment of distribution normality (Q-Q plots) at 23˚C.

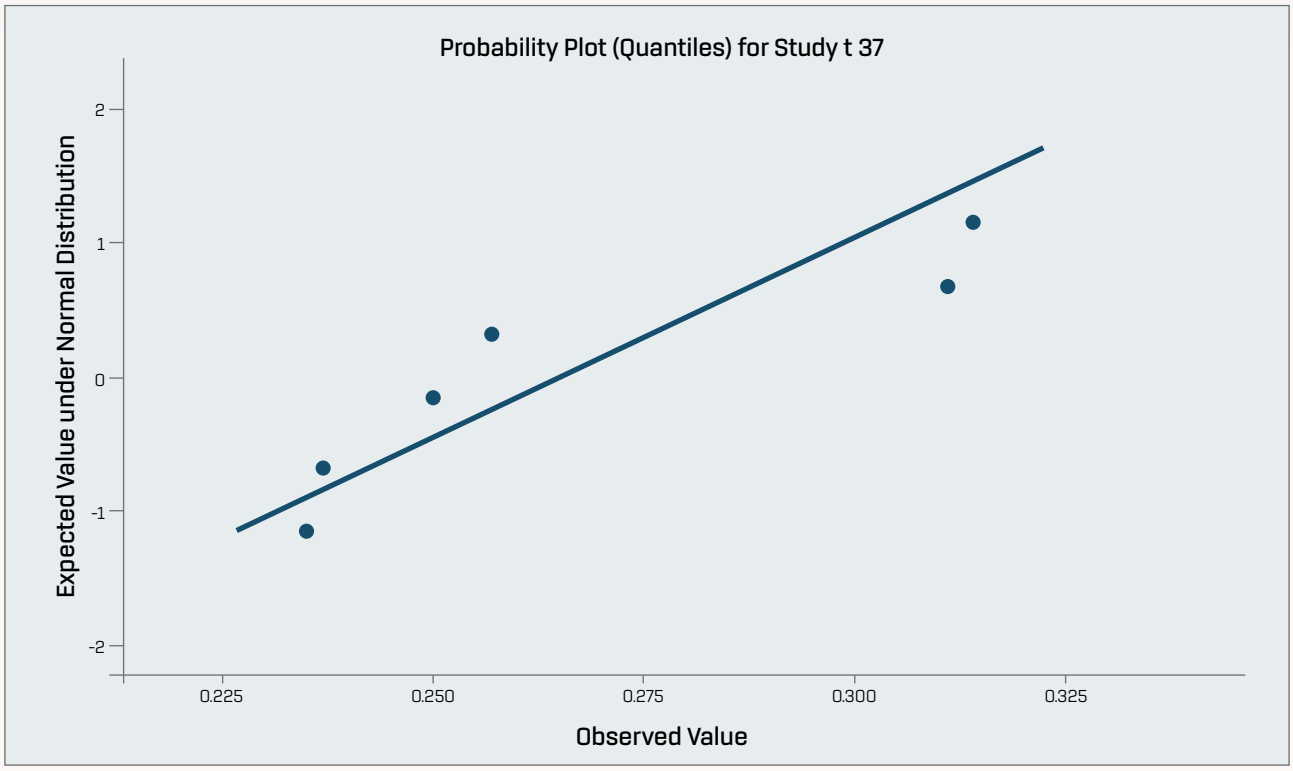

Figure 2. Visual assessment of distribution normality (Q-Q plots) at 37°C.

Thus, the graphical evaluation supports the statistical conclusion that the data distributions under both temperature conditions deviate from normality. This indicates that the empirical distribution is statistically significantly different from the normal distribution, and the null hypothesis of normality was rejected at the 0.05 significance level.

Further statistical analysis required the use of nonparametric methods, which do not assume a normal distribution of data. In such cases, parametric methods like Student's t-test are not appropriate.

Therefore, the nonparametric Mann-Whitney U test was chosen to compare two independent samples. This test does not require the assumption of a normal distribution and is resistant to outliers and skewed data. The obtained p-value of 0.001 is statistically significant ($p<0.05$), allowing us to reject the null hypothesis of equal distributions. This indicates that temperature has a significant effect on the studied indicator.

2. *Molecular genetic studies of the S. liquefaciens 1/2024 strain*

The investigation yielded a nucleotide sequence of 633 nucleotides, which has been registered in the GenBank database under the identifier PQ308601.1.

A preliminary comparison with the genomes in this database revealed 99.21% identity with other strains of the species (fig. 3), including the standard *S. liquefaciens* ATCC 27592. A dendrogram was built to illustrate the evolutionary connections between the examined strain and other species within the genus *Serratia*, placing the *S. liquefaciens* 1/2024 strain in the same clade as other strains of this species. The results of the phylogenetic analysis confirmed the classification of the investigated strain as belonging to the species *S. liquefaciens*.

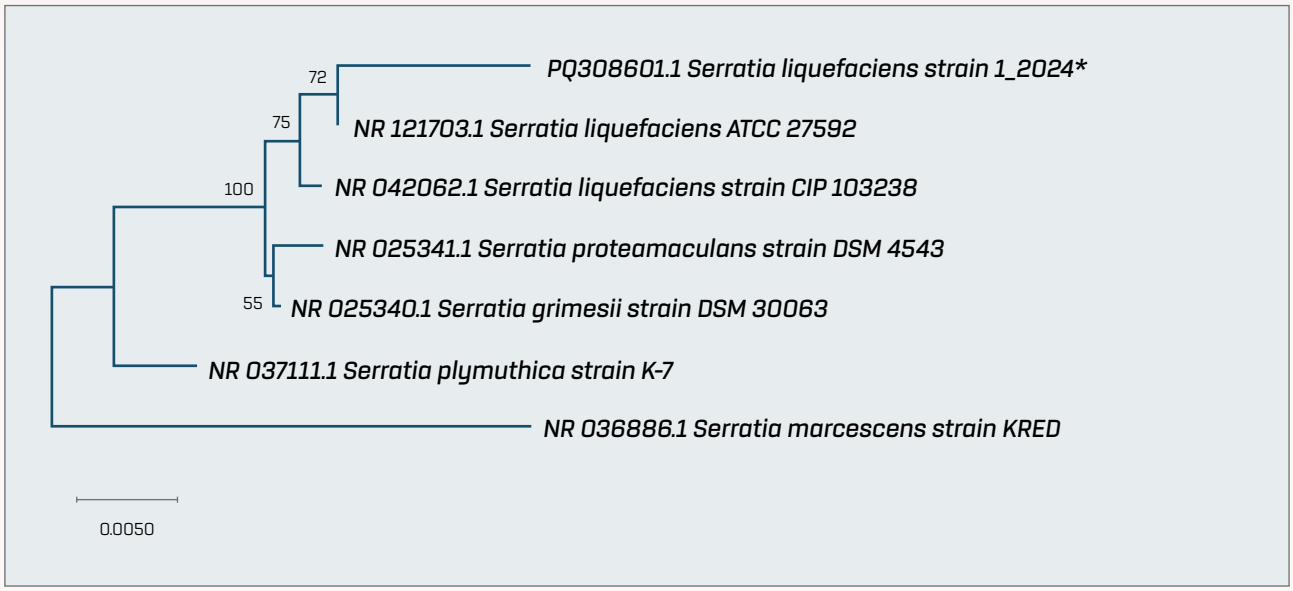

Figure 3. Dendrogram illustrating genetic similarity between *S. liquefaciens strain 1_2024* and other members of the Serratia genus.

DISCUSSION

The ubiquity of *S. liquefaciens* makes it a subject of particular concern within the framework of the "One Health" concept, which recognizes the close interdependence between the health of humans, domestic and wild animals, plants, and the environment, including entire ecosystems (30). *S. liquefaciens* is a notable opportunistic pathogen with zoonotic potential and is responsible for nosocomial infections, including those in veterinary settings. It exhibits resistance to multiple antibiotics and has the ability to form biofilms, thereby posing a threat to poultry, cattle, salmonids, trout, turbot, and various companion animals (16, 21, 31, 32, 33, 34, 35, 36).

S. liquefaciens is a member of the Enterobacteriaceae family and is prevalent in both environmental settings and cattle populations. Infection often occurs through water, feed, or infected ambient items. It is essential to consider the findings of several authors (37), which indicate that the source of histamine in seafood, which may lead to human food poisoning, is histamine-producing bacteria, such as *S. liquefaciens.*

Favorable factors for the penetration, reproduction, and pathogenic activity of *S. liquefaciens* in the animal body include stress of various origins (such as poor housing conditions, inadequate nutrition, and concurrent infections) as well as immunodeficiency states. In poultry, clinical manifestations may include septicaemia, respiratory symptoms, purulent skin and subcutaneous lesions, enteritis, arthritis, and tendovaginitis (18).

The optimal temperature for the proliferation of *S. liquefaciens* is 37°C. Under these conditions, motile cells with elevated proteolytic activity are capable of synthesizing pigment. Research indicates that certain *Serratia* strains can produce thermostable (ST) and thermolabile (LT) enterotoxins, similar to those produced by *Escherichia coli* (16).

The obtained isolate *S. liquefaciens* 1/2024 exhibited resistance to penicillin group antibiotics (Ampicillin/Sulbactam, Amoxicillin-Clavulanic acid, Ticarcillin/Clavulanic acid), cephalosporins (Cephalothin, Cefuroxime), among others, corroborating findings from several authors (14, 38).

It should be noted that the strain remains sensitive to carbapenems, fluoroquinolones, aminoglycosides, and tetracyclines, which may indicate the absence of specific resistance mechanisms to antimicrobial agents.

At present, antimicrobial resistance is considered a key factor contributing to pathogenicity, based on current scientific understanding. As a result, infections caused by antibiotic-resistant organisms in susceptible individuals can lead to prolonged treatment durations, increased mortality rates, and the dissemination of resistant bacterial clones in the environment. The growing prevalence of antibiotic resistance among pathogens poses a significant challenge to the healthcare system (39,40). The global scale of antibiotic resistance among microorganisms necessitates urgent action to prevent the emergence and spread of antibiotic-resistant strains (41, 42, 43).

Our findings demonstrate the ability of *S. liquefaciens 1/2024* strain to produce biofilms. Numerous authors (44, 45, 46) have noted that biofilm formation is a common ecological strategy among various bacteria, providing significant advantages such as increased resistance to antibiotics and the ability to evade host immune responses.

The experimental study investigated the effect of temperature (23 °C and 37 °C) on variables obtained from seven independent replicates in each group. Preliminary statistical analysis revealed that the sample data did not follow a normal distribution, confirming the need for nonparametric method of analysis.

Therefore, the Mann-Whitney U test, one of the most commonly used nonparametric tests for analyzing independent samples, was used to test the hypothesis that there were statistically significant differences between the groups. The analysis revealed a significant difference ($p = 0.001$), indicating that temperature has a substantial effect on the studied parameter. The obtained value of $p = 0.001$ is statistically significant ($p < 0.05$), allowing for the rejection of the null hypothesis of equal distributions. These findings highlight that temperature is a critical factor influencing the studied indicator. Therefore, the temperature regime should be carefully considered when conducting such experiments.

The Mann-Whitney U test is widely used in biomedical research (47), particularly when the data are ordinal or do not meet the assumptions of proportional odds. Additionally, several studies highlight that the Mann-Whitney U test is a reliable tool for analyzing non-normal distribution data and recommend its use in medical research (48). Therefore, the use of the Mann-Whitney U test for statistical analysis in this study is appropriate when the assumption of normal distribution is not met.

Thus, the obtained results allow us to conclude that the temperature regime influences the behavior or properties of the object under study. This indicates the need to consider the temperature factor when designing experiments and interpreting research findings, especially when environmental conditions may affect the outcome. Despite the absence of a normal distribution, which is common in small samples and experimental data in biology, medicine, and related sciences, the use of a nonparametric approach, specifically the Mann-Whitney test, ensured the reliability of the conclusions drawn.

The sequencing results of the 16S rRNA gene fragments, along with subsequent phylogenetic analysis, justified the inclusion of the *S. liquefaciens* 1/2024 strain in the GenBank NCBI database under the accession number PQ308601.1. This strain clustered with other strains of the species, notably the reference strain *S. liquefaciens* ATCC 27592, for which the complete genome sequence has been established (49, 50).

Consequently, the data obtained justify the use of the *S. liquefaciens* 1/2024 strain as a standard, namely for evaluating nutritional media productivity, conducting comparative assessments of field isolates, and testing novel antimicrobial drugs, among other applications.

Infectious diseases hinder sustainable societal development by affecting plant, animal, and human health, while also jeopardizing food security and the biodiversity of natural ecosystems. Contemporary challenges, such as climate change, population displacement due to armed conflicts, environmental and food issues, and the globalization of trade, are closely linked to the emergence of zoonotic diseases and have a detrimental impact on public health (1, 30, 40).

Research aimed at improving diagnostic techniques and studying the biological characteristics of infections is especially relevant in these challenging times.

CONCLUSIONS

1. The *S. liquefaciens* 1/2024 strain, isolated from chicken cloacal washings, exhibits typical characteristics of the *Serratia* genus and is pathogenic to white mice (10^8CFU).
2. It demonstrates biofilm-forming ability and multiple resistance to antimicrobial agents, including resistance to penicillins, cephalosporins, and fusidic acid.
3. Sequencing of the 16S rRNA gene fragment revealed 99.21% similarity to the reference strain *S. liquefaciens* ATCC 27592, and it is listed in the GenBank NCBI database under accession number PQ308601.1.

CONFLICT OF INTEREST

The authors declare no conflict of interest.

FUNDING

This research was carried out with the financial support of the Ministry of Education and Science of Ukraine under project number 110/4-pr-2023.

ETHICAL APPROVAL

This study was approved by the Bioethics Commission of the National University of Life and Environmental Sciences (NULES) of Ukraine, decision No. 022/2024, dated November 26, 2024.

REFERENCES

1. European Centre for Disease Prevention and Control. *Point prevalence survey of healthcare-associated infections and antimicrobial use in European acute care hospitals 2022-2023.* Stockholm: ECDC, 2024. https://doi.org/10.2900/88011.
2. Taxt AM, Eldholm V, Kols NI, Haugan MS, Raffelsberger N, Asfeldt AM, et al. A national outbreak of Serratia marcescens complex: investigation reveals genomic population structure but no source, Norway, June 2021 to February 2023. *Euro Surveill.* 2025;30(5):2400291. https://doi.org/10.2807/1560-7917.ES.2025.30.5.2400291.
3. Ayuzo-Del-Valle NC, Flores-Osorio X. Pink colored breast milk! Serratia marcescens infection, series of 4 cases. *Bol Med Hosp Infant Mex*. 2024;81(2):114-117. https://doi.org/10.24875/BMHIM.23000087.
4. Atta S, Perera C, Nayyar S, Kowalski RP, Jhanji V. An 18-Year Overview of Serratia marcescens Ocular Infection. *Eye Contact Lens.* 2021;1;47(8):471-475. https://doi.org/10.1097/ICL.0000000000000803.
5. Weakland DR, Smith SN, Bell B, Tripathi A, Mobley HLT. The Serratia marcescens Siderophore Serratiochelin Is Necessary for Full Virulence during Bloodstream Infection. *Infect Immun*. 2020;88(8):e00117-20. https://doi.org/10.1128/IAI.00117-20.
6. Friman MJ., Eklund MH, Pitkälä AH, Rajala-Schultz PJ, Rantala MHJ. Description of two Serratia marcescens associated mastitis outbreaks in Finnish dairy farms and a review of literature. *Acta Vet. Scand.* 2019;61:54. https://doi.org/10.1186/s13028-019-0488-7.
7. Stock I., Grueger T., Wiedemann B. Natural antibiotic susceptibility of strains of Serratia marcescens and the S. liquefaciens complex: S. liquefaciens sensu stricto, S. proteamaculans and S. grimesii. *Int J Antimicrob Agents*. 2003;22(1):35-47. https://doi.org/10.1016/S0924-8579(02)00163-2.
8. Millán-Lou MI, López C, Bueno J, Pérez-Laguna V, Lapresta C, Fuertes ME, et al. Successful control of Serratia marcescens outbreak in a neonatal unit of a tertiary-care hospital in Spain. Enferm Infecc Microbiol Clin (Engl Ed). 2022;40(5):248-254. https://doi.org/10.1016/j.eimce.2021.05.014
9. Van Houdt R, Van der Lelie D, Izquierdo JA, Aertsen A, Masschelein J, Lavigne R, et al. Genome Sequence of Serratia plymuthica RVH1, Isolated from a Raw Vegetable-Processing Line. Genome Announc. 2014;6;2(1):e00021-14. https://doi.org/10.1128/genomeA.00021-14
10. Fodor A., Palkovics L., Végh A. First report of Serratia marcescens from oleander in Hungary. Phytopathol. Mediterr. 2022;61, 311–317. https://doi.org/10.36253/phyto-13354.
11. Sijia Hu, Xinfu Li, Qiang Xiong. The Combination of Corona Discharge Plasma and ε-Polylysine for the Inactivation of Serratia liquefaciens, Journal of Food Protection, 2023;86(7):100078. https://doi.org/10.1016/j.jfp.2023.100078.
12. Belletti N, Garriga M, Aymerich T, Bover-Cid S. Inactivation of Serratia liquefaciens on dry-cured ham by high pressure processing, Food Microbiology, 2013;35(1):34-37, https://doi.org/10.1016/j.fm.2013.03.001.
13. Li X, Xiong Q, Zhou H, Xu B, Sun Y. Analysis of Microbial Diversity and Dynamics During Bacon Storage Inoculated With Potential Spoilage Bacteria by High-Throughput Sequencing. Frontiers in Microbiology. 2021;12: 713513. https://doi.org/10.3389/fmicb.2021.713513.
14. Mahlen SD. Serratia infections: from military experiments to current practice. Clin Microbiol Rev. 2011;24(4):755-91. https://doi.org/10.1128/CMR.00017-11.
15. Wen-Liang Yu, Wen-Chien Ko, Kuo-Chen Cheng, Hui-En Chen, Ching-Chien Lee, Yin-Ching Chuang. Institutional spread of clonally related Serratia marcescens isolates with a novel AmpC cephalosporinase (S4): a 4-year experience in Taiwan, Diagnostic Microbiology and Infectious Disease, 2008;61(4):460-467, https://doi.org/10.1016/j.diagmicrobio.2008.03.010/
16. Pérez-Viso B, Hernández-García M, Rodríguez CM, D Fernández-de-Bobadilla M, Serrano-Tomás MI, Sánchez-Díaz AM, et al. A long-term survey of Serratia spp. bloodstream infections revealed an increase of antimicrobial resistance involving adult population. Microbiol Spectr. Feb 2024;6;12(2):e0276223. https://doi.org/10.1128/spectrum.02762-23.
17. Empel J, Baraniak A, Literacka E, Mrówka A, Fiett J, Sadowy E, et al. Molecular Survey of β-Lactamases Conferring Resistance to Newer β-Lactams in Enterobacteriaceae Isolates from Polish Hospitals. Antimicrob Agents Chemother. 2008;52(7). https://doi.org/10.1128/AAC.00043-08.
18. Ishikawa K., Matsumoto T, Yasuda M, Uehara S, Muratani T, Yagisawa M, et al. The nationwide study of bacterial pathogens associated with urinary tract infections conducted by the Japanese Society of Chemotherapy. J. Infect. Chemother. 2011;17:126–138. https://doi.org/10.1007/s10156-010-0174-1.
19. Singh BR, Agri H, Karthikeyan R, Jayakumar V. Common Bacterial Causes of Septicaemia in Animals and Birds Detected in Heart Blood Samples of Referred Cases of Mortality in Northern India. *J Clin Med Img*. 2023;7(7):1-14. https://clinandmedimages.org/wp-content/uploads/2023/11/JCMI-v7-1689.pdf.
20. Friman MJ, Eklund MH, Pitkälä AH, Schultz PJ, Rantala MHJ. Description of two Serratia marcescens associated mastitis outbreaks in Finnish dairy farms and a review of literature. Acta Vet Scand, 2019;61(54). https://doi.org/10.1186/s13028-019-0488-7.
21. Harada K, Shimizu T, Ozaki H, Kimura Y, Miyamoto T, Tsuyuki Y. Characterization of Antimicrobial Resistance in Serratia spp. and Citrobacter spp. Isolates from Companion Animals in Japan: Nosocomial Dissemination of Extended-Spectrum Cephalosporin-Resistant Citrobacter freundii. Microorganisms, 2019;7(3):64. https://doi.org/10.3390/microorganisms7030064.

22. Allen JL, Doidge NP, Bushell RN, Browning GF, Marenda MS. Healthcare-associated infections caused by chlorhexidine-tolerant Serratia marcescens carrying a promiscuous IncHI2 multi-drug resistance plasmid in a veterinary hospital. PLoS One, 2022;17(3), e0264848. https://doi.org/10.1371/journal.pone.0264848.

23. Tavares-Carreon F, De Anda-Mora K, Rojas-Barrera IC, Andrade A. Serratia marcescens antibiotic resistance mechanisms of an opportunistic pathogen: a literature review. PeerJ. 2023;5(11):e14399. https://doi.org/10.7717/peerj.14399.

24. Clements T, Ndlovu T, Khan S, Khan W. Biosurfactants produced by Serratia species: Classification, biosynthesis, production and application. Appl Microbiol Biotechnol. 2019;103(2):589-602. https://doi.org/10.1007/s00253-018-9520-5.

25. Simmonds R. Chapter 4. Bioethics and animal use in programs of research, teaching, and testing. In: Weichbrod, R. H., Thompson, G. A. H., Norton, J. N. (Eds.). Management of animal care and use programs in research, education, and testing. 2nd edition. CRC Press, Taylor & Francis, Boca Raton. 2017;1-28. https://doi.org/10.1201/9781315152189-4.

26. The European Committee on Antimicrobial Susceptibility Testing. Routine and extended internal quality control for MIC determination and disk diffusion as recommended by EUCAST. Version 13.1, 2023. Access January 20th, 2025. http://www.eucast.org.

27. Stepanovic S, Vukovic D, Dakic I, Savic B, Svabic-Vlahovic M. A modified microtiter-plate test for quantification of staphylococcal biofilm formation. J Microbiol Methods. 2000;40(2):175-9. https://doi.org/10.1016/s0167-7012(00)00122-6

28. Tkachuk NV, Zelena LB, Parminska VS, Yanchenko VO, Demchenko AM. Identification of Heterotrophic Bacteria Isolated from Soil Ferrosphere and their Sensitivity to the Pesticide Linuron. Mikrobiol. Z. 2017; 79(4):75-87. https://doi.org/10.15407/microbiolj79.04.075

29. Tamura K, Stecher G, Peterson D, Filipski A, Kumar S. MEGA6: Molecular Evolutionary Genetics Analysis version 6.0. Molecular Biology and Evolution, 2013;30(12):2725–2729, https://doi.org/10.1093/molbev/mst197.

30. World Health Organization. One Health. Access February 16th, 2025: https://www.who.int/health-topics/one-health#tab=tab_1.

31. Papatsiros VG, Athanasiou LV, Spanou VM, Stylianaki I, Papakonstantinou G, Letsios M, et al. First case of Serratia liquefaciens isolated from urinary tract infection in sows and associated clinicopathological and pathological findings. Lett Appl Microbiol. 2020;70(4):259-262. https://doi.org/10.1111/lam.13267.

32. Franchini D, Paci S, Ciccarelli S, Valastro C, Greco G, Di Bello A. Chondroblastic Osteosarcoma Associated with Previous Chronic Osteomyelitis Caused by Serratia liquefaciens in a German Shepherd Dog. Vet Sci. 2022;9(3):96. https://doi.org/10.3390/vetsci9030096.

33. Machado SG, da Silva FL, Bazzolli DM, Heyndrickx M, Costa PM, Vanetti MC. Pseudomonas spp. and Serratia liquefaciens as Predominant Spoilers in Cold Raw Milk. J Food Sci. 2015;80(8):M1842-9. https://doi.org/10.1111/1750-3841.12957.

34. McIntosh D, Austin B. Recovery of an extremely proteolytic form of Serratia liquefaciens as a pathogen of Atlantic salmon, Salmo salar, in Scotland. Journal of Fish Biology, 1990;36, 765-772. https://doi.org/10.3390/biology12081135

35. Aydın SM, Erman Z, Bilgin OC. (2001). Investigations of Serratia liquefaciens infection in rainbow trout (Oncorhynchus mykiss Walbaum). *Turkish Journal of Veterinary & Animal Sciences.* 2001;*25*(5): 643-650. https://journals.tubitak.gov.tr/veterinary/vol25/iss5/2/

36. Starliper CE. Isolation of Serratia liquefaciens as a pathogen of Arctic char, Salvelinus alpinus (L.). *Journal of Fish Diseases*. 2008;24(1):53-56, https://doi.org/10.1046/j.1365-2761.2001.00266.

37. Oktariani AF, Ramona Y, Sudaryatma PE, Dewi IAMM, Shetty K. Role of Marine Bacterial Contaminants in Histamine Formation in Seafood Products: A Review. Microorganisms. 2022;10(6):1197. https://doi.org/10.3390/microorganisms10061197.

38. Livermore DM, Winstanley TG, Shannon KP. Interpretative reading: recognizing the unusual and inferring resistance mechanisms from resistance phenotypes. J. Antimicrob. Chemother. 2001.48(Suppl. 1):87–102. https://doi.org/10.1093/jac/48.suppl_1.87.

39. Van Duin D., Paterson DL. Multidrug-Resistant Bacteria in the Community: An Update. Infectious disease clinics of North America, 2020;34(4), 709–722. https://doi.org/10.1016/j.idc.2020.08.002.

40. Bava R, Castagna F, Lupia C, Poerio G, Liguori G, Lombardi R, et al. Antimicrobial Resistance in Livestock: A Serious Threat to Public Health. Antibiotics. 2024;13(6),551. https://doi.org/10.3390/antibiotics13060551.

41. Męcik M, Buta-Hubeny M, Paukszto Ł, Maździarz M, Wolak I, Harnisz M, et al. Poultry manure-derived microorganisms as a reservoir and source of antibiotic resistance genes transferred to soil autochthonous microorganisms, Journal of Environmental Management, 2023; 348:119303. https://doi.org/10.1016/j.jenvman.2023.119303.

42. Ding J, Yang W, Liu X, Zhao J, Fu X, Zhang F, et al. Hydraulic conditions control the abundance of antibiotic resistance genes and their potential host microorganisms in a frequently regulated river-lake system. Sci Total Environ. 2024;946:174143. https://doi.org/10.1016/j.scitotenv.2024.174143.

43. Liu M, Huang Y, Sun Y, Sun Y, Ren X, Xuan Y, et al. Analysis of antibiotic resistance genes and potential host microorganisms in atmospheric PM2.5 in the Beijing urban area, Journal of Environmental Chemical Engineering. 2025;13(2):115456. https://doi.org/10.1016/j.jece.2025.115456.

44. Rao W, Fang Z, Chen Z, Wu J, Fang X, Antibacterial mechanism of metabolites of Leuconostoc mesenteroides against Serratia liquefaciens,

LWT, 2023;187:115335. https://doi.org/10.1016/j.lwt.2023.115335

45. Gong J, Liu S, Wang H, Shao L, Chen S, Xu X, et al. Investigating meat-borne bacterial profiles related to biofilm formation: An in situ and in vitro assessment, Food Control, 2024;1572:110175. https://doi.org/10.1016/j.foodcont.2023.110175.
46. Fisher RG, 110 – Serratia, Editor(s): JCherry JD, Kaplan SL, Harrison GJ, Steinbach WJ, Hotez PJ, John V. Williams JV, Feigin and Cherry's Textbook of Pediatric Infectious Diseases (Ninth Edition), Elsevier, 2025, p.1098-1100.e3. https://doi.org/10.1056/NEJM197904193001604.
47. Park Y. Optimal two-stage group sequential designs based on Mann–Whitney–Wilcoxon test. PLOS ONE, 2025;20(2):e0318211. https://doi.org/10.1371/journal.pone.0318211.
48. Kishore K., Jaswal V. Statistics Corner: Wilcoxon–Mann–Whitney Test. Journal of Postgraduate Medical Education and Research, 2022;56(4):199–201. https://doi.org/10.2340/jrm.v57.42555
49. Nicholson WL, Leonard MT, Fajardo-Cavazos P, Panayotova N, Farmerie WG, Triplett EW, et al. Complete Genome Sequence of Serratia liquefaciens Strain ATCC 27592. Genome Announc. 2013;1(4):e00548-13. https://doi.org/10.1128/genomeA.00548-13.
50. Kleyn MS, Akinyemi MO, Bezuidenhout C, Adeleke RA. Draft genome sequences of three Serratia liquefaciens strains isolated from vegetables in South Africa. Microbiol Resour Announc. 2025:11;14(3):e0077224. https://doi.org/10.1128/mra.00772-24.

Date of receipt of the manuscript: 01.03.2025

Date of acceptance for publication: 18.12.2025

Liliia Vygovska, WoS Researcher ID: ADC-0717-2022, SCOPUS ID 57222986117;

Artem Ushkalov, SCOPUS ID 58069384100;

Liubov Zelena, WoS Researcher ID: IDH-7309-2013;

Ushkalov Valerii, WoS Researcher ID: AAS-4217-2020, SCOPUS ID 59473747300;

Yuriy Vishovan, SCOPUS ID 58643511800.

MEDICAL SCIENCES

OPEN ACCESS

SINGLE NUCLEOTIDE POLYMORPHISM TEST FOR RAPID DETECTION OF SARS-COV-2 LINEAGES IN THE REPUBLIC OF NORTH MACEDONIA

Gala MATEVSKA[1], Golubinka BOSHEVSKA[1,2], Elizabeta JANCHESKA[1], Teodora KAREVSKA[1], Maja VUKOVIKJ[1]

[1] Laboratory of Virology, Institute of Public Health, Skopje,
[2] Faculty of Medical Sciences, Goce Delcev University, Stip, North Macedonia

Corresponding author: Golubinka BOSHEVSKA, e-mail: golubinka.bosevska@ugd.edu.mk

https://doi.org/10.38045/ohrm.2026.1.04 CZU: [616.98:578.834.1]-07(497.17)

ABSTRACT

Introduction The coronavirus pandemic represents one of the most significant medical crises in recent history; therefore, rapid virus detection has become a critical component of public health practice. As the virus has undergone continuous mutations, the emergence of new variants has resulted in altered transmission dynamics, changes in disease severity, and implications for diagnostic testing. Although genomic sequencing is the most effective method for mutation detection, it remains time-consuming and expensive process.

Aim To present a testing algorithm and evaluate the use of single nucleotide polymorphism (SNP) melting curve PCR for the detection of SARS-CoV-2 lineages, which may inform modifications in public health control and preventive measures, as well as potential adjustments to PCR-based diagnostic tests.

Material and methods RNA extracted from 140 SARS-CoV-2 positive samples received in the National Reference Laboratory for Virology, at the Institute of Public Health – Skopje as part of the COVID-19 surveillance system where Ct value ≤ 25 were subjected to SNP testing.

Results Analysis of 140 SARS-CoV-2–positive samples collected between January and September 2022 using SNP testing revealed a predominance of the BA.4/BA.5 Omicron sublineages, accounting for 55.7% of cases.

Conclusions Targeted SNP assays enable rapid and accurate detection of mutations associated with specific SARS-CoV-2 Omicron sublineages, facilitating early identification of emerging variants. These results may subsequently be subjected to further investigation, ultimately contributing to an improved public health response.

Keywords Coronaviruses, Omicron, SARS-CoV-2, Melting curve analysis, Single Nucleotide Polymorphism.

TESTUL DE POLIMORFISM CU UN SINGUR NUCLEOTID PENTRU DETECTAREA RAPIDĂ A TULPINILOR SARS-COV-2 ÎN REPUBLICA MACEDONIA DE NORD

Introducere Pandemia de coronavirus reprezintă una dintre cele mai mari crize medicale din ultima vreme, prin urmare, detectarea rapidă a virusului a devenit o normalitate. Pe măsură ce virusul a suferit mutații, apariția de noi variante a dus la modificări ale dinamicii de transmitere și ale severității bolii, precum și remanieri în utilizarea testelor de diagnostic. Cea mai eficientă modalitate de a detecta mutațiile este secvențierea, care este un proces de durată și costisitor.

Scop Prezentarea unui algoritm de testare și elaborare a utilizării PCR cu curbă de topire a polimorfismului cu un singur nucleotid (SNP) pentru detectarea tulpinilor SARS-CoV-2, ceea ce poate duce la modificarea măsurilor de control al sănătății publice și a măsurilor preventive, dar și la posibile modificări ale testelor PCR, utilizate pentru detectarea SARS-CoV-2.

Material și metode ARN-ul extras din 140 de probe pozitive la SARS-CoV-2 recepționate în Laboratorul Național de Referință pentru Virusologie, la Institutul de Sănătate Publică - Skopje, ca parte a sistemului de supraveghere a COVID-19, unde valoarea Ct ≤ 25 a fost supusă testării SNP.

Rezultate Analiza a 140 de probe pozitive la SARS-CoV-2 din ianuarie până în septembrie 2022, utilizând testarea SNP, a identificat o prezență dominantă a subtulpinilor BA.4/BA.5 Omicron, reprezentând 55,7% dintre cazuri.

Concluzii Testele SNP specifice permit detectarea rapidă și precisă a mutațiilor legate de o subtulpină specifică a SARS-CoV-2 Omicron, ajutând la identificarea timpurie a variantelor emergente. Rezultatele obținute pot fi supuse, ulterior, unor examinări suplimentare, ceea ce ar putea genera un coeficient mai mare a cazurilor depistate.

Cuvinte-cheie Coronavirusuri, Omicron, SARS-CoV-2, analiza curbei de topire, polimorfism cu un singur nucleotid.

INTRODUCTION

In December 2019, cases with similar symptoms and clinical presentation caused by a new human pathogen were reported in Wuhan, China. The virus was named SARS-CoV-2 and the disease COVID-19. On March 11, 2020, the World Health Organization officially categorized the COVID-19 outbreak, a pandemic. The SARS-CoV-2 genome (30kb) has a single-stranded, positive-sense RNA. The main structural components of the virus are: glycoprotein S (Spike), membrane protein M, envelope protein E, and nucleocapsid protein N. In addition, the virus has six open reading frames. The RT-PCR test for detection of SARS-CoV-2 is recommended by WHO as first line test for detection of this virus. Rapid tests for antigen detection have also been developed (1, 2).

Since the appearance of SARS-CoV-2 in the human population, mutations had appeared in the virus's genome resulting in emergence of new variants (3). According to the infectious potential and virulence of the variants, the WHO classified them as Variants of Concern (VOCs), Variants of Interest (VOIs) and Variants Under Monitoring (VUMs). The VOCs are: Alfa (B.1.1.7), Beta (B.1.351), Gama (P.1), Delta (B.1.617.2) and Omicron (B.1.1.529). Currently the Omicron variant is circulating, from which several sub lineages evolved (4-15).

The Omicron variant was first detected on November 9, 2021, in the South African province of Gauteng. The number of confirmed infections per variant and the rapid emergence of each variant indicated that Omicron is more infectious than Delta and Beta (7). To date, it is the VOC with the highest number of non-synonymous mutations, most of which in the Spike protein and they cause increased transmission, disease severity, and immune response evasion (7). As such, the Omicron variant has received a lot of attention in healthcare around the world (11-14). More than 60 mutations have been identified in the Omicron variant, 30 of which are located in the S protein, with 15 in the RBD region. Compared to the other VOCs, Spike protein mutations in Omicron are 3-4 times more numerous including 30 substitutions: A67V, T95I, Y145D, L212I, G339D, S371L, S373P, S375F, K417N, N440K, G446S, S477N, T478K, E484A, Q493R, G496S, Q498R, N501Y, Y505H, T547K, D614G, H655Y, N679K, P681H, N764K, D796Y, N856K, Q954H, N969K, и L981F (13, 14, 16-18).

The Omicron variant initially gave rise to the BA.1 sublineage, followed by the more transmissible BA.2 sublineage, which rapidly became globally dominant. Comparison of the genetic profiles of the BA.1 and BA.2 sublineages revealed a total of 51 mutations across the genome, of which 32 are shared between the two sublineages (7, 13). Among the shared mutations, 21 occur in the spike (S) protein. Nineteen mutations define the unique genetic profiles of the respective sublineages, including 13 spike protein mutations specific to BA.1 (A67V, HV69del, T95I, VYY143del, N211del, L212I, 215EPEins, S371L, G446S, G496S, T547K, N856K, L981F) and seven spike protein mutations specific to BA.2 (T19I, LPPA24S, V213G, S371F, T376A, D405N, R408S) (7, 13, 16–20).

As the virus continued to evolve, the genetic sequences of the BA.4 and BA.5 sublineages were found to contain elements derived from both the BA.2 sublineage and the earlier Delta variant. At the Department of Virology, Institute of Public Health (IPH)–Skopje, a testing algorithm was developed using available commercial kits for the indirect detection of the emerging BA.4 and BA.5 sublineages. The assay targeted the L452R mutation, which is present in the Delta variant and in the BA.4 and BA.5 sublineages, but absent in BA.1 and BA.2. Consequently, in samples initially identified as BA.2, the detection of the L452R mutation suggested the presence of BA.4 or BA.5, prompting further sequencing for definitive genotyping (21).

To enhance epidemiological surveillance and ensure a rapid public health response, North Macedonia established the *National Program for Sequencing of SARS-CoV-2 and Other Highly Pathogenic Agents with Public Health Importance* in December 2021, with support from the World Health Organization. As part of this strategy, SNP testing was implemented as a pre-screening tool, particularly in view of the high cost of next-generation sequencing in low- and middle-income countries. SNP testing was used to differentiate between the BA.1 and BA.2 Omicron sublineages for diagnostic purposes and to select representative samples for sequencing in order to monitor viral evolution. This approach enables a strengthened public health response by facilitating timely implementation of appropriate control measures and optimization of diagnostic methods for the detection of emerging variants.

The aim of this study is to present a testing algorithm based on SNP melting curve PCR for the detection and differentiation of SARS-CoV-2 sublineages, with the potential to inform modifications of existing PCR-based diagnostic strategies. This method is particularly useful for targeted sampling during outbreak or cluster investigations. Routine screening of circulating variants and sublineages can thus be efficiently performed with high throughput, allowing for the selection of samples for additional next-generation sequencing while providing rapid and accurate results at a substantially lower cost.

MATERIALS AND METHODS

Materials

RNA was extracted from 140 samples received at the National Reference Laboratory for Virology, Institute of Public Health (IPH), Skopje, as part of the COVID-19 surveillance system. All samples tested positive for SARS-CoV-2 by real-time RT-PCR and had a cycle threshold (Ct) value ≤ 25. These samples were subjected to melting curve analysis.

Methods

RNA was extracted manually using the QIAamp Viral RNA (Qiagen) based on the manufacturer instructions. The principle is based on a combination of the selective binding capabilities of silica gel membranes and the centrifugation speed (22).

Melting Curve PCR

The principle of Melting Curve PCR is based on determining the melting point (Tm) of the DNA molecule. The Tm of DNA is the temperature at which half of the DNA molecules in the solution are denatured. It is monitored with fluorescent dyes intercalating with the DNA molecule and emitting a signal once bound to the still paired, double-stranded DNA. It depends on the number of G+C pairs in the target sequence, it's length and the ionic strength of the solution. The peak occurs at the temperature at which 50% of the DNA molecules are denatured. The analysis's dynamic approach enables rapid detection and genotyping. The result is used to confirm or exclude the presence of a specific single nucleotide polymorphism (SNP) characteristic for specific variants or sublineages (23, 24).

Reagents and Kits

Two commercial kits were used for SNP melting curve analysis:

1. VirSNiP SARS-CoV-2 Spike S371L/S373P Kit (Cat. No. 53-0827-96; TIB Molbiol) together with the corresponding Lyophilized 1-step RT-PCR Polymerase Mix (Cat. No. 90-9999-96; TIB Molbiol).
2. SARS-CoV-2 Delta Real-Time PCR Genotyping Kit (DNA Technology), which detects the L452R and T478K mutations. All procedures were performed according to the manufacturers' instructions.

The primers and probes in the VirSNiP kit target a specific region of the SARS-CoV-2 genome, generating distinct melting profiles depending on the mutation present. Detection of the S371L/S373P mutations indicates the BA.1 sublineage, whereas detection of the S371F/S373P mutations indicates the BA.2 sublineage (25). An additional assay targeting the L452R mutation, originally developed for Delta variant detection, was used to identify BA.4 or BA.5 sublineages (26).

The mastermix was prepared in a separate room under sterile conditions, in a PCR cabinet, according to the kit's protocol.

For the VirSNiP assay, the lyophilized 1-step RT-PCR Polymerase Mix was reconstituted with 990 µL buffer and gently mixed by pipetting. Primers and probes were rehydrated with 50 µL nuclease-free water, vortexed, and centrifuged before being added to the mastermix along with buffer, enzyme, and nuclease-free water. A volume of 15 µL mastermix was dispensed into each reaction tube, followed by the addition of 5 µL RNA sample (25).

For the purposes of this research, only the primers and probes for the L452R mutation were used from the SARS-CoV-2 DELTA REAL-TIME PCR Genotyping Kit. The buffer, enzyme and the PCR mix (primers and probes) were added to a 1,5µl tube and briefly vortexed. 15µl mastermix was placed into each tube, then 10µl from the RNA sample was added (26).

PCR amplification and melting curve analysis were performed using: PCR thermocycler (used: QuantStudio 5 Real-Time PCR System (manufacturer: Thermo Fisher Scientific – Waltham, Massachusetts, United States) and DTlite real-time PCR instrument (manufacturer: DNA Technology – Moscow, Russia).

Negative and positive controls were included in each PCR run to validate the reaction and monitor potential contamination. Two negative controls were used: one during nucleic acid extraction and one during RNA pipetting, along with a single positive control. Negative controls were required to show no fluorescence signal, whereas the positive control confirmed proper assay performance.

Results were interpreted based on the amplification curve and the cycle at which the fluorescence's exponential growth started. Where there is no signal the result is negative ("Undetermined"). This result should appear in the negative control. When analyzing the results, the focus is on the Amplification Plot and the Melting Curve Plot. Amplification should appear on the Amplification Plot in SARS-CoV-2 positive samples and a peak according to the detected mutation on the Melting Curve Plot. Negative controls should show no fluorescence in either plot. The detected Tm values were interpreted as follows: Tm = 53 °C indicated the BA.2 sublineage (S371F/S373P), Tm = 62 °C indicated the BA.1 sublineage (S371L/S373P), and Tm = 45 °C indicated a non-Omicron variant. Detection of two melting peaks in a single sample suggested either contamination or co-infection with multiple sublineages (25).

RESULTS

The Laboratory for Virology conducted routine testing as part of its central role in national surveillance and outbreak response, including the characterization of pathogens such as SARS-CoV-2 and identification of circulating sublineages to monitor their regional distribution. The results presented include analyses performed using the VirSNiP SARS-CoV-2 Spike S371L/S373P assay for the detection of BA.1 and BA.2 sublineages, as well as the SARS-CoV-2 Delta Real-Time PCR Genotyping Kit for the detection of sublineages indicative of BA.4 and BA.5.

Omicron sublineages circulating in Macedonia in January-September 2022

A total of 140 SARS-CoV-2 positive samples were selected for detection of Omicron sublineages with Melting Curve analysis. Using two different kits BA.1 was detected in 16 samples (11.4%), BA.2 was detected in 46 samples (32.9%) and sublineages indicative of BA.4 and BA.5 in 78 (55.7%) samples (fig. 1, 2).

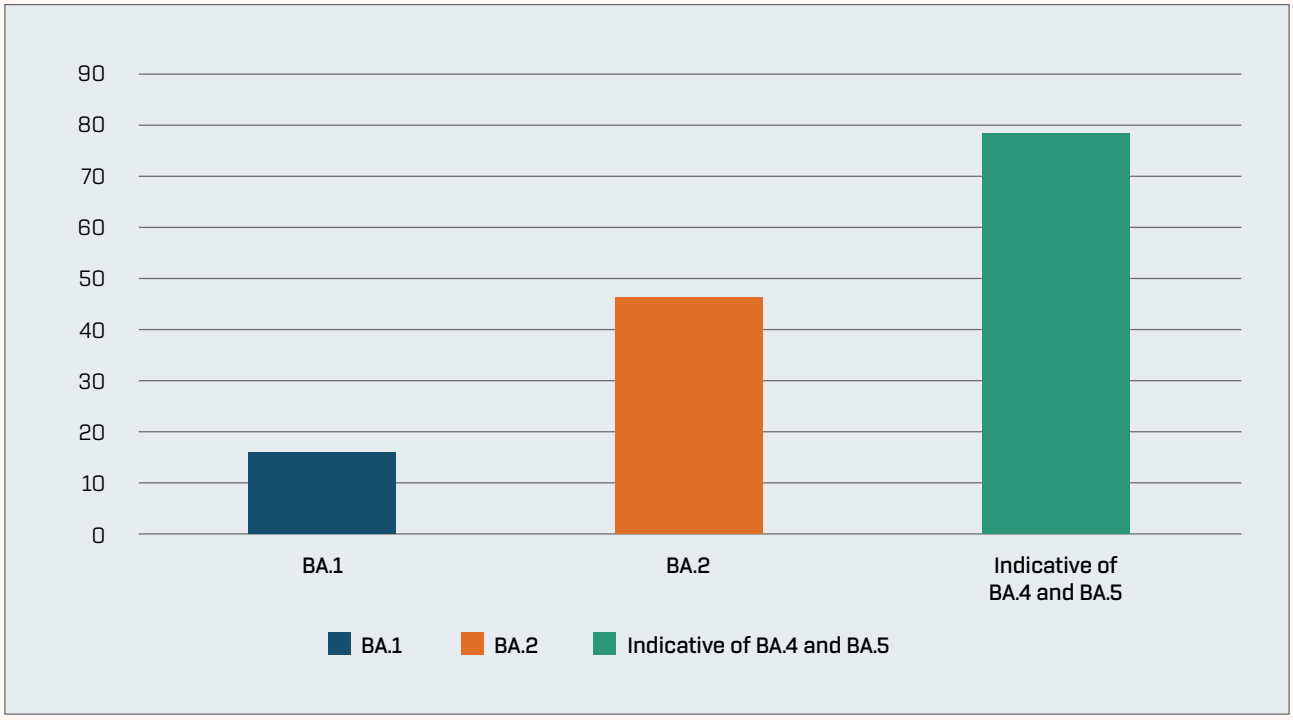

Figure 1. Number of Omicron sublineages between January-September 2022.

Appearance of Omicron sublineages according to collection date

All samples were collected between 10 January and 23 September 2022. The BA.1 sublineage circulated primarily from 10 January to 5 February 2022. The BA.2 sublineage subsequently emerged and increased in prevalence between 27 June and 30 June 2022, followed by a marked decline during the period from 3 August to 11 August 2022. From 23 August to 23 September 2022, a pronounced increase in cases indicative of the BA.4 and BA.5 sublineages was observed, while BA.2 circulation further decreased and BA.1 was no longer detected in the samples analyzed.

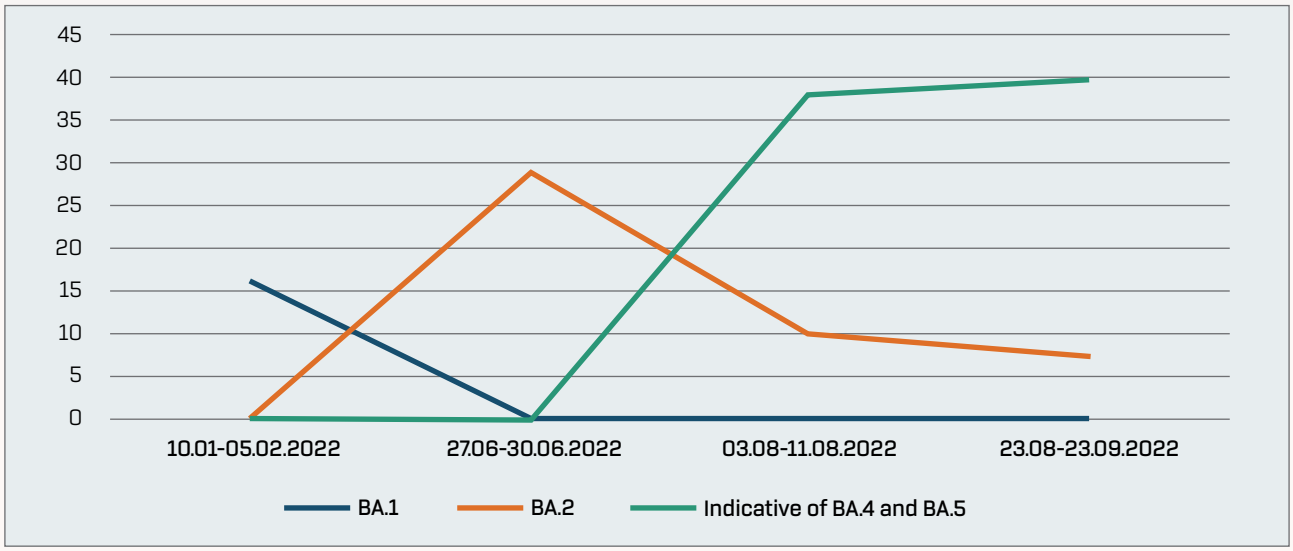

Figure 2. Emergence of Omicron sublineages, their increase and decrease according to their collection date.

City distribution

Figure 3 shows the distribution and number of patients in which the Omicron sublineages were detected.

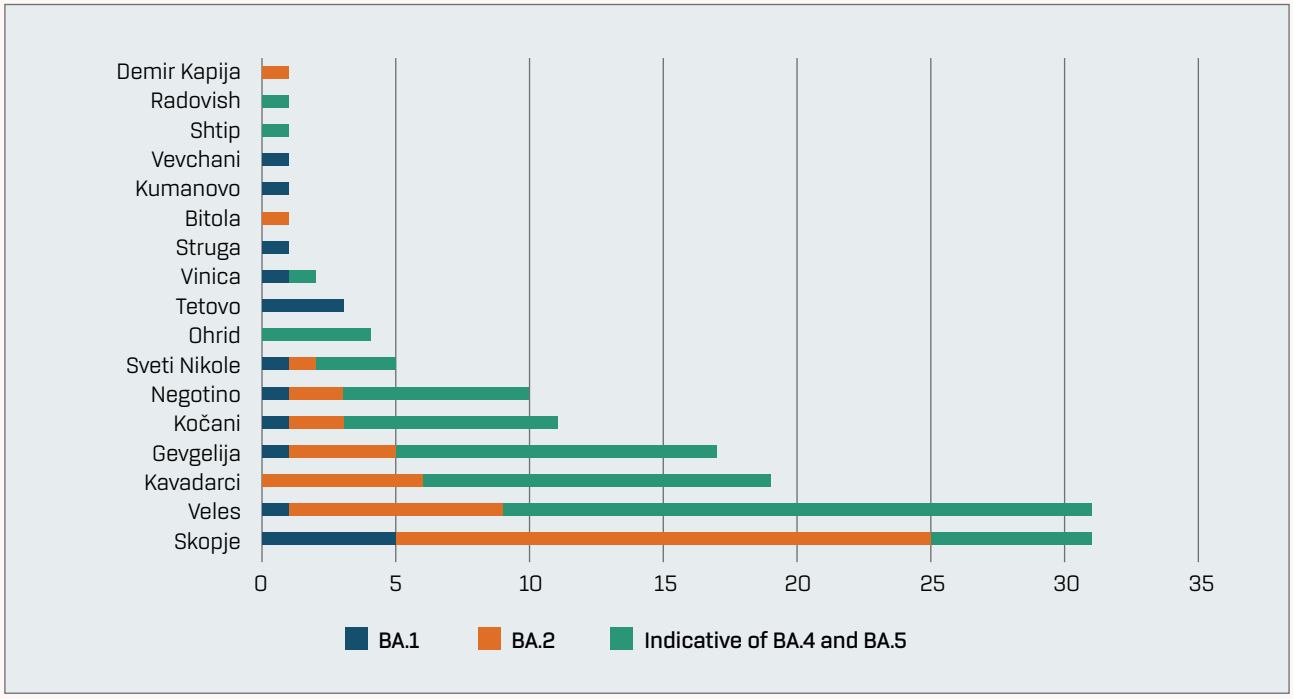

Figure 3. Distribution of Omicron sublineages across cities in Macedonia.

Distribution by sex and age

From all analyzed patients, 66 were male and 74 were female (fig. 4).

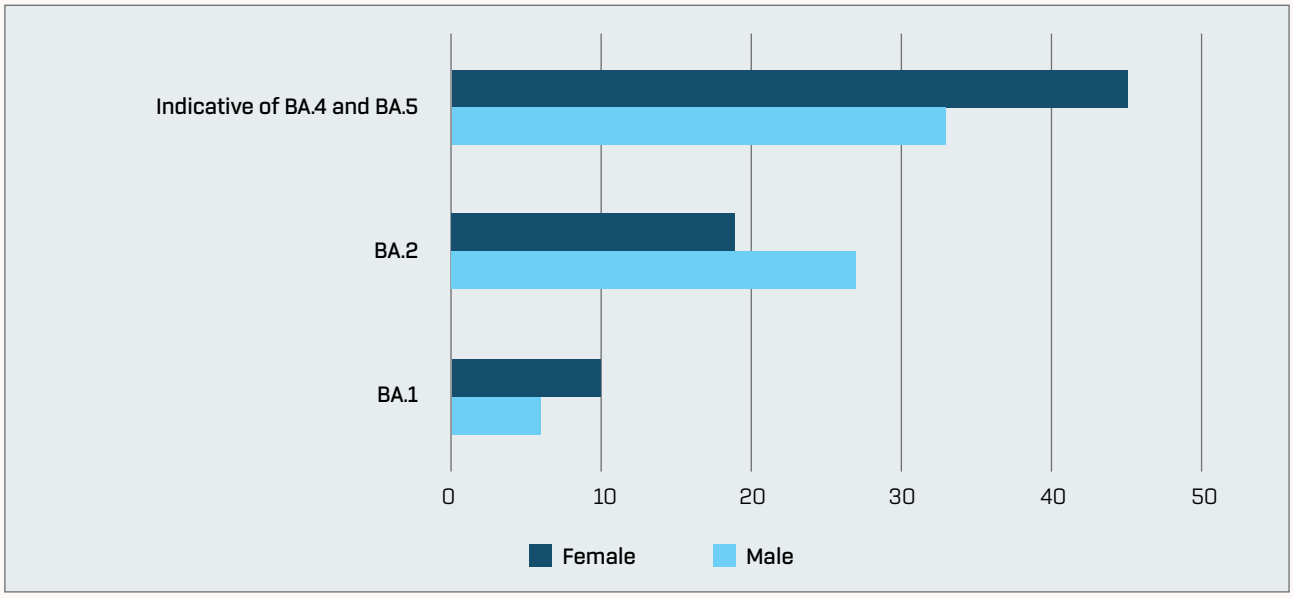

Figure 4. Distribution of Omicron cases and their sublineages, in men and women separately.

The majority of positive patients belong to the 30-64 age group (fig. 5). The exact ages of the patients range from 1 to 88 and the median age is 61,5.

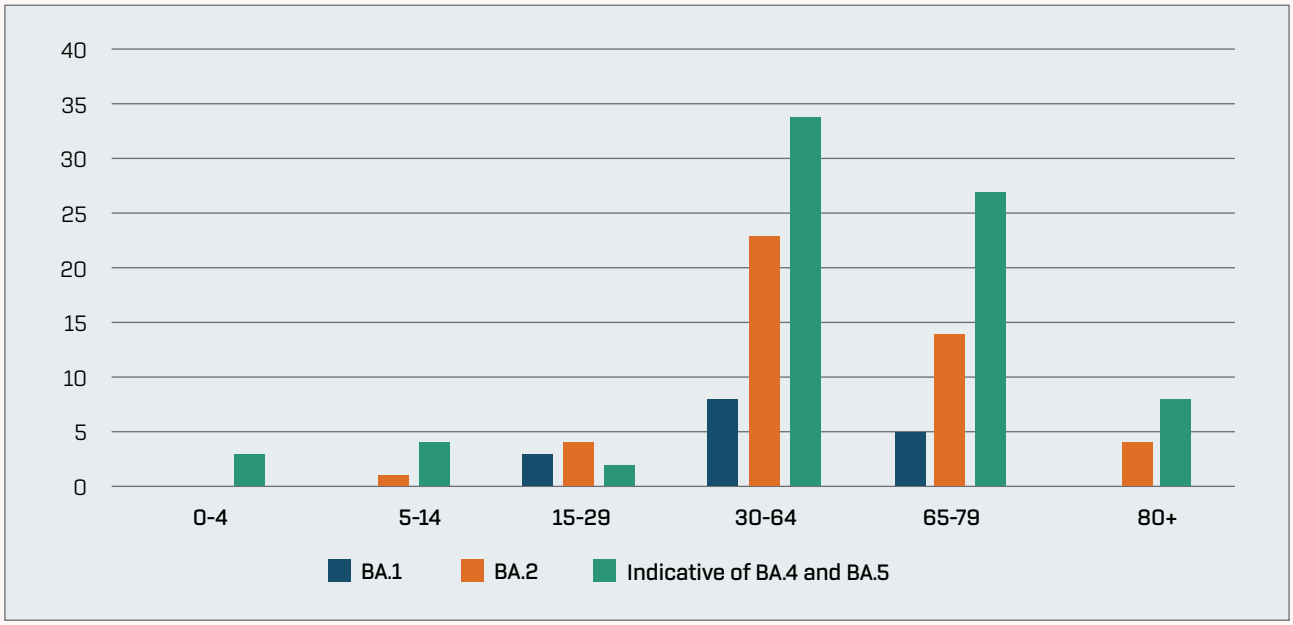

Figure 5. Distribution of Omicron patients and their sublineages across all age groups.

DISCUSSION

Real time surveillance of the prevalence and spread of circulating SARS-CoV-2 variants in the country enables early detection of new VOCs and VOIs with possible emergence of new SARS-CoV-2 variants and sublineages as a result of the appearance of new mutations in the genome.

The performance of laboratory diagnostic assays, particularly PCR-based methods, may be affected by the emergence of new variants. Therefore, rapid detection of genetic changes is critical to allow timely adaptation of diagnostic kits and to ensure continued accuracy of testing. For routine screening and differentiation of the BA.1 and BA.2 sublineages, melting curve analysis demonstrated satisfactory performance, particularly due to its short turnaround time of approximately 53 minutes. These assays complement sequencing-based surveillance by enabling monitoring of variants circulating at frequencies below 5%, thereby increasing the overall number of samples under surveillance (27). Furthermore, melting curve analysis facilitates the rapid design of new primer sets targeting mutations specific to newly emerging variants. In this study, only samples with Ct values ≤ 25 were included, as lower Ct values indicate higher viral RNA concentrations and are associated with improved assay reliability and result quality (26).

During the period from January to August 2022, a clear replacement of the BA.1 sublineage by BA.2 was observed, followed by the emergence and increasing circulation of BA.4 and BA.5 sublineages (28). Consequently, BA.1 accounted for the smallest proportion of detected cases, while the majority were indicative of BA.4 and BA.5. Although these sublineages were initially classified as VOCs, the European Centre for Disease Prevention and Control (ECDC) de-escalated BA.2, BA.4, and BA.5 from VOC status on 3 March 2023, as they were no longer circulating at that time (29).

The majority of analyzed positive cases were from Skopje, as a capital city with largest number of SARS-CoV-2 cases, and from Veles. However, in order to get a representative picture of the Omicron positive cases in the country, it is recommended to select a specific number of samples for SNP assay based on the number of detected SARS-CoV-2 cases and the proportional distribution of circulating variants across regions.

No association was observed between SARS-CoV-2 infection and patient age or sex. The highest number of cases occurred in individuals aged 30–64 years, while the lowest number was observed among children aged 0–4 years. A limitation of this study is that only a small proportion of the total SARS-CoV-2–positive cases during the study period was included. However, existing literature indicates that SARS-CoV-2 infection and Omicron sublineages are distributed across all age groups and are not significantly influenced by patient age or sex (7).

Eventually, the existing tests may stop detecting the positive cases due to acquired mutations or may not be able to differentiate the sublineages. Therefore, it is recommended that diagnostic kits target multiple genomic regions to ensure sustained performance. In periods of high variant prevalence, melting curve analysis provides an efficient method for continuous variant monitoring, significantly reducing reliance on sequencing, which requires longer processing times, specialized bioinformatics expertise, higher reagent costs, and extensive instrument calibration and maintenance.

According to the *National Program for Sequencing of SARS-CoV-2 and Other Highly Pathogenic Agents with Public Health Importance*, a minimum of 10% of randomly selected positive pre-screening samples are planned to undergo sequencing to estimate the prevalence of circulating variants. Conse-

quently, mutation detection assays such as melting curve analysis are widely employed in resource-limited settings to monitor how genomic mutations influence viral transmission and clinical presentation. This information is essential for vaccine development and supports the modeling of public health prevention and control strategies aimed at limiting the spread of highly pathogenic variants.

LIMITATIONS

A limitation of this study is the potential for false-positive results, which may arise from non-specific binding of probes or primers, as well as from sample contamination. Conversely, false-negative results may occur due to improper sample storage conditions, including prolonged exposure to light, inappropriate temperatures, or repeated freeze–thaw cycles.

An additional limitation relates to the selected time intervals, which were determined by the availability of the diagnostic kits used in this study. These constraints resulted from global delays and increased demand for testing during the COVID-19 pandemic, particularly following the emergence of the Omicron variant. During these periods, the laboratory team employed alternative testing assays and surveillance strategies that are not included in the present analysis.

CONCLUSIONS

1. Molecular techniques, due to their high specificity, sensitivity, and flexibility, have a significant and broad applicability in the detection and monitoring of viral infections.
2. Melting Curve analysis, based on the detection of a specific SNP, enables rapid and accurate identification of mutations, allowing precise discrimination of Omicron sublineages.
3. This approach is particularly valuable for the selection of samples for sequencing, especially when changes in the clinical or epidemiological patterns of viral infections are observed.
4. The method facilitates early detection of emerging viral variants and supports the timely implementation of appropriate public health measures.
5. The results obtained can be further subjected to additional analyses of public health relevance, contributing to the optimization of diagnostic strategies and strengthening epidemiological surveillance systems.

CONFLICT OF INTEREST

None declared.

ETHICAL APPROVAL

Ethical considerations are addressed within the *National Program for Sequencing of SARS-CoV-2 and Other Highly Pathogenic Agents with Public Health Importance*. The program stipulates that all positive samples are anonymized through coding, ensuring that no direct link exists between patient identity and SNP or sequencing results. Metadata are linked to SNP and sequencing data solely for epidemiological analysis and the implementation of public health measures, without any possibility of identifying individual patients.

REFERENCES

1. Holmes EC, Goldstein SA, Rasmussen AL, et al. The origins of SARS-CoV-2: A critical review. *Cell*. 2021;184(19):4848-4856. https://doi.org/10.1016/j.cell.2021.08.017.
2. Wang MY, Zhao R, Gao LJ, Gao XF, Wang DP, Cao JM. SARS-CoV-2: Structure, Biology, and Structure-Based Therapeutics Development. *Front Cell Infect Microbiol*. 2020;10:587269. https://doi.org/10.3389/fcimb.2020.587269.
3. World Health Organization. Interim guidance, Diagnostic testing for SARS-CoV-2, 11 September 2020. Accessed March 20th, 2023. https://iris.who.int/bitstream/handle/10665/334254/WHO-2019-nCoV-laboratory-2020.6-eng.pdf?sequence=1odic.
4. World Health Organization. WHO announces simple, easy-to-say labels for SARS-CoV-2 Variants of Interest and Concern, 31 May 2021, Accessed March 3rd, 2023. https://www.who.int/news/item/31-05-2021-who-announces-simple-easy-to-say-labels-for-sars-cov-2-variants-of-interest-and-concern.
5. Coronaviridae Study Group of the Internation al Committee on Taxonomy of Viruses. The species Severe acute respiratory syndrome-related coronavirus: classifying 2019-nCoV and naming it SARS-CoV-2. *Nat Microbiol*. 2020;5(4):536-544. https://doi.org/10.1038/s41564-020-0695-z
6. Huang C, Wang Y, Li X, et al. Clinical features of patients infected with 2019 novel coronavirus in Wuhan, China. *Lancet*. 2020;395(10223):497-506. https://doi.org/10.1016/S0140-6736(20)30183-5
7. World Health Organization. Coronavirus. Accesed April 14th 2023. https://www.who.int/health-topics/coronavirus#tab=tab_1.
8. Acuti Martellucci C, Flacco ME, Cappadona R, Bravi F, Mantovani L, Manzoli L. SARS-CoV-2 pandemic: An overview. *Adv Biol Regul*. 2020;77:100736. https://doi.org/10.1016/j.jbior.2020.100736.
9. Hardenbrook NJ, Zhang P. A structural view of the SARS-CoV-2 virus and its assembly. *Curr Opin Virol*. 2022;52:123-134. https://doi.org/10.1016/j.coviro.2021.11.011.
10. Watanabe Y, Allen JD, Wrapp D, McLellan JS, Crispin M. Site-specific glycan analysis of the SARS-CoV-2 spike. *Science*. 2020;369(6501):330-333. https://doi.org/10.1126/science.abb9983.
11. Sánchez-Morales L, Sánchez-Vizcaíno JM, Pérez-Sancho M, Domínguez L, Barroso-Arévalo S. The Omicron (B.1.1.529) SARS-CoV-2 variant of concern also affects companion animals. *Front Vet Sci*. 2022;9:940710. https://doi.org/10.3389/fvets.2022.940710
12. Kandeel M, Mohamed MEM, Abd El-Lateef HM, Venugopala KN, El-Beltagi HS. Omicron variant genome evolution and phylogenetics. *J Med Virol*. 2022;94(4):1627-1632. https://doi.org/10.1002/jmv.27515
13. He X, Hong W, Pan X, Lu G, Wei X. SARS-CoV-2 Omicron variant: Characteristics and prevention. *MedComm (2020)*. 2021;2(4):838-845. https://doi.org/10.1002/mco2.110
14. Liu H, Wei P, Kappler JW, Marrack P, Zhang G. SARS-CoV-2 Variants of Concern and Variants of Interest Receptor Binding Domain Mutations and Virus Infectivity. *Front Immunol*. 2022;13:825256. https://doi.org/10.3389/fimmu.2022.825256
15. World Health Organization. Tracking SARS-CoV-2 variants. Accessed May 10th, 2023. https://www.who.int/activities/tracking-SARS-CoV-2-variants.
16. Korber B, Fischer WM, Gnanakaran S, et al. Tracking Changes in SARS-CoV-2 Spike: Evidence that D614G Increases Infectivity of the COVID-19 Virus. *Cell*. 2020;182(4):812-827.e19. https://doi.org/10.1016/j.cell.2020.06.043
17. Plante JA, Liu Y, Liu J, et al. Spike mutation D614G alters SARS-CoV-2 fitness. *Nature*. 2021;592(7852):116-121. https://doi.org/10.1038/s41586-020-2895-3
18. Volz E, Hill V, McCrone JT, et al. Evaluating the Effects of SARS-CoV-2 Spike Mutation D614G on Transmissibility and Pathogenicity. *Cell*. 2021;184(1):64-75.e11. https://doi.org/10.1016/j.cell.2020.11.020
19. Majumdar S, Sarkar R. Mutational and phylogenetic analyses of the two lineages of the Omicron variant. *J Med Virol*. 2022;94(5):1777-1779. https://doi.org/10.1002/jmv.27558
20. Alkhatib M, Salpini R, Carioti L, et al. Update on SARS-CoV-2 Omicron Variant of Concern and Its Peculiar Mutational Profile. *Microbiol Spectr*. 2022;10(2):e0273221. https://doi.org/10.1128/spectrum.02732-21
21. Tegally H, Moir M, Everatt J, et al. Emergence of SARS-CoV-2 Omicron lineages BA.4 and BA.5 in South Africa. *Nat Med*. 2022;28(9):1785-1790. https://doi.org/10.1038/s41591-022-01911-2
22. QIAGEN https://www.qiagen.com/dk/resources/resourcedetail?id=c80685c0-4103-49ea-aa72-8989420e3018&lang=en. Accessed March 23, 2023.
23. Pryor RJ, Wittwer CT. Real-time polymerase chain reaction and melting curve analysis. In: Walker M. J., ed. *Methods in Molecular Biology*. New Jersey: Humana Press; 2006;336:19-32. https://doi.org/10.1385/1-59745-074-X:19
24. Sit BHM, Po KHL, Cheung YY, et al. Detection of SARS-CoV-2 VOC-Omicron using commercial sample-to-answer real-time RT-PCR platforms and melting curve-based SNP assays. *J Clin Virol Plus*. 2022;2(3):100091. https://doi.org/10.1016/j.jcvp.2022.100091
25. TIB MOLBIOL https://www.tib-molbiol.de/fileadmin/user_upload/Covis-19/VirSNiP/Manuals/53-0827-96_VirSNP_S371L-S373P_V211129_09634835001.pdf. Accessed March 23, 2023.
26. Kit protocol for SARS-CoV-2 DELTA REAL-TIME PCR Genotyping Kit by the manufacturer DNA Technology.
27. European Center for Disease and Control. Sequencing of SARS-CoV-2 – first update. Accessed: April 18th 2022. https://www.ecdc.europa.eu/en/publications-data/sequencing-sars-cov-2.
28. Park, Kyemyung et al. Omicron Subvariants, Including BA.4 and BA.5, Substantially Preserve T Cell Epitopes of Ancestral SARS-CoV-2. *Immune network* 2022;3;22(4):e29. https://doi.org/10.4110/in.2022.22.e29.
29. European Centre for Disease Prevention and Control. ECDC de-escalates BA.2, BA.4 and BA.5 from its list of variants of concern, March 3rd 2023, Accessed November, 1st 2025. https://www.ecdc.europa.eu/en/news-events/ecdc-de-escalates-ba2-ba4-and-ba5-its-list-variants-concern.

Date of receipt of the manuscript: 07.03.2025
Date of acceptance for publication: 18.12.2025
Golubinka Boshevska, WoS Researcher ID: LRT-9770-2024, SCOPUS ID 57325991500

MEDICAL SCIENCES

OPEN ACCESS

CLINICAL, BIOCHEMICAL, AND GENETIC DISTINCTIONS IN PATIENTS WITH MITOCHONDRIAL INVOLVEMENT VERSUS OTHER GENETIC DISORDERS

Doina SECU, Daniela BLANITA, Natalia USURELU, Victoria SACARA

Institute of Mother and Child, Chisinau, Republic of Moldova

Corresponding author:Secu Doina, e-mail: secudoina95@gmail.md

https://doi.org/10.38045/ohrm.2026.1.05 CZU: 616-056.7:[575.224:576.311.347]

ABSTRACT

Introduction Mitochondrial diseases are clinically and genetically heterogeneous disorders characterized by respiratory chain dysfunction, often mimicking other multisystem genetic conditions, necessitating an integrated clinical, biochemical, and molecular diagnosis. This study aims to compare the clinical, biochemical, and genetic profiles of patients with mitochondrial involvement and those with other inherited genetic disorders.

Material and methods We analyzed 81 patients with suspected mitochondrial disease (Nijmegen Mitochondrial Disease Score ≥3), categorized into Group 1 (mitochondrial involvement) and Group 2 (other inherited disorders). Clinical, biochemical, instrumental, and molecular evaluations were performed using qPCR-HRM and Sanger sequencing, with data analyzed through descriptive statistics and non-parametric tests.

Results Group 1 showed significantly higher rates of severe neuromuscular impairment, skill regression, ocular abnormalities, elevated plasma lactate and alanine, and characteristic neuroimaging findings, including basal ganglia abnormalities and cerebral-cerebellar atrophy. Genetic analysis identified phenotype-associated mutations in 32 patients, primarily affecting Complex I and V subunits and mitochondrial RNA genes, often involving multiple respiratory chain sites. Group 2 comprised a range of genetically confirmed non-mitochondrial disorders, identified through targeted genomic testing.

Conclusions This study highlights the crucial role of integrated clinical, biochemical, and genomic approaches, emphasizing the importance of comprehensive molecular testing and multidisciplinary evaluation in addressing the diagnostic complexities of overlapping genetic disorders.

Keywords Mitochondrial diseases, mitochondrial DNA, Sanger sequencing, qPCR-HRM.

CARACTERISTICI CLINICE, BIOCHIMICE ȘI GENETICE DISTINCTIVE LA PACIENȚII CU AFECTARE MITOCONDRIALĂ COMPARATIV CU ALTE AFECȚIUNI GENETICE EREDITARE

Introducere Bolile mitocondriale reprezintă tulburări clinice și genetice eterogene, caracterizate prin disfuncția lanțului respirator, frecvent mimând alte afecțiuni genetice multisistemice, ceea ce impune un diagnostic integrat clinic, biochimic și molecular. Acest studiu își propune să compare profilurile clinice, biochimice și genetice ale pacienților cu afectare mitocondrială și ale celor diagnosticați cu alte boli genetice ereditare.

Material și metode Au fost analizați 81 de pacienți cu suspiciune de boală mitocondrială (Scor clinic Nijmegen ≥3), împărțiți în două grupuri-țintă: grupul 1 (afectare mitocondrială) și grupul 2 (alte afecțiuni ereditare). Evaluările clinice, biochimice, instrumentale și moleculare au inclus qPCR-HRM și secvențierea Sanger, iar datele au fost analizate prin statistica descriptivă și teste neparametrice.

Rezultate Grupul 1 a prezentat rate semnificativ mai mari de afectare neuromusculară severă: pierderea achizițiilor motorii, anomalii oculare, lactat și alanină plasmatică crescute, precum și modificări neuroimagistice caracteristice (afectarea ganglionilor bazali, atrofie cerebrală și cerebeloasă). Testele genetice au identificat mutații asociate fenotipului la 32 dintre pacienți, predominant în subunitățile Complexelor I și V și genele ARN mitocondrial, adesea cu implicare concomitentă a mai multor complexe respiratorii. Grupul 2 a inclus o varietate de afecțiuni genetice non-mitocondriale, confirmate prin teste genomice țintite.

Concluzii Studiul subliniază rolul esențial al abordării integrate clinic, biochimic și genomic, accentuând testarea moleculară completă și evaluarea multidisciplinară pentru a depăși complexitatea diagnosticului în afecțiunile genetice suprapuse.

Cuvinte-cheie Boli mitocondriale, ADN mitocondrial, secvențiere Sanger, qPCR-HRM.

INTRODUCTION

Mitochondrial diseases represent a clinically and genetically heterogeneous group of disorders caused by dysfunction of the mitochondrial respiratory chain, predominantly affecting tissues with high energy demands. With an estimated prevalence of approximately 1 in 4,300 individuals, they are among the most common inherited metabolic disorders (1). However, establishing a definitive diagnosis remains challenging due to the nonspecific and overlapping nature of clinical manifestations, which often mimic those of other multisystem genetic conditions (2, 3).

In the absence of universally reliable biomarkers, the diagnostic evaluation of patients with suspected mitochondrial involvement often relies on integrative clinical scores, such as the Nijmegen Mitochondrial Disease Score (NMDS) (4). These tools incorporate clinical symptoms, biochemical findings, and instrumental investigations to guide further testing. However, their utility in distinguishing mitochondrial involvement from other genetic disorders remains limited, particularly in the absence of molecular confirmation.

In this context, targeted molecular screening approaches, such as High-Resolution Melting qPCR (qPCR-HRM) for common mitochondrial DNA mutations, followed by Sanger sequencing of coding mitochondrial genes in high-scoring patients, can enhance diagnostic accuracy. Importantly, a substantial proportion of individuals referred for suspected mitochondrial disease are ultimately found to harbor pathogenic variants associated with non-mitochondrial genetic syndromes, many of which present with phenotypes that closely resemble mitochondrial disorders.

This study aims to conduct a comparative analysis of the clinical, biochemical, and genetic features of patients with mitochondrial involvement, defined by the presence of mitochondrial DNA mutations consistent with the individual phenotype, and those diagnosed with other inherited genetic disorders.

MATERIALS AND METHODS

This research was designed as an observational, prospective study and was conducted between March 2021 and November 2024 at the National Center for Reproductive Health and Medical Genetics, Institute of Mother and Child, Republic of Moldova.

Patient Selection and Cohort Overview

Patient selection was based on clinical suspicion of mitochondrial disease, assessed using the Nijmegen Mitochondrial Disease Score (NMDS), a validated, domain-based diagnostic tool that integrates clinical manifestations, metabolic and biochemical abnormalities, neuroimaging findings, and, in its original form, muscle biopsy and respiratory chain enzymology (4). In the original scoring system, NMDS values of 0–1 indicate that mitochondrial disease is unlikely; scores of 2–4 suggest possible mitochondrial disease; 5–7 indicate probable disease; and scores of 8 or higher are consistent with definite mitochondrial involvement.

In this study, a modified version of the NMDS was implemented to accommodate local diagnostic constraints. The entire biopsy and enzymatic domain (Section IV of the original NMDS), which includes histopathological features such as ragged-red fibers, cytochrome c oxidase–negative fibers, and respiratory chain complex deficiencies, was omitted due to the limited availability of

muscle biopsy and enzymatic testing in our setting. The modified NMDS was therefore calculated using only the remaining domains: clinical, biochemical/metabolic, and neuroimaging criteria. Importantly, the internal scoring within each retained category remained unchanged; as a result, while the maximum attainable score was reduced, the relative weight and discriminative structure of the scale were preserved.

Given that the modification reduced the maximum attainable score, a threshold of ≥3 points was retained to preserve diagnostic sensitivity. This decision was supported by two considerations: first, published NMDS classifications indicate that scores of 3 or higher already correspond to the "possible mitochondrial disease" category, capturing early or partially expressed phenotypes; second, preliminary assessment of our dataset showed that maintaining this threshold ensured adequate inclusion of patients who were later found to carry pathogenic mitochondrial variants, whereas increasing it would have excluded clinically relevant cases. The resulting modified NMDS thus represents a pragmatic and context-adapted approach that preserves the scale's discriminatory structure in the absence of biopsy data.

Written informed consent was obtained from all patients or their legal guardians prior to inclusion, ensuring voluntary participation and compliance with ethical research standards.

A total of 240 patients with a modified NMDS ≥3 were initially enrolled. From this cohort, 81 patients for whom a molecular genetic result suggestive of a specific diagnosis had been received were selected for comparative analysis:

- Group 1 (n = 37): Patients with mitochondrial involvement, defined by the presence of mitochondrial DNA variants, identified via qPCR-HRM or Sanger sequencing, that correlated with the patient's clinical phenotype, as well as five patients with variants in nuclear genes related to mitochondrial function, identified through next-generation sequencing or targeted Sanger analysis.
- Group 2 (n = 44): Patients with other inherited genetic disorders, diagnosed through targeted gene panels, clinical exome sequencing, or other molecular approaches.

Clinical and Laboratory Assessment

All patients included in the study underwent a detailed clinical assessment, including both medical history and neurological examination. Standard laboratory testing comprised hematological parameters, kidney and liver function, serum electrolytes, blood gas analysis, lactate, creatine kinase, and uric acid. In addition, ammonia levels, urinary organic acid analysis, acylcarnitine profile, and plasma amino acid profiles were included, when available, as part of the extended metabolic assessment. Complementary instrumental evaluations, such as electromyography, electroencephalography, electrocardiography, audiometry, and cerebral imaging (MRI or CT) were performed based on symptomatology to evaluate multisystemic or neurological involvement.

Molecular and Genetic Profiling

All patients first underwent molecular prescreening at the Scientific Laboratory of Human Molecular Genetics, Institute of Mother and Child, using a high-resolution melting (qPCR-HRM) assay targeting seven recurrent mitochondrial DNA point mutations (m.3243A>G, m.8344A>G, m.8993T>G/C, m.13513G>A, m.3460G>A, m.11778G>A, and m.14484T>C). The assay was specifically optimized for the detection of these canonical pathogenic variants, with its analytical performance validated using synthetic oligonucleotide

controls encompassing both wild-type and mutant sequences, thereby providing internal reference standards for melting-curve profiling and calibration. Given the intrinsic limitations of HRM in reliably detecting variants at low heteroplasmic levels, the workflow was systematically complemented by PCR-RFLP analysis, with fragment ratios quantified in ImageJ to obtain a semi-quantitative estimation of heteroplasmy. Importantly, all cases with positive, borderline, or otherwise inconclusive HRM signatures were advanced to confirmatory Sanger sequencing of the corresponding mitochondrial regions, ensuring definitive molecular characterization and mitigating the risk of false-positive or unresolved findings.

Patients with a modified Nijmegen score of ≥6, as well as those exhibiting suggestive or ambiguous findings on the initial screening assay, were referred for targeted mitochondrial genome sequencing using Sanger sequencing by capillary electrophoresis. This analysis encompassed all 13 protein-coding mitochondrial genes, along with the adjacent mitochondrial rRNA and tRNA regions, ensuring coverage of genomic loci with established relevance to primary mitochondrial pathology. All detected variants were systematically evaluated and classified according to the American College of Medical Genetics and Genomics (ACMG) criteria, using curated reference databases and established interpretation frameworks.

For individuals assigned to Group 2, comprehensive genomic analyses, including whole-exome sequencing (WES), whole-genome sequencing (WGS), targeted multigene panels, and, in rare cases, array comparative genomic hybridization (aCGH), were performed in ISO 15189-accredited laboratories, ensuring methodological rigor, reproducibility, and full compliance with international quality standards. WES was conducted using commercially available exome capture kits such as Agilent SureSelect or IDT xGen, and sequenced on high-throughput instruments to achieve a mean coverage of ≥100× across coding regions, with over 98% of bases covered at ≥20×. Targeted NGS panels encompassing 50–480 genes were sequenced on benchtop or mid-throughput platforms with average coverage exceeding 150× and >99% of targeted regions covered at ≥30×. WGS was performed with PCR-free library preparation to attain an average genome-wide depth of approximately 30×. All sequencing datasets were processed through standardized bioinformatic pipelines, including alignment to the human reference genome, variant calling, annotation, and, when indicated, copy-number assessment using dedicated computational tools. Detected variants were rigorously interpreted following ACMG-AMP 2015 guidelines and classified as pathogenic, likely pathogenic, or variants of uncertain significance, providing a consistent and clinically meaningful framework for molecular diagnosis.

Statistical Analysis

Descriptive statistics were used to summarize clinical, laboratory, and instrumental findings. The normality of continuous variables was assessed using the Shapiro-Wilk test, confirming approximately normal distributions. Accordingly, comparisons of continuous variables were performed using independent samples t-test or one-way ANOVA, while categorical variables were analyzed with the Chi-square test. All statistical analyses were conducted in IBM SPSS Statistics (version 27.0), with significance set at $p < 0.05$.

RESULTS

Analysis of the molecular findings alongside clinical and biochemical data revealed significant differences between patients exhibiting mitochondrial DNA variants correlated with their phenotype and those diagnosed with alternative genetic conditions.

Clinically, both groups exhibited overlapping features such as developmental delay, hypotonia, and seizures; however, several manifestations were significantly more prevalent among patients with mitochondrial involvement. Severe neuromuscular impairment ($\chi^2 = 6.16$, $p = 0.013$) and regression of previously acquired skills ($\chi^2 = 4.52$, $p = 0.033$) were more frequently observed in Group 1, reflecting the progressive and multisystemic nature characteristic of mitochondrial dysfunction. In addition, ocular abnormalities, particularly ophthalmoplegia ($\chi^2 = 7.70$, $p = 0.006$) and optic nerve atrophy ($\chi^2 = 4.94$, $p = 0.026$), were significantly associated with this group. In contrast, dysmorphic features ($\chi^2 = 4.30$, $p = 0.038$) and intellectual disability ($\chi^2 = 3.92$, $p = 0.048$) were more commonly reported among patients in Group 2. An overview of the clinical signs and symptoms observed in both groups, including the percentage of affected patients and the corresponding p-values for features reaching statistical significance, is presented in Figure 1.

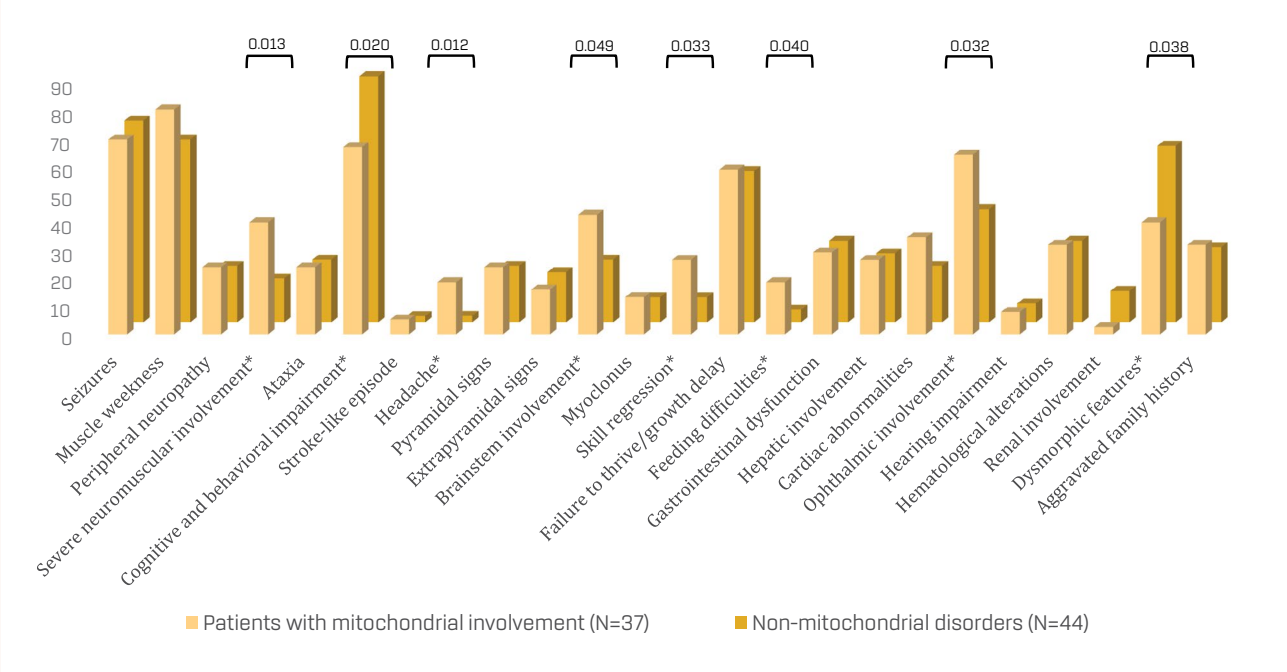

Figure 1. Prevalence of clinical features in patients with mitochondrial and other genetic disorders (p-values indicate intergroup significance).

Biochemically, plasma lactate levels were significantly higher in the mitochondrial group compared to the non-mitochondrial group (mean 3.6 mmol/L vs. 2.2 mmol/L), with one-way ANOVA revealing a robust group effect ($F(1, 74) = 9.74$, $p = 0.003$). This suggests that elevated lactate may serve as a relevant indicator in the context of mitochondrial involvement. Additionally, plasma alanine levels were significantly higher in patients with mitochondrial involvement (mean ± SD: 441 ± 45 µmol/L) compared to those with other genetic disorders (262 ± 22 µmol/L; $p < 0.001$), as revealed by independent samples t-test, thereby reinforcing the potential utility of amino acid profiling in the biochemical evaluation of suspected mitochondrial dysfunction.

Mean values of several biochemical markers, including creatine kinase (CK: 281 ± 66 U/L vs. 210 ± 32 U/L), lactate dehydrogenase (LDH: 541 ± 175 U/L vs. 395 ± 3 U/L), alanine aminotransferase (ALT: 93 ± 49 U/L vs. 49 ± 8 U/L), and aspartate aminotransferase (AST: 247 ± 193 U/L vs. 68 ± 12 U/L), were higher in the mitochondrial group compared to the non-mitochondrial group. However, none of these differences reached statistical significance, limiting their individual diagnostic utility in distinguishing between the two conditions. Other specialized metabolic investigations, such as ammonia levels, urinary organic acid analysis, and acylcarnitine profiling, did not reveal statistically significant differences between groups, but remain essential components of a comprehensive diagnostic workup given their potential to uncover subtle metabolic abnormalities.

Electrophysiological studies revealed abnormal electromyography findings in 27% of Group 1 patients compared to 21% in Group 2, while abnormal electroencephalography patterns were observed in 57% and 65%, respectively. These differences were not statistically significant. However, significant deviations on electrocardiograms were more frequently detected in Group 1 (χ^2 = 4.108, p = 0.043), underscoring the cardiovascular involvement associated with mitochondrial dysfunction. Neuroimaging abnormalities were observed in 75.7% of patients with mitochondrial involvement compared to 68.2% in the non-mitochondrial group. Notably, Group 1 exhibited a significantly higher prevalence of basal ganglia alterations (χ^2 = 4.95, p = 0.026) as well as cerebral and cerebellar atrophy (χ^2 = 6.16, p = 0.013), highlighting characteristic neuroanatomical changes associated with mitochondrial pathology. Figure 2 illustrates the percentage of patients in both groups exhibiting biochemical, instrumental, and neuroimaging abnormalities, with p-values indicated for statistically significant differences.

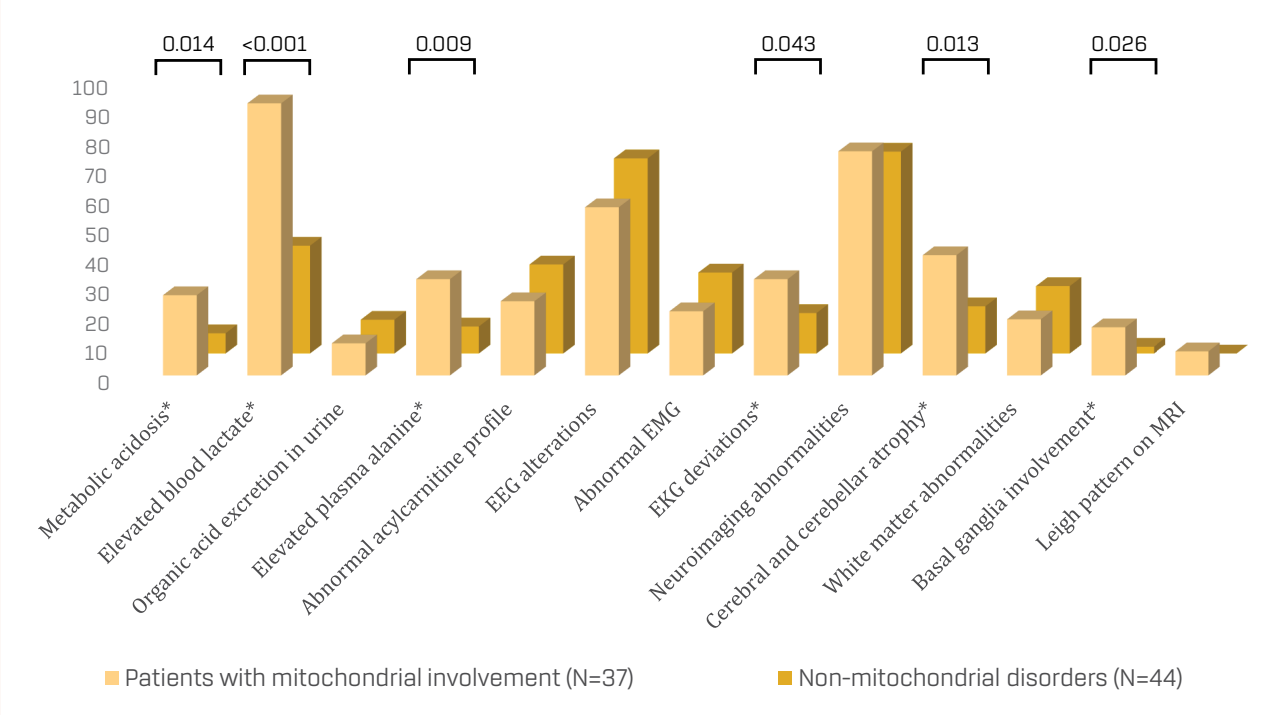

Figure 2. Prevalence of biochemical, instrumental, and neuroimaging abnormalities in patients with mitochondrial and other genetic disorders (p-values indicate intergroup significance).

Legend: EEG – Electroencephalography; EMG – Electromyography; EKG – Electrocardiography; MRI – Magnetic Resonance Imaging.

Genetic investigations further elucidated the molecular basis of the observed clinical and laboratory features. Eight patients were identified with common pathogenic point mutations through qPCR-HRM screening, including m.3243A>G (n=3), m.8993T>G (n=2), m.11778G>A (n=1), and m.3460G>A (n=2). Subsequent Sanger sequencing of the mitochondrial genome, focusing primarily on protein-coding genes, uncovered additional variants.

The identified variants predominantly involved genes encoding subunits of Complex I (*MT-ND* genes), representing 25.0% of cases, followed by mitochondrial RNA genes at 21.9%, Complex V subunits (*MT-ATP* genes) at 15.6%, and genes associated with Complex III (*MT-CYB*) and Complex IV (*MT-CO2*), each accounting for 3.1%. A notable proportion of patients (31.3%) harbored mutations affecting multiple respiratory chain complexes, suggesting broader mitochondrial dysfunction. However, the presence of combined complex involvement did not correlate significantly with increased clinical severity ($p = 0.064$). Figure 3 presents the gene-level distribution of variants detected in patients with mitochondrial involvement, highlighting the most frequently affected genes within this group.

Among the subset of patients who underwent partial mitochondrial genome sequencing, 19 individuals (59.4%) were found to carry pathogenic or likely pathogenic variants, while 13 (40.6%) harbored variants of uncertain significance (VUS). However, when considering the entire group of patients with mitochondrial involvement, including those harboring pathogenic variants in nuclear genes implicated in mitochondrial dysfunction, approximately 65% carried pathogenic or potentially pathogenic variants, and around 35% had VUS. Most of these uncertain variants were located in genes encoding Complex I subunits (34.1%), followed by Complex V (29.2%) and Complex IV (17.0%). Notably, individuals with pathogenic or likely pathogenic variants exhibited significantly higher NMDS scores compared to those with VUS ($\chi^2 = 6.82$, $p = 0.033$), suggesting a greater clinical impact in genetically confirmed cases.

Within the subgroup of patients carrying nuclear gene mutations associated with mitochondrial dysfunction, pathogenic variants were identified in genes involved in key aspects of mitochondrial maintenance and metabolism. These included *POLG* (n = 2), which encodes the mitochondrial DNA polymerase essential for mtDNA replication and repair; *TWNK* (n = 1) and *DGUOK* (n = 1), both critical for mitochondrial DNA maintenance; *ETHE1* (n = 1), implicated in sulfide detoxification within the mitochondrial matrix; and *OPA1* (n = 1), a gene involved in mitochondrial inner membrane fusion and cristae remodeling. Notably, the patient with the *OPA1* mutation also carried the common pathogenic mtDNA variant m.3243A>G, suggesting a potential synergistic effect in disease expression.

Figure 3 presents the gene-level distribution of variants detected in patients with mitochondrial involvement, highlighting the most frequently affected genes within this group.

In contrast, Group 2 encompassed a heterogeneous array of inherited disorders that phenotypically overlapped with mitochondrial disease. These included syndromic or multisystemic genetic conditions (36.4%), neurometabolic disorders (27.3%), ion channelopathies and epileptic encephalopathies (18.2%), neuromuscular disorders (11.3%), and chromosomal microdeletion syndromes (6.8%). The gene-specific distribution of variants identified in Group 2 is presented in Figure 4, highlighting the relative frequency of each affected gene within the spectrum of non-mitochondrial genetic disorders. Diagnostic confirmation in this group was achieved through targeted next-generation sequencing (NGS) panels, clinical exome sequencing, or array comparative genomic hybridization (aCGH), depending on the clinical suspicion. In

several cases, functional studies such as neurotransmitter metabolite profiling or advanced neuroimaging (including MR spectroscopy) were essential to support the genetic findings and to delineate the pathophysiological mechanism.

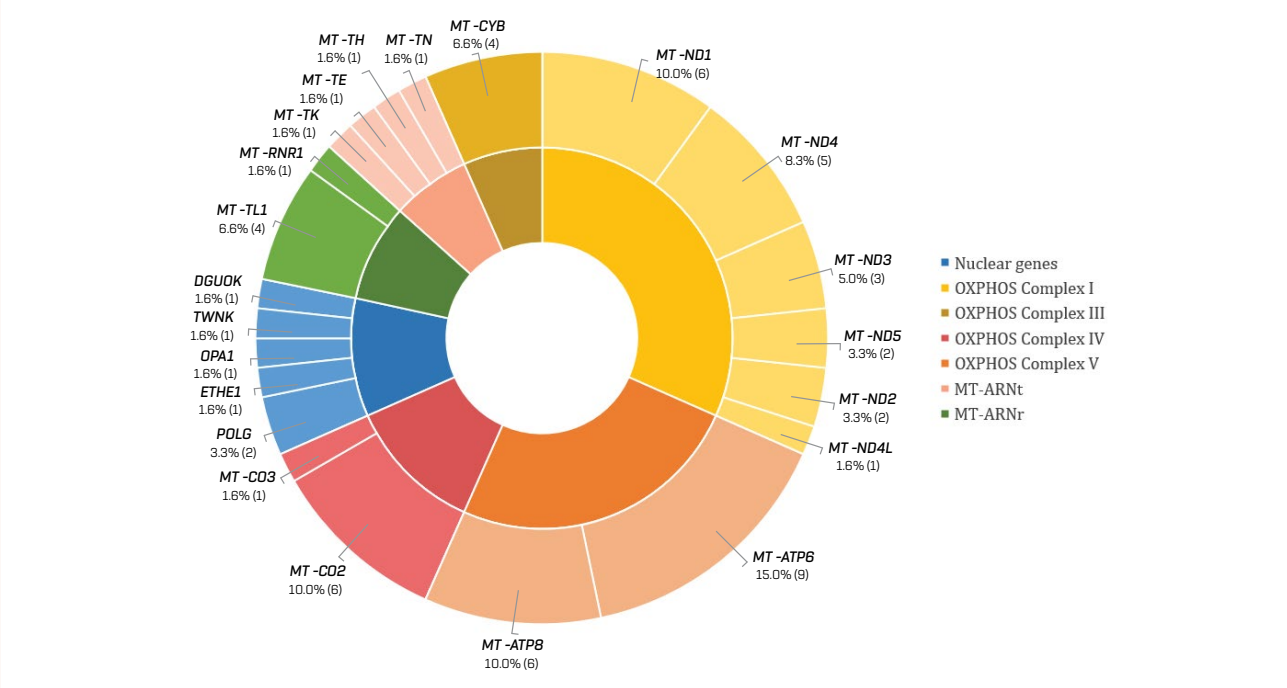

Figure 3. Distribution of identified variants by gene in Group 1, representing patients with mitochondrial involvement.

Legend: OXPHOS – Oxidative Phosphorylation genes; MT-ARNt – Mitochondrial transfer RNA genes; MT-ARNr – Mitochondrial ribosomal RNA genes.

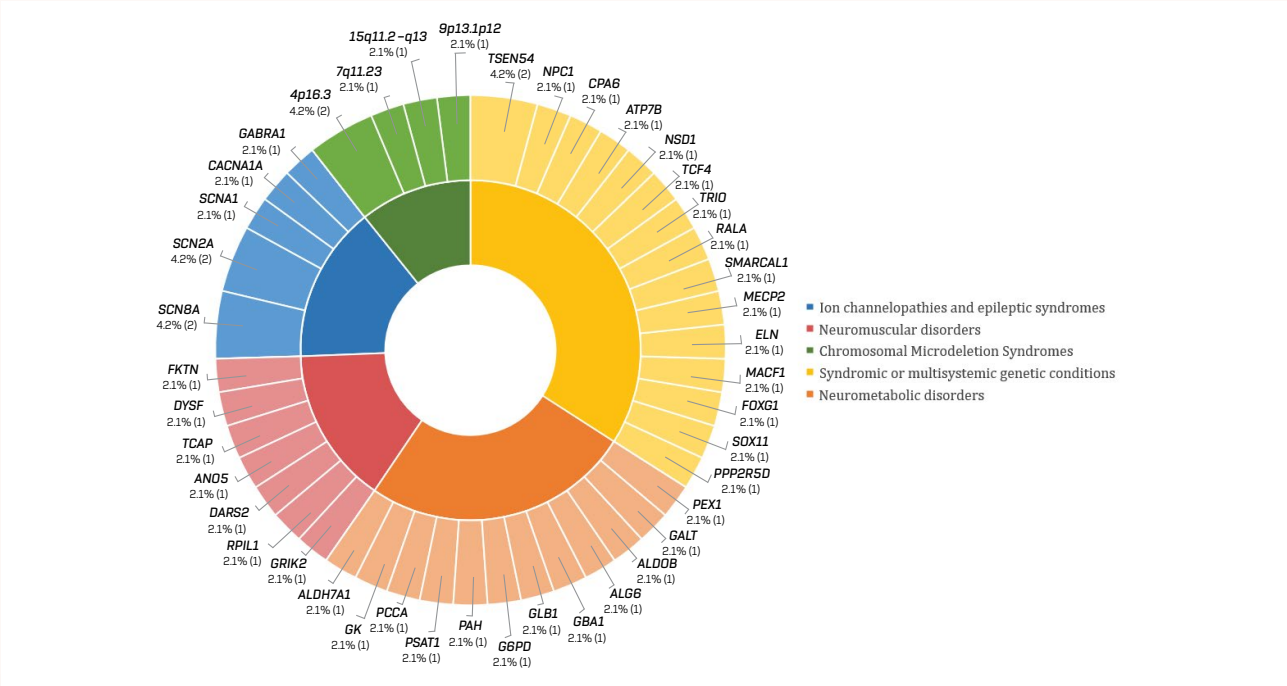

Figure 4. Gene-level distribution of variants identified in Group 2, encompassing patients with other inherited genetic disorders.

DISCUSSIONS

This comparative study highlights critical distinctions in clinical, biochemical, and genetic characteristics of patients with confirmed mitochondrial involvement versus those with other inherited genetic disorders presenting with overlapping phenotypes. Our findings underscore the complexity of diagnosing mitochondrial diseases and reinforce the need for integrated, multidisciplinary approaches that combine molecular genetics, biochemical profiling, and detailed clinical assessment. The Nijmegen Mitochondrial Disease Score proved to be a valuable and practical tool in this study, effectively guiding patient selection and supporting the differentiation between mitochondrial and non-mitochondrial genetic disorders. Its integration of clinical, biochemical, and instrumental parameters enhances diagnostic precision, reaffirming its established role as a cornerstone in the initial evaluation and stratification of patients with suspected mitochondrial pathology.

Severe neuromuscular involvement observed in patients with mitochondrial pathology is consistent with well-documented clinical phenotypes extensively described in the literature (5,6). The predominance of multisystemic manifestations, with at least three organ systems affected in most cases, further supports the systemic nature of mitochondrial dysfunction, as previously reported (7). Additionally, the frequent occurrence of ocular abnormalities, including ophthalmoplegia and optic atrophy, aligns with established mitochondrial syndromes, reflecting mitochondrial vulnerability in highly energy-dependent tissues (8).

Biochemically, the significant elevation of plasma lactate and alanine levels reinforces their utility as reliable metabolic biomarkers in suspected mitochondrial disease. The absence of significant differences in other specialized metabolic assays underscores their supportive role rather than a definitive diagnostic capacity within the broader clinical context.

Genetic analyses identified mitochondrial DNA mutations associated with well-characterized syndromes such as Leigh syndrome, Leber Hereditary Optic Neuropathy (LHON), and Mitochondrial Encephalomyopathy, Lactic Acidosis, and Stroke-like episodes (MELAS), alongside nuclear gene mutations linked to Mitochondrial DNA Depletion Syndrome (*OPA1* gene) and Progressive Sclerosing Poliodystrophy (*POLG* gene). However, in certain cases, the detected genetic variants only partially explain the patients' phenotypes or are currently insufficient to definitively establish a diagnosis of a mitochondrial syndrome, highlighting the evolving nature of genotype-phenotype correlations in mitochondrial pathology. Moreover, variants of uncertain significance identified in mitochondrial genes account for a substantial proportion of findings, underscoring the complexity of genetic interpretation and the need for ongoing functional studies and longitudinal clinical correlation to clarify their pathogenic potential and contribution to disease phenotypes.

Despite providing valuable insights, this study has inherent limitations. The partial sequencing approach limited full genomic coverage, potentially overlooking rare or novel variants. The sample size, although robust, may restrict the statistical power for detecting subtle associations. Moreover, the absence of muscle biopsy and enzymatic activity data, due to limited availability, precluded a more integrative pathological correlation. Importantly, this work underscores the critical need for next-generation sequencing (NGS) technologies to improve diagnostic resolution by enabling comprehensive interrogation of mitochondrial and nuclear genomes. NGS has become a widely adopted approach, facilitating precise genotype-phenotype correlations in mitochondrial diseases and their mimics, as increasingly reflected in the current literature (9, 10).

CONCLUSIONS

1. The Nijmegen Mitochondrial Disease Score proved valuable not only as a screening instrument but also as an indicator of disease severity, showing significant correlations with key clinical features and neuroimaging abnormalities. Elevated plasma lactate and alanine levels emerged as robust biochemical markers associated with mitochondrial pathology.
2. Molecular investigations revealed a broad spectrum of mitochondrial DNA and nuclear gene variants, with a notable impact of Complex V subunit mutations on phenotype severity. Pathogenic variants were linked to higher clinical burden, underscoring the importance of comprehensive genomic analysis.
3. Integrating clinical, biochemical, imaging, and genetic data allowed for refined patient stratification, emphasizing the diagnostic value of a sequential molecular testing approach. Collectively, these findings support early, multidisciplinary evaluation, incorporating next-generation sequencing, to improve diagnostic precision and guide personalized clinical management in suspected mitochondrial disorders.

CONFLICT OF INTEREST The authors declare no conflict of interest.

ACKNOWLEDGMENTS This study was supported by the institutional research project “Diagnosis and Monitoring of Genetic Diseases in the Prevention of Maternal and Child Health Disorders” (Project No. 140102, DiMoGEN).

ETHICAL APPROVAL The study was approved by the Research Ethics Committee of the State University of Medicine and Pharmacy “Nicolae Testemițanu” (Decision No. 3, dated 09.09.2020).

REFERENCES

1. Schlieben LD, Prokisch H. The Dimensions of Primary Mitochondrial Disorders. *Front Cell Dev Biol*. 2020;8:600079. https://doi.org/10.3389/fcell.2020.600079.
2. Gropman AL, Uittenbogaard MN, Chiaramello AE. Challenges and opportunities to bridge translational to clinical research for personalized mitochondrial medicine. *Neurotherapeutics*. 2024;21(1):e00311. https://doi.org/ 10.1016/j.neurot.2023.e00311.
3. Forny P, Footitt E, Davison JE, et al. Diagnosing Mitochondrial Disorders Remains Challenging in the Omics Era. *Neurol Genet*. 2021;7(3):e597. https://doi.org/10.1212/NXG.0000000000000597.
4. Morava E, Van Den Heuvel L, Hol F, et al. Mitochondrial disease criteria: Diagnostic applications in children. *Neurology*. 2006;67(10):1823-6. https://doi.org/10.1212/01.wnl.0000244435.27645.54.
5. Nascimento A, Ortez C, Jou C, O'Callaghan M, Ramos F, Garcia-Cazorla À. Neuromuscular Manifestations in Mitochondrial Diseases in Children. *Semin Pediatr Neurol*. 2016;23(4):290-305. https://doi.org/10.1016/j.spen.2016.11.004.
6. Kuusik B, Mithal DS. Updates on neurologic manifestations of mitochondrial disease. *Curr Opin Pediatr*. 2025;37(1):107-111. https://doi.org/10.1097/MOP.0000000000001418.
7. Mancuso M. Complex neurological and multisystem presentations in mitochondrial disease. *Handb Clin Neurol*. 2023;194:117-124. https://doi.org/10.1016/B978-0-12-821751-1.00003-8.
8. Chen BS, Harvey JP, Gilhooley MJ, Jurkute N, Yu-Wai-Man P. Mitochondria and the eye—manifestations of mitochondrial diseases and their management. *Eye (Lond)*. 2023;37(12):2416-2425. https://doi.org/10.1038/s41433-023-02523-x.
9. Davis RL, Kumar KR, Puttick C, et al. Use of Whole-Genome Sequencing for Mitochondrial Disease Diagnosis. *Neurology*. 2022;99(7):e730-e742. https://doi.org/10.1212/WNL.0000000000200745.
10. Swalwell H, Kirby DM, Blakely EL, et al. Respiratory chain complex I deficiency caused by mitochondrial DNA mutations. *European Journal of Human Genetics*. 2011;19(7):769-775. https://doi.org/10.1038/ejhg.2011.18.

Date of receipt of the manuscript: 26.06.2025

Date of acceptance for publication: 18.12.2025

Secu Doina, WoS Researcher ID: AEB-7004-2022;

Daniela BLĂNIȚĂ, WoS Researcher ID: JFS-5994-2023;

Natalia UȘURELU, WoS Researcher ID: NQF-0089-2025, SCOPUS ID 56334943600;

Victoria SACARĂ, WoS Researcher ID: Y-3880-2018, SCOPUS ID 57205301327.

BIOLOGICAL SCIENCES

OPEN ACCESS

ASTAXANTHIN AND CELLULAR METABOLITES PRODUCTION IN *HAEMATOCOCCUS LACUSTRIS* EXPOSED TO SILVER NANOPARTICLES

Liliana CEPOI[1], Ludmila RUDI[1], Tatiana CHIRIAC[1], Vera MISCU[1], Ecaterina PLINGAU[1]

[1] Technical University of Moldova, Institute of Microbiology and Biotechnology, Republic of Moldova

Coresponding author: Liliana Cepoi, e-mail: liliana.cepoi@imb.utm.md

https://doi.org/10.38045/ohrm.2026.1.06 CZU: 582.263:620.3:546.57

ABSTRACT

Introduction Silver nanoparticles (AgNPs) can modulate microalgal metabolism in a dose-dependent and stage-specific manner. *Haematococcus lacustris*, a key astaxanthin-producing microalga, is highly sensitive to environmental stressors that regulate the transition from the green vegetative stage to the red aplanospore stage.

Material and methods The effects of 10 nm and 20 nm citrate-stabilized AgNPs (0.01–5 mg L^{-1}) were assessed on biomass, cellular metabolites, photosynthetic pigments, lipids, and astaxanthin. Nanoparticles were introduced on day 3, with analyses performed at the end of the green (day 9) and red stages (day 16).

Results Low to moderate AgNPs concentrations (0.01–1 mg L^{-1}) increased biomass, proteins, carbohydrates, and lipids during the green stage, while 5 mg L^{-1} inhibited growth and pigments and elevated MDA levels. In the red stage, all concentrations reduced final biomass; however, 10 nm AgNPs at 0.01–0.5 mg L^{-1} boosted astaxanthin (by up to ~30%) and lipids (by up to ~96%). Higher doses, along with all 20 nm AgNP treatments, suppressed astaxanthin accumulation.

Conclusions *H. lacustris* exhibits a hormetic response to AgNPs: mild exposure stimulates key metabolites, while higher concentrations become inhibitory. Nanoparticle size, dose, and timing are crucial for precisely directing metabolic pathways and improving astaxanthin yield.

Keywords *Haematococcus lacustris*, silver nanoparticles, astaxanthin, metabolites, oxidative stress, hormesis.

ASTAXANTINA ȘI PRODUCEREA METABOLIȚILOR CELULARI ÎN *HAEMATOCOCCUS LACUSTRIS* EXPUS LA NANOPARTICULE DE ARGINT

Introducere Nanoparticulele de argint (AgNPs) pot modula metabolismul microalgelor într-un mod dependent de concentrație și de stadiul fiziologic. *Haematococcus lacustris*, un important producător de astaxantină, prezintă o sensibilitate sporită la factorii de stres care reglează tranziția de la faza de celule verzi vegetative la cea de aplanospori roșii.

Material și metode Au fost evaluate efectele AgNP-urilor de 10 nm și 20 nm (0,01–5 mg L^{-1}) asupra biomasei, metaboliților celulari, pigmenților fotosintetici, lipidelor și astaxantinei. Nanoparticulele au fost adăugate în ziua a 3-a, iar analizele au fost efectuate la sfârșitul fazei de celule vegetative (ziua a 9-a) și al fazei de aplanospori (ziua a 16-a).

Rezultate Concentrațiile mici și moderate de AgNPs (0,01–1 mg L^{-1}) au stimulat biomasa, proteinele, carbohidrații și lipidele în faza de celule vegetative, în timp ce 5 mg L^{-1}au inhibat creșterea și conținutul de pigmenți și au crescut nivelul MDA. În faza de aplanospori, toate concentrațiile au redus biomasa finală; totuși, AgNP de 10 nm la 0,01–0,5 mg L^{-1} au intensificat sinteza de astaxantină (până la ~30%) și de lipide (până la ~96%). Dozele mai mari și toate tratamentele cu AgNPs de 20 nm au redus semnificativ astaxantina.

Concluzii *H. lacustris* manifestă un răspuns hormetic la AgNPs: expunerea moderată stimulează metaboliții valoroși, în timp ce concentrațiile ridicate devin inhibitoare. Dimensiunea nanoparticulelor, doza aplicată și durata expuneriit constituie factori determinanți în modularea controlată a metabolismului celular și în optimizarea producției de astaxantină.

Cuvinte-cheie *Haematococcus lacustris*, nanoparticule de argint, astaxantină, metaboliți, stres oxidativ, răspuns hormetic.

INTRODUCTION

Nanotechnology is among the most dynamic frontiers of modern science, with applications expanding from engineering to biomedicine. This growth is driven by the unique physicochemical properties of nanomaterials, including nanoscale dimensions, a high specific surface area, and enhanced reactivity (1, 2). As their use has broadened, so have concerns regarding their toxicological impact, as numerous studies indicate that some nanomaterials can induce oxidative stress, cellular damage, and systemic toxicity, particularly at high concentrations or in unsuitable formulations (3). At the same time, a deeper understanding of their mechanisms of action has shifted the focus from simply avoiding toxicity toward exploring their potential for the controlled, beneficial stimulation of cellular processes (4, 5). This new perspective has opened new nanobiotechnological applications, including those involving microalgae, where nanoparticles may modulate oxidative stress and enhance the biosynthesis of high-value metabolites such as lipids, carotenoids, proteins, and exopolysaccharides (6–8).

Despite increasing interest, the biological responses of microalgae to nanoparticle exposure remain poorly understood. These responses are highly variable, depending critically on nanoparticle type, concentration, and the physiological state of the organism. (6, 8, 9). Among different nanomaterials, silver nanoparticles (AgNPs) are particularly noteworthy because of their dual biological effects, where they can either stimulate or inhibit cellular processes, depending on size, concentration, and surface properties. When carefully controlled, moderate oxidative stress induced by AgNPs may act as a metabolic signa, promoting the synthesis of bioactive compounds (8, 10, 11).

The green microalga *Haematococcus lacustris* (formerly *Haematococcus pluvialis*) is a model organism in phycobiotechnology due to its exceptional capacity to accumulate astaxanthin, a carotenoid with strong antioxidant properties and significant pharmaceutical, nutraceutical, cosmetic, and aquaculture relevance (12–16). In addition to astaxanthin, *H. lacustris* produces considerable amounts of lipids, proteins, and carbohydrates, further enhancing its biotechnological value (12, 13).

The life cycle of *Haematococcus lacustris* consists of two distinct morphological and physiological stages: a vegetative green stage and a red aplanospore (or cyst) stage, with the latter characterized by the extensive accumulation of carotenoids. These stages also differ structurally. Green vegetative cells possess a relatively fragile cell wall that allows the direct extraction of intracellular components. In contrast, red aplanospores develop a thick, resilient cell wall that, while providing protection, substantially complicates metabolite extraction, requiring specific cell disruption or pretreatment procedures. Due to these structural and functional differences, each stage must be evaluated separately, when assessing nanoparticle effects on growth and metabolite biosynthesis – particularly in the case of astaxanthin (13, 17–21).

In this context, this study examines the impact of silver nanoparticles on astaxanthin accumulation and cellular metabolite profiles in *Haematococcus lacustris* CNMN-AV-05, specifically comparing its green

and red developmental stages. The responses to 10 and 20 nm AgNPs were evaluated by measuring biomass, major biochemical components, lipids, and astaxanthin, in order to clarify how nanoparticle exposure influences growth and metabolism across the two developmental stages.

MATERIALS AND METHODS

Microalgal Strain and Culture Conditions

The green microalga *Haematococcus lacustris* CNMN-AV-05 (NCNM, Technical University of Moldova) was used in all experiments. Starter cultures were maintained as aplanospores under continuous illumination (150 $\mu mol \cdot m^{-2} \cdot s^{-1}$, measured using a quantum light meter, LI-250A, LI-COR Biosciences, USA) at 26–28 °C in the mineral medium described below.

For experimental assays, cultures were inoculated at 0.2 g $DW \cdot L^{-1}$ in 50 mL working volumes (100 mL Erlenmeyer flasks) and cultivated under continuous light (75 $\mu mol \cdot m^{-2} \cdot s^{-1}$) with shaking twice daily during 10 min. The medium pH remained stable (6.8–7.0). The mineral medium contained ($g \cdot L^{-1}$): $NaNO_3$ 0.3; KH_2PO_4 0.02; K_2HPO_4 0.08; $MgSO_4 \cdot 7H_2O$ 0.01; $ZnSO_4 \cdot 7H_2O$ 0.0001; $MnSO_4 \cdot 5H_2O$ 0.0015; $CuSO_4 \cdot 5H_2O$ 0.00008; H_3BO_3 0.0003; $(NH_4)_6Mo_7O_{24} \cdot 4H_2O$ 0.0003; $Fe_2(SO_4)_3$ 0.013; EDTA 0.0075.

Silver Nanoparticles

Citrate-stabilized silver nanoparticles (AgNPs) of 10 nm (Lot MKCK8345) and 20 nm (Lot MKCM2276) were obtained from Sigma-Aldrich (Optical Density (OD) = 1; Polydispersity Index (PDI) < 0.2; TEM-verified size ±0.2 nm). Prior to use, stock suspensions were vortexed and briefly sonicated, then diluted in sterile medium immediately before addition to cultures.

After introduction, AgNPs remained visually stable throughout the experiment, with no sedimentation, flocculation; given the low working concentrations, no optical effects were expected. Seven concentrations were tested: 0, 0.01, 0.05, 0.1, 0.5, 1.0, and 5 $mg \cdot L^{-1}$. Nanoparticles were added on day 3, at the transition from germination to the green vegetative stage.

Experimental Design

Two experimental series were conducted – one for each AgNP size (10 nm and 20 nm).

For each concentration, three independent replicates were prepared for each sampling time.

Biomass was harvested at day 9 – end of the green vegetative stage, and at day 16 – end of the red aplanospore stage (after increasing illumination to 150 $\mu mol \cdot m^{-2} \cdot s^{-1}$ from day 14 to induce carotenoid accumulation).

After harvesting, biomass was washed with distilled water and resuspended to a standard concentration of 10 $mg \cdot mL^{-1}$ for biochemical assays.

Sample Preparation for Biochemical Analyses

Due to structural differences between stages, biomass was processed as follows:

a) Green stage (motile cells) – biomass subjected to three freeze–thaw cycles (–20 °C / +25 °C) to disrupt cells; homogenates used for protein, carbohydrate, pigment, lipid, and MDA assays.

b) Red stage (aplanospores) – aplanospores possess a thick, resistant wall; therefore biomass was subjected to acid hydrolysis (0.1 M HCl, 90 °C, 10 min), washed 3× with water, the pellet was used for astaxanthin extraction, residual material was used for lipid quantification.

Biomass Quantification

Biomass concentration was determined spectrophotometrically at 680 nm (green cells) and 565 nm (red aplanospores). Calibration curves were constructed separately for each cell type within the OD range 0.01–0.40 (7-point curves; $R^2 > 0.99$), and samples were diluted with fresh medium to fall within this linear interval.

Biochemical Analyses

Biochemical assays were performed on biomass standardized to 10 mg/mL, with cell disruption adapted to each stage: freeze–thaw cycles for green cells and mild acid hydrolysis (0.1 M HCl, 90°C, 10 min) for aplanospores.

Protein content was measured using a modified Folin–Ciocalteu assay (22). Absorbance was recorded at 750 nm, and concentrations were calculated from a BSA calibration curve.

Total carbohydrates were quantified by the anthrone method, heating samples with anthrone–H_2SO_4 and reading absorbance at 620 nm, using a glucose calibration curve.

Pigments (chlorophylls and carotenoids) were extracted in 96% ethanol, and absorbance at 649, 665, and 450 nm was used to calculate chlorophyll *a*, chlorophyll *b*, and total carotenoids according to Lichtenthaler (1987) (23).

Total lipids were quantified by the phosphovanillin colorimetric method (24). Green-stage biomass was extracted with chloroform–ethanol; for red-stage biomass, lipids were measured from the residue remaining after astaxanthin extraction. Absorbance was measured at 520 nm, and lipid content was determined using an oleic acid standard curve.

Lipid peroxidation was assessed via the Thiobarbituric Acid-Malondialdehyde (TBA–MDA) assay, measuring absorbance at 535 nm (corrected at 600 nm). MDA content was calculated using $\varepsilon = 1.56 \times 10^5\ M^{-1} \cdot cm^{-1}$.

Astaxanthin was extracted from hydrolyzed aplanospores with 96% ethanol, and absorbance at 478 nm was converted to concentration using a calibration curve of pure astaxanthin (≥97%).

Statistical Analysis

All experiments were performed in triplicate, and results are expressed as mean ± standard deviation (SD). Statistical differences between treatments and controls were assessed using one-way ANOVA, followed by Welch's t-test for unequal variances. Differences were considered statistically significant at $p < 0.05$.

RESULTS

Effects of AgNPs on Biomass and Cellular Metabolites of *Haematococcus lacustris* in the Green Stage

Exposure of *H. lacustris* to silver nanoparticles produced clear, concentration-dependent changes in biomass and cellular metabolite content at the end of the green growth phase (fig. 1–4). In terms of growth (fig. 1), both 10 nm and 20 nm AgNPs stimulated biomass accumulation at low and moderate concentrations.

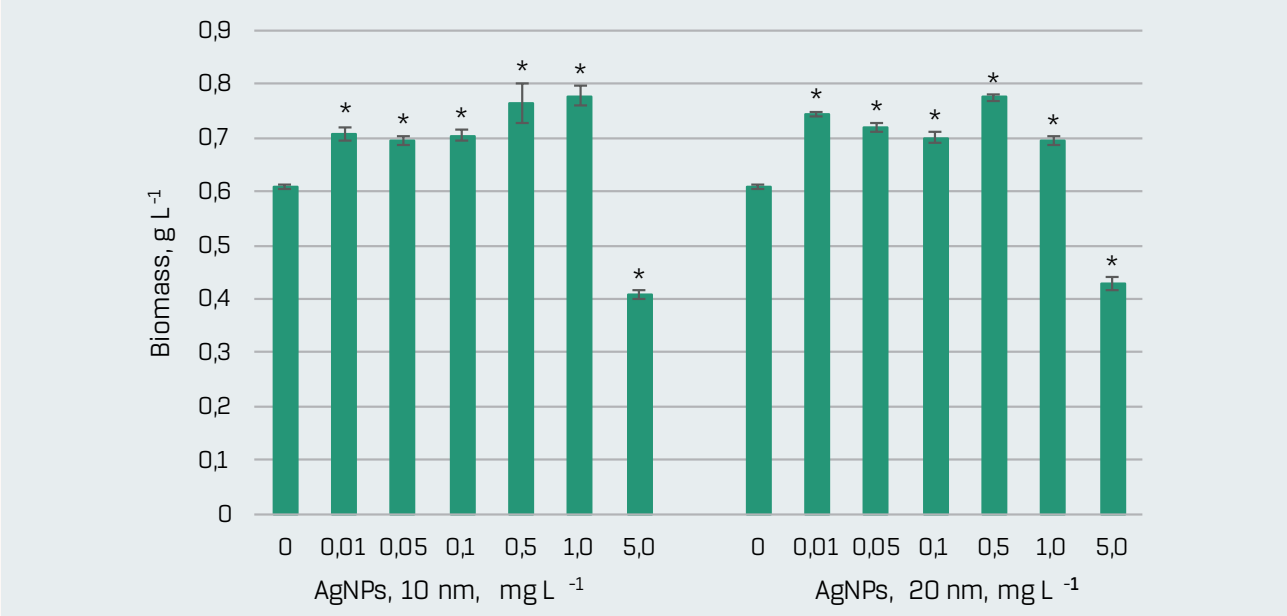

Figure 1. Biomass (g L^{-1}) of *Haematococcus lacustris* accumulated during the green stage following exposure to 10 nm and 20 nm AgNPs at various concentrations (mg L^{-1}). 0 – control; data are presented as mean ± SD (n = 3). Statistical significance is indicated relative to the control: * – $p < 0.05$.

For 10 nm AgNPs, 0.01–0.1 mg L^{-1} increased biomass by ~14–16%, while 0.5–1.0 mg L^{-1}produced stronger stimulation, up to ~26–28% above the control. A similar pattern was observed for 20 nm AgNPs, with biomass increases of ~14% at 0.01 mg L-1 and ~27% at 0.5–1.0 mg L^{-1}. In contrast, the highest concentration (5.0 mg L^{-1}) inhibited growth,

reducing biomass by ~30–33% for both nanoparticle sizes. Thus, AgNPs enhanced green-stage biomass within an optimal concentration window, while excessive doses were clearly detrimental.

Protein and carbohydrate contents also responded positively to AgNP treatment, although with different sensitivities (fig. 2). For proteins, all tested concentrations of both 10 nm and 20 nm AgNPs led to significant increases relative to the control. In cultures treated with 10 nm AgNPs, protein content rose by ~9–16%, with the strongest effects at 0.1–1.0 mg L^{-1}. For 20 nm AgNPs, the stimulatory effect was more pronounced, with increases of ~14–25% in the same concentration range, indicating that both size and dose influence protein accumulation.

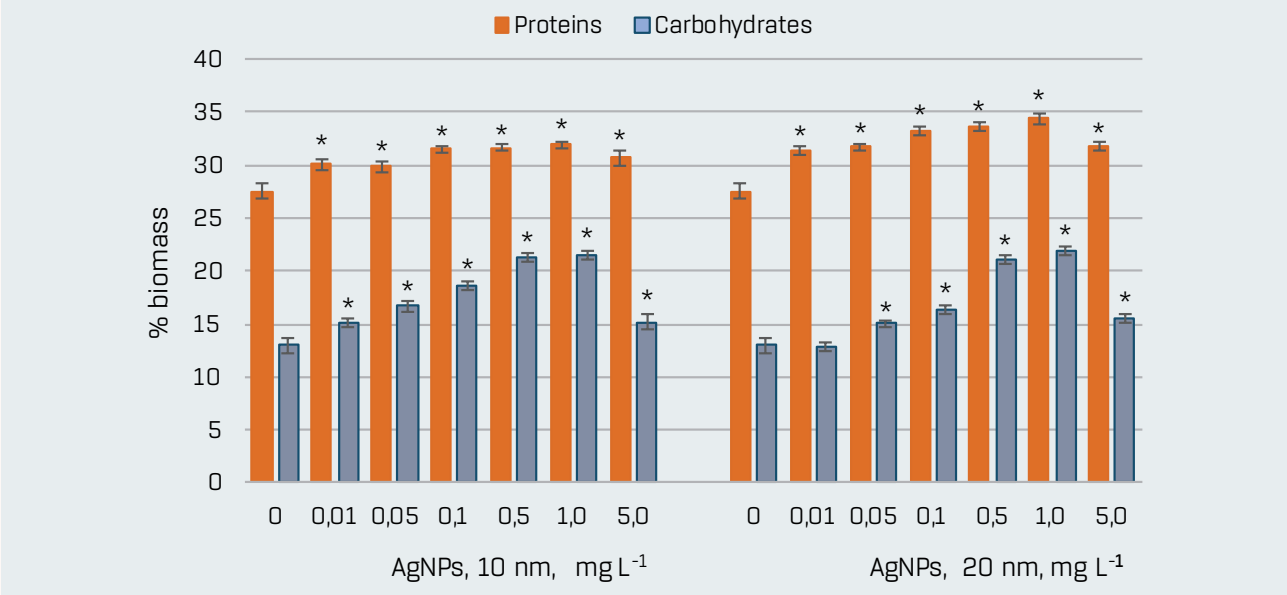

Figure 2. Protein and carbohydrate content (% of biomass) in *Haematococcus lacustris* collected at the end of the green phase after exposure to 10 nm and 20 nm AgNPs (mg L^{-1}). 0 = control; mean ± SD (n = 3); * $p < 0.05$ vs. control.

Carbohydrates displayed an even more marked stimulation. In the presence of 10 nm AgNPs, carbohydrate content increased at all concentrations, with moderate rises (~16%) at 0.01 and 5.0 mg L-1 and stronger enhancement (up to ~65%) at 0.05–1.0 mg/L. Treatment with 20 nm AgNPs similarly elevated carbohydrate levels at 0.05–5.0 mg L^{-1}, with maximal increases of ~62–68% at 0.5–1.0 mg L^{-1}, while 0.01 mg L^{-1} induced no detectable change. Overall, these results indicate that AgNPs, particularly in the intermediate range of 0.05–1.0 mg L^{-1}, strongly stimulate primary carbon storage in the green stage.

The pigment profile was more sensitive to AgNP exposure, especially at higher concentrations (fig. 3). For 10 nm AgNPs, total chlorophyll content remained comparable to the control at 0.01–0.5 mg L^{-1}, but declined by ~16% at 1.0 mg L^{-1} and ~29% at 5.0 mg L^{-1}. In cultures treated with 20 nm AgNPs, 0.01–0.05 mg L^{-1} had little effect on chlorophylls, whereas 0.1–5.0 mg L^{-1} induced a progressive reduction, reaching ~31% at 5.0 mg L^{-1}.

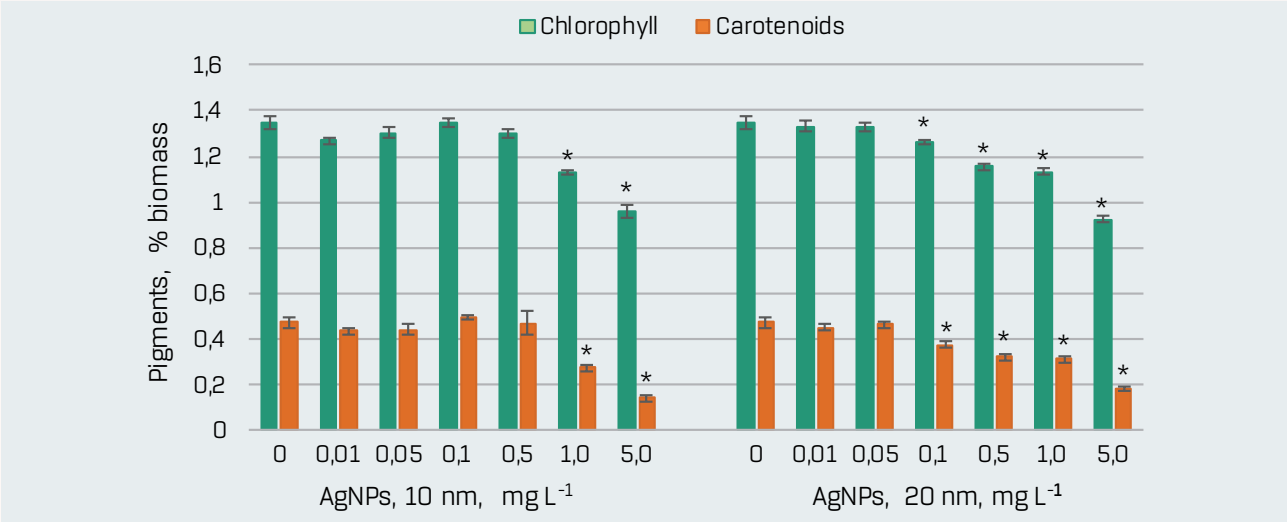

Figure 3. Total chlorophyll and carotenoid content (% biomass) in *Haematococcus lacustris* at the end of the green phase following exposure to 10 nm and 20 nm AgNPs (mg L^{-1}). 0 = control; mean ± SD (n = 3); * $p < 0.05$.

Total carotenoids followed a similar pattern. For 10 nm AgNPs, concentrations up to 0.5 mg L^{-1} did not substantially modify carotenoid levels, but 1.0 mg L^{-1} and 5.0 mg L^{-1} caused strong decreases of ~42% and ~70%, respectively. With 20 nm AgNPs, slight changes were observed at 0.01–0.05 mg L^{-1}, while 0.1–5.0 mg L^{-1} produced pronounced reductions (about 20–61%). These trends indicate that, unlike proteins and carbohydrates, photosynthetic pigments are relatively stable under low AgNP doses but highly susceptible to inhibition at ≥1.0 mg L^{-1}.

Lipid content and malondialdehyde (MDA) levels, used as indicators of carbon allocation and oxidative stress, are shown in Figure 4. In the presence of 10 nm AgNPs, lipid content increased moderately (~12%) at 0.05–0.1 mg L^{-1} and more strongly (~31–42%) at 0.5–5.0 mg L^{-1}. For 20 nm AgNPs, significant lipid stimulation (~24–65%) was observed mainly at 0.5–5.0 mg L^{-1}, whereas lower concentrations had little effect.

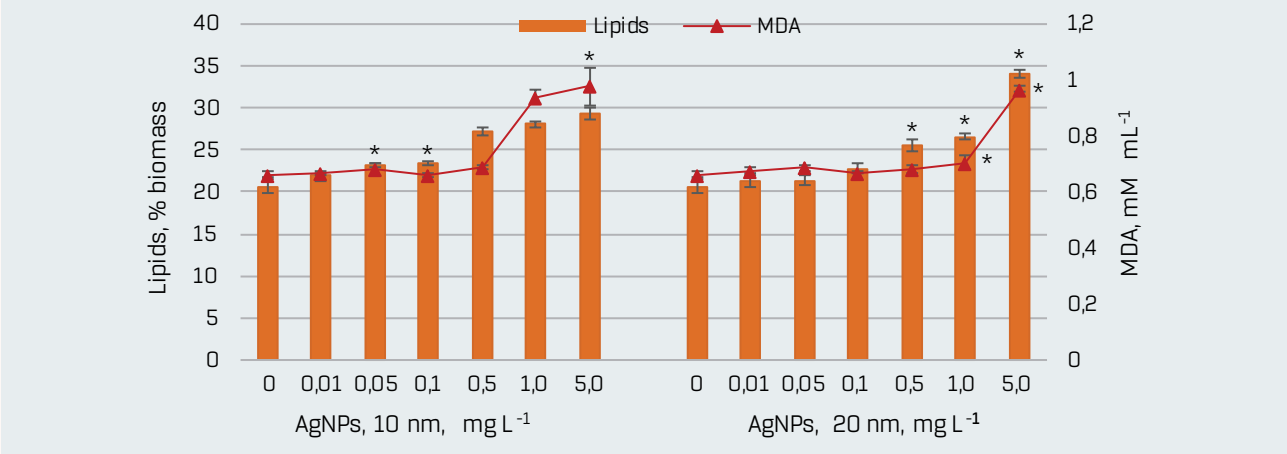

Figure 4. Lipid content (% biomass) and MDA levels (mM mL^{-1}) in *Haematococcus lacustris* at the end of the green stage following exposure to 10 nm and 20 nm AgNPs (mg L^{-1}). 0 = control; mean ± SD (n = 3); * $p < 0.05$ vs. control.

MDA levels remained close to control values at 0.01–0.5 mg L^{-1} for both nanoparticle sizes, indicating that these doses did not induce marked lipid peroxidation. However, at 1.0–5.0 mg L^{-1}, MDA increased substantially: for 10 nm AgNPs by ~42–47%, and for 20 nm AgNPs by ~6–46%. Thus, high AgNP concentrations that suppress pigments and growth are also associated with oxidative damage, whereas low–moderate doses stimulate biomass and metabolite accumulation without clear signs of stress.

Effects of AgNPs on Biomass, Astaxanthin, and Lipids in the Red Aplanospore Stage

At the red cyst (aplanospore) stage, the impact of AgNPs differed from that observed in the green phase, reflecting the shift towards stress-induced carotenoid and lipid accumulation (fig. 5, 6).

Biomass accumulation was consistently inhibited by AgNP exposure at the end of the cultivation cycle (fig. 5). Even the lowest concentrations (0.01–0.1 mg L^{-1}) caused moderate declines of ~5–7% for 10 nm AgNPs and ~4–8% for 20 nm AgNPs. At higher doses (0.5–5.0 mg L^{-1}), the reduction in aplanospore biomass became more pronounced, reaching ~10–35% for 10 nm particles and ~14–40% for 20 nm particles. These results suggest that although AgNPs can transiently stimulate biomass in the green stage, their prolonged presence ultimately limits final biomass at the red stage.

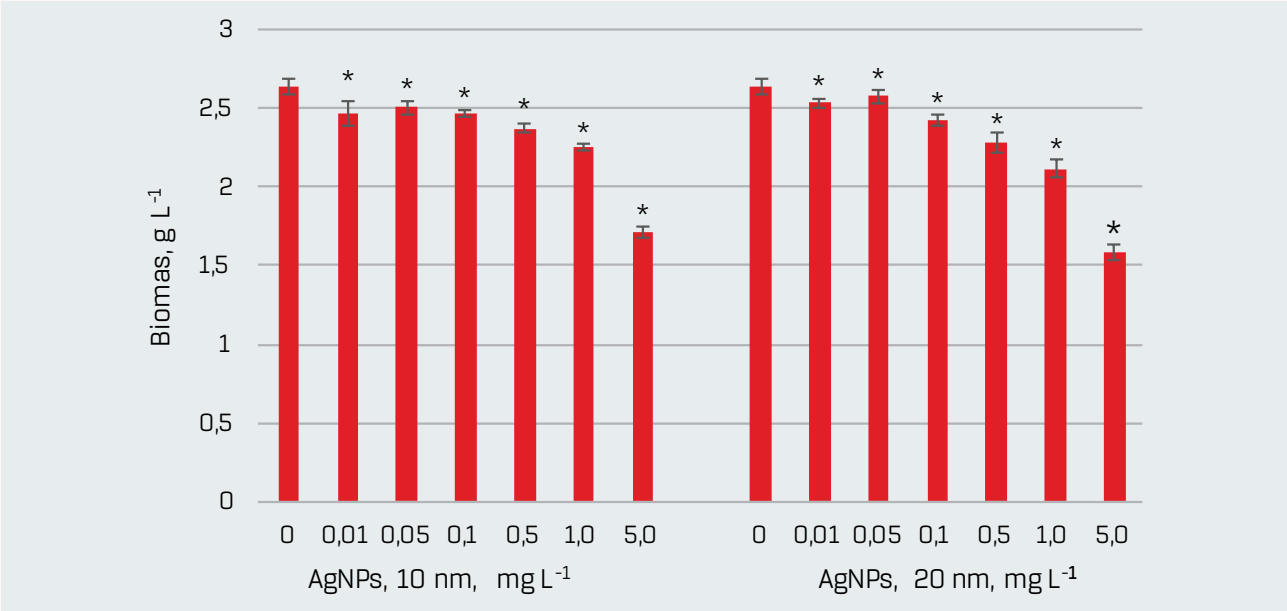

Figure 5. Biomass (g/L) of Haematococcus lacustris at the red cyst (aplanospore) stage following exposure to 10 nm and 20 nm AgNPs (mg L^{-1}). 0 = control; mean ± SD (n = 3); * $p < 0.05$ vs. control.

Astaxanthin accumulation in aplanospores exhibited a clear biphasic, concentration-dependent response (fig. 6). In cultures treated with 10 nm AgNPs, low concentrations (0.01–0.5 mg L^{-1}) stimulated astaxanthin biosynthesis, with increases of up to ~30% relative to the con-

trol, the highest value being observed at 0.1 mg L^{-1}. This indicates that mild nanoparticle-induced stress can act as a trigger for astaxanthin overproduction. Conversely, higher concentrations (1.0 and 5.0 mg L^{-1}) inhibited carotenoid accumulation, reducing astaxanthin content by ~5% and ~26%, respectively.

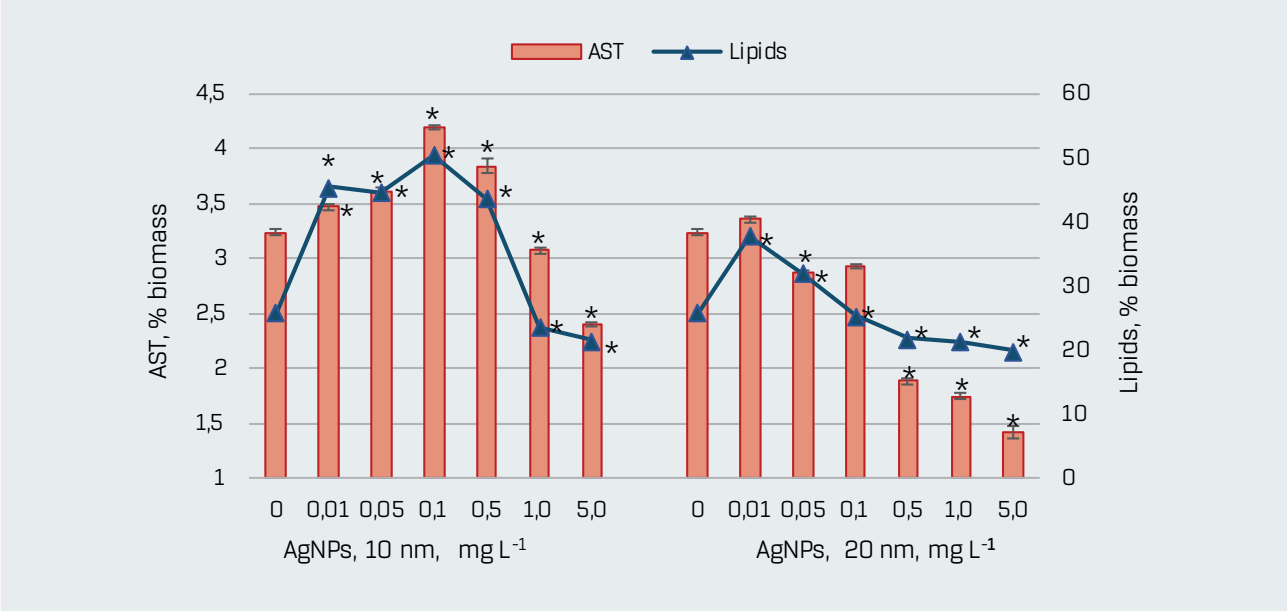

Figure 6. Astaxanthin (AST) and lipid content (% biomass) in *Haematococcus lacustris* at the aplanospore stage after exposure to 10 nm and 20 nm AgNPs (mg L^{-1}). 0 = control; mean ± SD (n = 3); * $p < 0.05$ vs. control.

For 20 nm AgNPs, the response pattern was different. Even at relatively low concentrations (0.05–0.1 mg L^{-1}), astaxanthin content already tended to decrease (by ~9–12%), and all concentrations from 0.5 to 5.0 mg L^{-1} strongly suppressed astaxanthin formation, with reductions of ~42–56%. These findings indicate that, at the aplanospore stage, 10 nm AgNPs at low–moderate doses can be exploited to enhance astaxanthin production, while 20 nm particles are largely inhibitory across the tested range.

The lipid content of aplanospores was also strongly affected by AgNPs (Figure 6). In the presence of 10 nm nanoparticles, concentrations between 0.01 and 0.5 mg L-1 markedly increased lipids, with rises of ~69–96% compared to the control, suggesting an intensified accumulation of energy-rich storage compounds in response to mild nanoparticle stress. At higher concentrations (1.0–5.0 mg L^{-1}), lipid levels declined by ~9–23%, paralleling the inhibition of astaxanthin.

For 20 nm AgNPs, lipid stimulation was restricted to the lowest concentrations (0.01–0.05 mg L^{-1}), where increases of ~24–47% were observed. At 0.5–5.0 mg L^{-1}, lipid content decreased significantly, with reductions comparable to those seen for astaxanthin (about 9–23%).

DISCUSSIONS

The present study analyzed the effects of silver nanoparticles on *Haematococcus lacustris* at two key physiological stages – green vegetative cells and red aplanospores – to reveal stage-specific metabolic responses and their relevance for astaxanthin and lipid production. Administering 10 nm and 20 nm AgNPs at the onset of the green stage enabled the evaluation of nanoparticle action during intensive biosynthesis as well as during the subsequent stress-driven transition to the red stage.

A biphasic effect on biomass formation was observed. During the green stage, low and moderate AgNP concentrations (≤1 mg L^{-1}) stimulated biomass accumulation, whereas 5 mg L^{-1} inhibited growth. Comparable stimulatory effects of low AgNP doses have been reported for *Porphyridium purpureum* and *Chlamydomonas reinhardtii* (25, 26). However, inhibition of biomass formation is the predominant outcome described in the literature, especially at ≥1 mg L-1 AgNPs, as demonstrated for *Nannochloropsis oculata, Dunaliella salina*, and several filamentous green algae (27–29). The final biomass collected at the aplanospore stage was reduced at all AgNP doses, indicating that prolonged exposure, even at low levels, ultimately constrains culture productivity. This is consistent with reports highlighting the overall high toxicity of silver nanoparticles to microalgae (30).

In the green stage, *H. lacustris* showed enhanced protein and carbohydrate content across nearly all treatments, pointing to intensified primary metabolism. Similar increases – interpreted as adaptive responses to moderate oxidative stress – were reported for *Oedogonium*, *Ulothrix, Cladophora,* and *Spirogyra* exposed to low AgNP concentrations (33). In contrast to these species, where stress-induced accumulation occurred alongside biomass inhibition, *H. lacustris* in our study exhibited metabolite increases associated with biomass stimulation, suggesting that the stress level induced by low–moderate AgNPs concentrations remained compensable during the vegetative stage.

Chlorophyll and carotenoids were more sensitive indicators of AgNP toxicity. Although pigment levels remained close to control values at ≤0.5 mg L^{-1}, clear declines occurred at 1–5 mg L^{-1} for both nanoparticle sizes, consistent with the well-documented suppression of photosynthetic pigments under AgNP exposure (34, 35). The carotenoid-to-chlorophyll ratio (Car/Chl), a marker of photosynthetic functionality, remained within the characteristic range for the green stage at 0.01–0.5 mg L^{-1} AgNPs, confirming maintenance of primary metabolism under low stress. In contrast, higher concentrations that reduced chlorophyll also altered the Car/Chl ratio, indicating impaired pigment homeostasis.

Lipid content exhibited concentration-dependent stimulation in the green stage, reflecting adaptive remodeling of membrane systems under stress, a phenomenon widely described for microalgae exposed to adverse conditions (8, 37, 38). The increase in lipids observed at both nanoparticle sizes suggests activation of compensatory responses, while elevated MDA levels at ≥1 mg L^{-1} indicate that excessive nanoparticle doses trigger oxidative damage. The correlation between lipids and MDA supports this interpretation.

At the aplanospore stage, the metabolic pattern changed. Low concentrations of 10 nm AgNPs stimulated astaxanthin accumulation, while higher doses inhibited it. Published data similarly describe both suppressive and stimulatory effects of AgNPs on astaxanthin, depending on dose, exposure duration, and physiological state (21, 31). In our study, 20 nm AgNPs caused inhibition at nearly all concentrations, highlighting that nanoparticle size is an important determinant of stress sensitivity.

A strong positive correlation between total carotenoids (green stage) and astaxanthin (red stage) indicates that precursor availability influences final pigment accumulation. At the same time, the negative correlations between lipid content in green and red stages suggest dynamic redistribution of metabolic resources during stress adaptation. Lipids, which function as storage matrices for astaxanthin, showed a strong positive association with astaxanthin levels in the red stage, supporting the interdependence of these biosynthetic pathways.

Overall, the findings show that *H. lacustris* exhibited a clear hormetic response to silver nanoparticles. Low concentrations of 10 nm AgNPs enhanced biomass formation and stimulated the accumulation of primary metabolites, lipids, and astaxanthin, whereas higher doses surpassed the cellular tolerance threshold, resulting in pigment degradation, oxidative damage, and reduced astaxanthin synthesis. The ability of *H. lacustris* to withstand moderate stress and redirect its metabolism toward protective and storage compounds, such as carotenoids and lipids, highlights its adaptive plasticity and suggests opportunities for controlled metabolic enhancement, provided nanoparticle exposure remains within non-inhibitory ranges.

These stage-dependent responses underscore the importance of nanoparticle dose, size, and timing of application in determining whether their effects are stimulatory or toxic.

CONCLUSIONS

1. This study has proved that silver nanoparticles induced distinct, stage-specific responses in *Haematococcus lacustris*, with direct implications for biomass accumulation, astaxanthin synthesis, and cellular metabolite profiles.
2. Low to moderate concentrations of 10 nm AgNPs stimulated biomass production during the green stage and enhanced lipid and astaxanthin accumulation during the red aplanospore stage, suggesting that controlled nanoparticle-induced stress can be exploited to boost valuable metabolites. In contrast, higher concentrations of 10 nm AgNPs and all tested doses of 20 nm AgNPs markedly suppressed biomass and astaxanthin production, indicating increased toxicity associated with larger particle size and elevated exposure levels.

3. These findings confirmed a hormetic response, in which metabolic stimulation was restricted to a narrow exposure window, while excessive nanoparticle-induced oxidative stress led to inhibitory effects.
4. Overall, this knowledge has provided a scientific basis for developing controlled, nanoparticle-assisted strategies to enhance microalgal bioproduct yields while minimizing adverse toxic effects.

ETHICAL APPROVAL

Was not required for this study, as the research did not involve human participants, animals, or interventions subject to ethical committee review.

CONFLICT OF INTEREST

The authors declare no conflicts of interest. The funders had no role in the design of the study; in the collection, analyses, or interpretation of data; in the writing of the manuscript; or in the decision to publish the results.

AUTHOR CONTRIBUTIONS

Conceptualization, L.C. and L.R.; methodology, L.R., T.C. and V.M.; investigation, V.M., T.C. and E. P.; data curation, L.R.; writing – original draft preparation, L.C. and T.C; writing – review and editing L.C.; project administration, L.C. All authors have read and agreed to the published version of the manuscript.

FUNDING

This research was funded by National Agency for Research and Development, Republic of Moldova, Project 24.80012.7007.08 SE" Oxidative stress as a tool in production of microalgae derived antioxidant astaxanthin".

REFERENCES

1. Bayda S, Adeel M, Tuccinardi T, Cordani M, Rizzolio F. The History of Nanoscience and Nanotechnology: From Chemical–Physical Applications to Nanomedicine. *Molecules*. 2019;25(1):112. https://doi.org/10.3390/molecules25010112
2. Malik S, Muhammad K, Waheed Y. Nanotechnology: A Revolution in Modern Industry. *Molecules*. 2023;28(2):661. https://doi.org/10.3390/molecules28020661
3. Kumah EA, Fopa RD, Harati S, Boadu P, Zohoori FV, Pak T. Human and environmental impacts of nanoparticles: a scoping review of the current literature. *BMC Public Health*. 2023;23(1):1059. https://doi.org/10.1186/s12889-023-15958-4
4. Iavicoli I, Leso V, Fontana L, Calabrese E. Nanoparticle Exposure and Hormetic Dose–Responses: An Update. *IJMS*. 2018;19(3):805. https://doi.org/10.3390/ijms19030805
5. Reetu, Clifford M, Prakash R, Rai MP. Latest advances and status analysis of nanomaterials for microalgae photosystem, lipids and biodiesel: A state of art. *Journal of Environmental Chemical Engineering*. 2023;11(1):109111. https://doi.org/10.1016/j.jece.2022.109111
6. Yuan X, Gao X, Liu C, et al. Application of Nanomaterials in the Production of Biomolecules in Microalgae: A Review. *Marine Drugs*. 2023;21(11):594. https://doi.org/10.3390/md21110594
7. Liu Y, Wang S, Wang Z, Ye N, Fang H, Wang D. TiO2, SiO2 and ZrO2 Nanoparticles Synergistically Provoke Cellular Oxidative Damage in Freshwater Microalgae. *Nanomaterials*. 2018;8(2):95. https://doi.org/10.3390/nano8020095
8. Vargas-Estrada L, Torres-Arellano S, Longoria A, Arias DM, Okoye PU, Sebastian PJ. Role of nanoparticles on microalgal cultivation: A review. *Fuel*. 2020;280:118598. https://doi.org/10.1016/j.fuel.2020.118598
9. Déniel M, Errien N, Daniel P, Caruso A, Lagarde F. Current methods to monitor microalgae-nanoparticle interaction and associated effects. *Aquatic Toxicology*. 2019;217:105311. https://doi.org/10.1016/j.aquatox.2019.105311
10. Alishah Aratboni H, Rafiei N, Mehdizadeh Allaf M, et al. Nanotechnology: An outstanding tool for increasing and better exploitation of microalgae valuable compounds. *Algal Research*. 2023;71:103019. https://doi.org/10.1016/j.algal.2023.103019
11. Huang Y, Gao M, Wang W, et al. Effects of manufactured nanomaterials on algae: Implications and applications. *Front Environ Sci Eng*. 2022;16(9):122. https://doi.org/10.1007/s11783-022-1554-3
12. Mularczyk M, Michalak I, Marycz K. Astaxanthin and other Nutrients from Haematococcus pluvialis – Multifunctional Applications. *Marine Drugs*. 2020;18(9):459. https://doi.org/10.3390/md18090459
13. Oslan SNH, Tan JS, Oslan SN, et al. Haematococcus pluvialis as a Potential Source of Astaxanthin with Diverse Applications in Industrial Sectors: Current Research and Future Directions. *Molecules*. 2021;26(21):6470. https://doi.org/10.3390/molecules26216470
14. Abdelazim K, Ghit A, Assal D, et al. Production and therapeutic use of astaxanthin in the nanotechnology era. *Pharmacol Rep*. 2023;75(4):771-790. https://doi.org/10.1007/s43440-023-00488-y
15. Dang Y, Li Z, Yu F. Recent Advances in Astaxanthin as an Antioxidant in Food Applications. *Antioxidants*. 2024;13(7):879. https://doi.org/10.3390/antiox13070879
16. Sun L, Li Y, Yang A, Xie M, Xiong R, Huang C. Astaxanthin: A comprehensive review of synthesis, biological activities and applications. *Food Chemistry*. 2025;488:144847. https://doi.org/10.1016/j.foodchem.2025.144847
17. Lutzu GA, Concas A, Damergi E, Chen L, Zhang W, Liu T. Production of Carotenoids and Astaxanthin from Haematococcus pluvialis Cultivated Under Mixotrophy Using Brewery Wastewater: Effect of Light Intensity and Cultivation Time. *Applied Sciences*. 2024;14(21):9704. https://doi.org/10.3390/app14219704
18. Samhat K, Kazbar A, Takache H, et al. Optimization of continuous astaxanthin production by Haematococcus pluvialis in nitrogen-limited photobioreactor. *Algal Research*. 2024;80:103529. https://doi.org/10.1016/j.algal.2024.103529
19. Zarei Z, Zamani H. Biorefinery approach to stimulate astaxanthin and biofuel generation in microalga Haematococcus pluvialis under different light irradiance. *Clean Techn Environ Policy*. 2024;26(10):3333-3347. https://doi.org/10.1007/s10098-024-02803-4
20. Do TT, Ong BN, Le TL, et al. Growth of Haematococcus pluvialis on a Small-Scale Angled Porous Substrate Photobioreactor for Green Stage Biomass. *Applied Sciences*. 2021;11(4):1788. https://doi.org/10.3390/app11041788
21. Venckus P, Endriukaitytė I, Čekuolytė K, Gudiukaitė R, Pakalniškis A, Lastauskienė E. Effect of Biosynthesized Silver Nanoparticles on the Growth of the Green Microalga Haematococcus pluvialis and Astaxanthin Synthesis. *Nanomaterials*. 2023;13(10):1618. https://doi.org/10.3390/nano13101618
22. Lowry OliverH, Rosebrough NiraJ, Farr AL, Randall RoseJ. Protein measurement with the folin phenol reagent. *Journal of Biological Chemistry*. 1951;193(1):265-275. https://doi.org/10.1016/S0021-9258(19)52451-6
23. Lichtenthaler HK, Wellburn AR. Determinations of total carotenoids and chlorophylls *a* and *b* of leaf extracts in different solvents. *Biochemical Society Transactions*. 1983;11(5):591-592. https://doi.org/10.1042/bst0110591
24. Park J, Jeong HJ, Yoon EY, Moon SJ. Easy and rapid quantification of lipid contents of marine dinoflagellates using the sulpho-phospho-vanillin method. *ALGAE*. 2016;31(4):391-401. https://doi.org/10.4490/algae.2016.31.12.7

25. Rudi L, Cepoi L, Chiriac T, Djur S, Valuta A, Miscu V. Effects of Silver Nanoparticles on the Red Microalga Porphyridium purpureum CNMN-AR-02, Cultivated on Two Nutrient Media. *Marine Drugs*. 2024;22(5):208. https://doi.org/10.3390/md22050208

26. Sendra M, Yeste MP, Gatica JM, Moreno-Garrido I, Blasco J. Direct and indirect effects of silver nanoparticles on freshwater and marine microalgae (Chlamydomonas reinhardtii and Phaeodactylum tricornutum). *Chemosphere*. 2017;179:279-289. https://doi.org/10.1016/j.chemosphere.2017.03.123

27. Fazelian N, Movafeghi A, Yousefzadi M, Rahimzadeh M, Zarei M. Impact of silver nanoparticles on the growth, fatty acid profile, and antioxidative response of Nannochloropsis oculata. *Acta Physiol Plant*. 2020;42(7):126. https://doi.org/10.1007/s11738-020-03101-4

28. Dash A, Singh AP, Chaudhary BR, Singh SK, Dash D. Effect of Silver Nanoparticles on Growth of Eukaryotic Green Algae. *Nano-Micro Lett*. 2012;4(3):158-165. https://doi.org/10.1007/BF03353707

29. Johari SA, Sarkheil M, Behzadi Tayemeh M, Veisi S. Influence of salinity on the toxicity of silver nanoparticles (AgNPs) and silver nitrate (AgNO3) in halophilic microalgae, Dunaliella salina. *Chemosphere*. 2018;209:156-162. https://doi.org/10.1016/j.chemosphere.2018.06.098

30. Lau ZL, Low SS, Ezeigwe ER, et al. A review on the diverse interactions between microalgae and nanomaterials: Growth variation, photosynthetic performance and toxicity. *Bioresource Technology*. 2022;351:127048. https://doi.org/10.1016/j.biortech.2022.127048

31. Cepoi L, Rudi L, Chiriac T, Plingau E, Valuta A, Miscu V. The effect of silver nanoparticles on the microalgae haematococcus pluvialis. In: Proceedings of the 16th International Conference on Nanomaterials – Research & Application (NANOCON 2024), Brno, Czech Republic, 16–18 October 2024.2025:220-225. https://doi.org/10.37904/nanocon.2024.5021

32. Shah MdMR, Liang Y, Cheng JJ, Daroch M. Astaxanthin-Producing Green Microalga Haematococcus pluvialis: From Single Cell to High Value Commercial Products. *Front Plant Sci*. 2016;7. https://doi.org/10.3389/fpls.2016.00531

33. Hasnain M, Munir N, Abideen Z, Dias DA, Aslam F, Mancinelli R. Applying Silver Nanoparticles to Enhance Metabolite Accumulation and Biodiesel Production in New Algal Resources. *Agriculture*. 2022;13(1):73. https://doi.org/10.3390/agriculture13010073

34. Pham TL. Effect of Silver Nanoparticles on Tropical Freshwater and Marine Microalgae. *Journal of Chemistry*. 2019;2019:1-7. https://doi.org/10.1155/2019/9658386

35. Liu W, Majumdar S, Li W, Keller AA, Slaveykova VI. Metabolomics for early detection of stress in freshwater alga Poterioochromonas malhamensis exposed to silver nanoparticles. *Sci Rep*. 2020;10(1):20563. https://doi.org/10.1038/s41598-020-77521-0

36. Solovchenko AE, Chivkunova OB, Maslova IP. Pigment composition, optical properties, and resistance to photodamage of the microalga Haematococcus pluvialis cultivated under high light. *Russ J Plant Physiol*. 2011;58(1):9-17. https://doi.org/10.1134/S1021443710061056

37. Alishah Aratboni H, Rafiei N, Garcia-Granados R, Alemzadeh A, Morones-Ramírez JR. Biomass and lipid induction strategies in microalgae for biofuel production and other applications. *Microb Cell Fact*. 2019;18(1):178. https://doi.org/10.1186/s12934-019-1228-4

38. Wang F, Liu T, Guan W, et al. Development of a Strategy for Enhancing the Biomass Growth and Lipid Accumulation of Chlorella sp. UJ-3 Using Magnetic Fe3O4 Nanoparticles. *Nanomaterials*. 2021;11(11):2802. https://doi.org/10.3390/nano11112802

39. Mattson MP, Calabrese EJ, eds. *Hormesis: A Revolution in Biology, Toxicology and Medicine.* Humana Press; 2010. https://doi.org/10.1007/978-1-60761-495-1

Date of receipt of the manuscript: 10.12.2025

Date of acceptance for publication: 18.12.2025

Liliana Cepoi, WoS Researcher ID: J-9640-2019, SCOPUS ID 55246094000;

Ludmila Rudi, WoS Researcher ID: AAY-3219-2020, SCOPUS ID 55681134100;

Tatiana Chiriac, WoS Researcher ID: AIB-8864-2022, SCOPUS ID 38861074900;

Vera Miscu, SCOPUS ID 55681134100.

EXPERT OPINION – AVIS D'EXPERT

MEDICAL SCIENCES

OPEN ACCESS

METAGENOMICS AT THE INTERFACE OF DIAGNOSTICS AND SURVEILLANCE: A NEAR-TERM PERSPECTIVE

Dániel CADAR

Bernhard Nocht Institute for Tropical Medicine, WHO Collaborating Centre for Arbovirus and Hemorrhagic Fever Reference and Research, National Reference Centre for Tropical Infectious Diseases Hamburg, Germany

INTRODUCTION

The global landscape of infectious diseases is undergoing rapid and profound change. Increased human mobility, climate-driven shifts in vector ecology, intensified human-animal-environment interactions, and geopolitical instability have collectively amplified the risk of emerging and re-emerging infectious diseases. At the same time, public health systems are increasingly confronted with pathogens that are unexpected, genetically diverse, or poorly represented in existing diagnostic panels. These developments highlight the growing limitations of exclusively targeted diagnostic approaches and underscore the need for broader, more adaptive tools.

In this context, metagenomic sequencing has emerged as a transformative technology. By enabling unbiased detection and genomic characterization of pathogens directly from clinical, environmental, or animal samples, metagenomics offers capabilities that extend far beyond conventional diagnostics. While historically confined to research and outbreak investigations, metagenomics is now approaching a level of maturity that warrants serious consideration for integration into routine diagnostics and risk-oriented surveillance frameworks.

METAGENOMICS AND DISEASES WITH INCREASED RISK

Diseases with increased epidemic or pandemic potential, particularly zoonotic and vector-borne infections, pose unique diagnostic and surveillance challenges. These pathogens often circulate at low levels, exhibit substantial genetic diversity, and may evade detection by assays designed for known targets. In such scenarios, metagenomic sequencing provides a critical advantage by enabling the detection of both expected and unexpected agents without prior assumptions.

Metagenomics is especially valuable for early-phase outbreak detection, investigation of unexplained clinical syndromes, and identification of novel or divergent pathogens. It also facilitates the detection of co-infections and mixed microbial communities, which may influence disease severity or transmission dynamics. Importantly, the genomic information generated through metagenomic analysis supports downstream applications such as phylogenetic reconstruction, source attribution, and monitoring of viral evolution capabilities that are essential for informed public health decision-making.

From a biosafety and biosecurity perspective, metagenomics also strengthens preparedness against deliberate or accidental biological events. The ability to rapidly characterize unknown biological agents enhances situational awareness and supports timely risk assessment in complex or ambiguous scenarios.

THE ROLE OF METAGENOMICS IN ROUTINE DIAGNOSTICS

Despite its clear strengths, metagenomics has not yet replaced targeted diagnostics in routine laboratory settings. Targeted PCR-based assays remain indispensable due to their superior sensitivity, speed, and cost-effectiveness for known pathogens and high-throughput screening applications. However, metagenomics should not be viewed as a competing approach, but rather as a complementary one.

A realistic near-term vision involves tiered diagnostic strategies, in which targeted assays serve as the first-line tools, while metagenomic sequencing is applied selectively, when routine diagnostics fail, when unusual epidemiological patterns emerge, or when genomic resolution is required. Such hybrid approaches maximize diagnostic yield while maintaining operational feasibility and cost control.

Recent advances are accelerating the transition of metagenomics toward routine use. Improvements in sample preparation, host nucleic acid depletion, sequencing chemistry, and bioinformatic automation are steadily enhancing analytical sensitivity and reducing turnaround times. At the same time, declining sequencing costs and increased computational capacity are making metagenomic workflows more accessible to public health laboratories.

ONE HEALTH AND INTEGRATED SURVEILLANCE

One of the most significant strengths of metagenomics lies in its applicability across the human-animal-environment interface. Many high-risk pathogens circulate silently in wildlife or vectors long before they cause detectable human disease. Integrating metagenomic surveillance across these domains enables earlier detection of spillover events and provides insights into ecological drivers of emergence.

By generating comparable genomic data from diverse sample types, metagenomics supports integrated One Health surveillance frameworks and facilitates data sharing across sectors. This is particularly important in regions where pathogen diversity is high but genomic data remains scarce. Expanding metagenomic surveillance in such settings can help close existing knowledge gaps and improve global preparedness.

CHALLENGES AND FUTURE DIRECTIONS

For metagenomics to be fully integrated into routine diagnostics and surveillance, several challenges must be addressed. Standardization of laboratory workflows, validation criteria, and data interpretation frameworks is essential to ensure reproducibility and comparability across laboratories. Clear guidance is also needed on result reporting, including thresholds for diagnostic significance and strategies to distinguish true pathogens from contaminants or background flora.

Capacity building remains a critical priority. Investments in training, infrastructure, and interdisciplinary collaboration are required to ensure that metagenomic data can be generated, interpreted, and acted upon effectively. Importantly, ethical and data governance considerations must be addressed, particularly with respect to data sharing and the handling of sensitive genomic information.

CONCLUSION

Metagenomic sequencing is no longer a distant prospect but a rapidly maturing technology with tangible relevance for routine diagnostics and high-risk disease surveillance. While targeted assays will continue to form the backbone of diagnostic testing, metagenomics offers unparalleled breadth and genomic resolution, enabling detection and characterization of pathogens that would otherwise remain undetectable.

The near future of diagnostics will be defined not by the replacement of existing methods, but by their intelligent integration. By combining targeted testing with selective metagenomic analysis, public health systems can enhance preparedness, improve outbreak response, and strengthen biosafety and biosecurity in an increasingly complex global health landscape.

REQUIREMENTS FOR AUTHORS

Rules of drafting

The manuscript (written in English and French) should be in accordance with the guidelines published in: *Uniform Requirements for Manuscripts Submitted to Biomedical Journal (1994) Lancet 1996, 348, V2; 1-4* (www.icmje.org). The manuscripts should be written in font Cambria, size 11 points, spaced at 1.0, fully justified alignment, fields 2 cm on all sides. All pages must be numbered consecutively (in the right bottom corner) and continuously. Abbreviations should be explained at first occurrence in the text and should not be excessively used. The manuscripts must not exceed the number of words (without the title, affiliation, abstract and references): review articles – 4,500 words; research articles – 3,000 words; expert opinions – 2,500 words; case presentation – 1,700 words; experimental and clinical notes – 1,300 words; book reviews and presentations – 2,000 words; teaching articles – 4,000 words. The volume of tables and figures should not exceed 1/3 from the volume of the manuscript. The journal reserves the right to make any other formatting changes. Rejected manuscripts are not returned.

All manuscripts submitted for publication should be accompanied by two abstracts: in the language of origin of the article and English.

Title and authors

The title should be as short as possible (maximum – 120 signs with spaces), relevant for the manuscript content. The names of the authors should be written in full: name, surname (*e.g.:* Jon JONES). Affiliation should include: Department/Unit/Chair, University/Hospital, City, Country of each author. Beneath the affiliation, the author`s details and contact information – e-mail address (*e.g.:* corresponding author: Jon Jones, e-mail: jon.jones@gmail.com).

The structure of the manuscript

The manuscript should comprise the following sub- headings (capitalized):

- **SUMMARY**
- **INTRODUCTION** (will reflect the topical ity and the general presentation of the problem studied, purpose and hypothesis of the study)
- **MATERIAL AND METHODS**
- **RESULTS**
- **DISCUSSIONS**
- **CONCLUSIONS**
- **CONFLICT OF INTERESTS**
- **ACKNOWLEDGEMENT** (optional)
- **ETHICAL APPROVAL** (specify the presence or absence of a positive opinion from the ethics committee: no, date, institution ad informed consent)
- **REFERENCES**

The **summary** should contain 1,600 signs with spaces:

- **Introduction**
- **Material and methods**
- **Results**
- **Conclusions**
- **Key words:** 3-5 words

The summary should not include tables, charts, and bibliographic notes; information not included in the article.

Figures. The text included in figures should be written in font Cambria, 10 point. Each figure should be accompanied by a heading and legend. They should be numbered with Arabic numerals and placed in parentheses (*e.g.:* fig. 1). Both the title (*e.g.* Figure 1) and legend are centred, below the figure.

Tables. The text included in tables should be written in font Cambria, 10 point. Each table should be accompanied by a heading. Tables should be inserted into the text and adjusted to the width of the page. The tables are numbered in Arabic numerals and mentioned in body text in parentheses (*e.g.* tab. 1). The title of the table is centred on the top of the table (*e.g.* Table 1).

References are numbered in the order they appear in the paper. The reference sources are cited at the end of the article by using AMA style and will include only the references cited within the text (the reference is numbered within round parentheses). The intext citations that appear more than once are numbered similarly as in the first citation. The number of references should not exceed 50 sources. The scientific authors are responsible for the accuracy of their writings. The reference list should include only those references that have been consulted by the authors of the manuscript. The elements of the reference sources are written exactly in accordance with the requirements.

For more information see: http://journal.ohrm. bba.md/index.php/journal-ohrm-bba-md/editing_ guidelines

CERINȚE PENTRU AUTORI

Reguli de tehnoredactare

Pregătirea manuscrisului (elaborat în limbile engleză și franceză) va fi în conformitate cu instrucțiunile publicate în: *Uniform Requirements for Manuscripts Submitted to Biomedical Journals (1994) Lancet 1996, 348, V2; 1-4* (www.icmje.org). Manuscrisele trebuie să fie cu font Cambria, dimensiune 11 puncte, spațiat la interval 1,0, aliniere justificată, câmpurile 2 cm pe toate laturile. Toate paginile trebuie să fie numerotate consecutiv (în colțul de jos, în partea dreaptă) și să includă numerotarea continuă a paginilor. Abrevierile trebuie să fie explicate la prima apariție în text și nu trebuie utilizate excesiv. Manuscrisele nu trebuie să depășească (fără a număra titlul, afilierea, rezumatul și referințele): pentru articole de sinteză/referate – 4500 de cuvinte; pentru articole de cercetare – 3000 de cuvinte; pentru opinii ale experților – 2500 de cuvinte; prezentare de caz și imagini din practica clinică/laborator – 1700 de cuvinte; note experimentale și clinice – 1300 de cuvinte; recenzii și prezentări de carte – 2000 de cuvinte; articole didactice – 4000 de cuvinte. Volumul tabelelor și figurilor nu trebuie să depășească 1/3 din volumul manuscrisului. Revista își rezervă dreptul de a face orice alte modificări de formatare. Manuscrisele respinse nu sunt returnate.

Toate manuscrisele transmise spre publicare trebuie să fie însoțite de două rezumate: în limba de origine al articolului și în limba engleză.

Titlul și autorii

Titlul ar trebui să fie cât mai scurt posibil (maximum – 120 de semne cu spații), elocvent pentru conținutul manuscrisului. Numele autorilor vor fi scrise deplin: prenume, nume de familie (*ex:* Ion RUSU). Afilierea va include: Secția/Departamentul/Catedra, Universitatea/Spitalul, Orașul, Țara pentru fiecare autor. Se vor menționa obligatoriu, mai jos, datele autorului corespondent și informațiile de contact – adresa de e-mail (*ex:* autor corespondent: Ion Rusu, e-mail: ion.rusu@gmail.com).

Structura manuscrisului

Manuscrisul va cuprinde următoarele subtitluri (scrise cu majuscule):

- **REZUMAT** (vezi cerințele mai jos)
- **INTRODUCERE** (se va reflecta actualitatea și prezentarea generală a problemei studiate, scopul și ipoteza studiului)
- **MATERIAL ȘI METODE**
- **REZULTATE**
- **DISCUȚII**
- **CONCLUZII**
- **CONFLICT DE INTERESE**
- **MULȚUMIRI ȘI FINANȚARE** (optional)
- **APROBAREA ETICĂ** (se va specifica prezența sau lipsa avizului pozitiv de la comitetul de etică: nr, data, instituția și acordul informat)
- **REFERINȚE**

Rezumatul va conține până la 1600 de semne cu spații și va cuprinde:

- **Introducere**
- **Material și metode**
- **Rezultate**
- **Concluzii**
- **Cuvinte-cheie**: 3-5 cuvinte

În rezumat nu vor fi incluse tabele, grafice și note bibliografice; informații care nu sunt prezentate în studiu.

Figuri. Textul inclus în figuri trebuie să fie scris cu font Cambria, dimensiune 10 puncte. Fiecare figură trebuie să fie însoțită de titlu și legendă. Ele vor fi numerotate cu cifre arabe și vor fi menționate în text în paranteze (*ex:* fig. 1). Titlul (*ex:* Figura 1) și legenda figurii trebuie să fie scrisă centrat, sub figură.

Tabele. Textul inclus în tabele trebuie să fie scris cu font Cambria, dimensiune 10 puncte. Fiecare tabel trebuie să fie însoțită de titlu. Tabelele vor fi inserate în text, fără a depăși lățimea unei pagini. Ele vor fi numerotate cu cifre arabe și vor fi menționate în text în paranteze (*ex:* tab. 1). Titlul tabelului va fi poziționat deasupra tabelului centrat (*ex:* Tabelul 1).

Referințele trebuie să fie numerotate în ordinea apariției în text. Citarea sursei de referință va fi conform stilului *AMA*, plasată la sfârșitul articolului și va include doar referințele citate în text (menționând numărul de referință în paranteză rotundă). Dacă aceeași referință este citată de mai multe ori, ea va fi trecută în text cu același număr ca la prima citare. Numărul total de referințe nu va depăși 50 de surse. Acuratețea datelor ține de responsabilitatea autorului.

Pentru mai multe informații consultații: http://journal.ohrm.bba.md/index.php/journal-ohrm-bba-md/editing_guidelines

EXIGENCES POUR LES AUTEURS

Normes de rédaction

La préparation des manuscrits (rédigés en anglais et français) sera conforme aux instructions publiées dans *Uniform Requirements for Manuscripts Submitted to Biomedical Journals (1994) Lancet 1996, 348, V2; 1-4* (www.icmje.org). Les manuscrits doivent être en police Cambria, taille 11 points, espacés à l'intervalle 1,0, alignement justifié, champs 2 cm de tous les côtés. Toutes les pages doivent être numérotées consécutivement (dans le coin inférieur droit) et inclure une numérotation continue des pages. Les abréviations doivent être expliquées lors de la première apparition dans le texte et ne doivent pas être utilisées de manière excessive. Les manuscrits ne doivent pas dépasser (sans mentionner le titre, l'affiliation, le résumé et la bibliographie) le volume suivant: pour articles de synthèse/rapports – 4500 mots; pour les articles de recherche – 3000 mots; pour les opinions d'experts – 2500 mots; présentation de cas et photos de la pratique clinique/de laboratoire – 1700 mots; notes expérimentales et cliniques – 1300 mots; commentaires et présentations de livres – 2000 mots; articles pédagogiques – 4000 mots. Le volume des tableaux et des figures ne doit pas dépasser 1/3 du volume du manuscrit. La revue se réserve le droit d'apporter toute autre modification de formatage. Les manuscrits rejetés ne sont pas retournés.

Tous les manuscrits à publier doivent être accompagnés par deux résumés: dans la langue originale et en anglais.

Titre et auteurs

Le titre doit être le plus court que possible (maximum – 120 signes avec espaces), éloquent pour le contenu du manuscrit. Les noms des auteurs seront écrits complets: prénom, nom (*ex:* Albert LEBRUN). Quant à l'affiliation, on devra indiquer: Section/Département/Chaire, Université/Hôpital, Ville, Pays – pour chaque auteur. Les données de l'auteur correspondant et les coordonnées – adresse e-mail (*ex:* auteur correspondant: Albert Lebrun, e-mail: albert.lebrun@gmail.com) seront obligatoires ci-dessous.

Structure du manuscrit

Le manuscrit comprendra les sous-titres suivants (avec lettres majuscules):

- **RÉSUMÉ** (voir les exigences ci-dessous)
- **INTRODUCTION** (reflétera l'actualité et la présentation générale du problème étudié, le but et l'hypothèse de l'étude)
- **METHODES**
- **RESULTATS**
- **DISCUSSIONS**
- **CONCLUSIONS**
- **CONFLIT D'INTERETS**
- **REMERCIEMENTS ET FINANCEMENT**
- **APPROBATION ÉTHIQUE** (préciser la présence ou l'absence d'avis favorable du comité d'éthique: no, date, institution et consentement éclairé)
- **REFERENCES**

Le **résumé** contiendra 1600 signes avec espaces:

- **Introduction**
- **Méthodes**
- **Résultats**
- **Conclusions**
- **Mots clés**: 3-5mots.

Le résumé ne comprendra pas des tableaux, graphiques et des notes bibliographiques; des informations non présentées dans l'étude.

Figures. Le texte inclus dans les figures doit être écrit avec police Cambria, taille 10 points. Chaque figure doit être accompagné par un titre et une légende. Ceuxci seront numérotés avec des chiffres arabes et mentionnés dans le texte entre parenthèses (*ex:* fig. 1). Le titre (*ex:* Figure 1) et la légende de la figure doivent être centrés, au-dessous de la figure.

Tableaux. Le texte inclus dans les tableaux doit être écrit avec police Cambria, taille 10 points. Chaque tableau doit être accompagné par un titre. Les tableaux seront numérotés avec des chiffres arabes, mentionnés dans le texte entre parenthèses (*ex:* tab. 1), et seront insérés dans le texte, sans dépasser la largeur d'une page. Le titre du tableau sera placé au-dessus du tableau, centré (*ex:* Tableau 1).

Les **références** doivent être numérotées dans l'ordre où elles apparaissent dans le texte. La citation de la source de référence sera de style *AMA*, placée à la fin de l'article et n'inclura que des références citées dans le texte (mentionnant le numéro de référence entre parenthèses rondes). Si la même référence est citée plusieurs fois, elle sera transmise dans le texte avec le même numéro que celui de la première citation. Le nombre total de références ne dépassera pas 50 sources. La responsabilité pour l'exactitude des données est à la charge de l'auteur. Il faut indiquer dans le manuscrit seulement les références vraiment consultées par les auteurs. Les composants des sources de référence doivent être rédigés strictement selon les exigences.

Pour plus d'informations, voir: http://journal.ohrm. bba.md/index.php/journal-ohrm-bba-md/editing_ guidelines

The *One Health* concept

Globally, the One Health concept is a worldwide strategy to expand interdisciplinary collaborations and communications in all aspects related to the health care of humans, domestic animals or wildlife, which can no longer be approached separately, but only jointly.

One Health addresses not only human and animal disease concerns, but also issues related to lifestyle, diet, exercise, the impact of different types of human-animal relationships, and environmental exposures that can affect both populations. In order to achieve the expected effects, it is also necessary to educate the population to make them aware of the risk factors and benefits of prevention, as well as communication and understanding between patients and healthcare providers.

HUMAN HEALTH

The WHO defined health in 1946 as “a state of complete physical, mental and social well-being and not merely the absence of disease or infirmity”, with the later addition of “the capacity to lead a socially and economically productive life”.

ANIMAL HEALTH

The OIE defines animal welfare in 2008: an animal is in good condition if it is healthy, enjoys comfort, is well fed, is safe, is able to display its innate (natural) behavior and does not suffer from unpleasant conditions such as pain, fear and stress.

PLANT AND ENVIROMENTAL HEALTH

Environmental health refers to those aspects of human health that include the quality of life determined by physical, biological, socio-economic and psycho-social factors in the environment. The interrelationships of people with the environment concern medicine, when an ecological system is in a state of equilibrium, the health of the population prevails.


Scopus

CORE

OpenAIRE

Academic
Resource
Index
ResearchBib

Instrumentul
Bibliometric Național
www.ibn.idsi.md

CYBERLENINKA

НАУЧНАЯ ЭЛЕКТРОННАЯ
БИБЛИОТЕКА
LIBRARY.RU

ROAD
Directory of Open Access
scholarly Resources

WORLD of JOURNALS

DOAJ
DIRECTORY OF
OPEN ACCESS
JOURNALS

INTERNET ARCHIVE

BŞM

We are
Crossref
Member

OCLC
WorldCat

Google Scholar